3C tecnología
Glosas de innovacion aplicadas a la pyme

Ed. 42_Vol. 11_N.º 2
August - December 2022

ISSN: 2254-3376

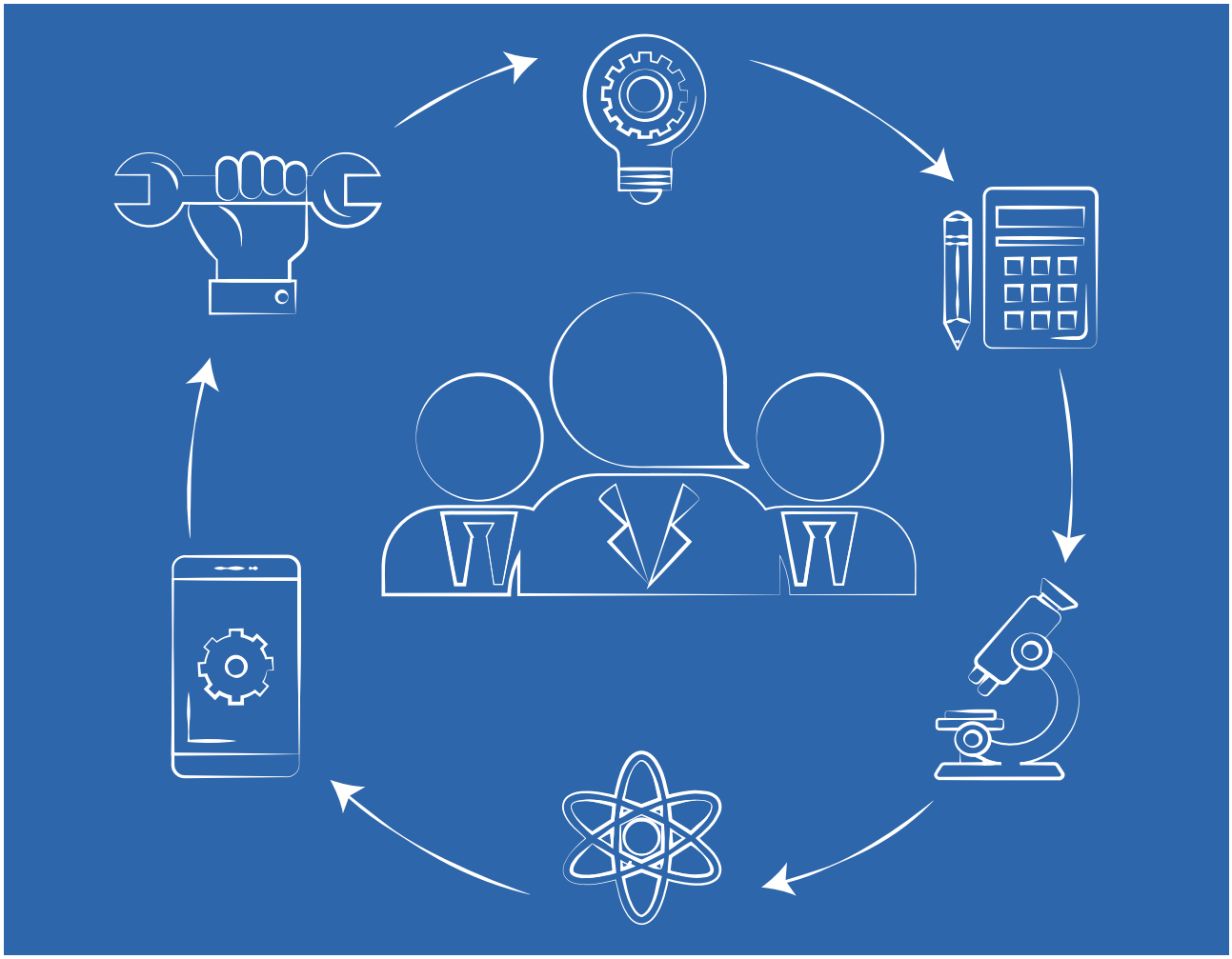

https://doi.org/10.17993/3ctecno/2022.v11n2e42

3C Tecnología. Glosas de innovación aplicadas a la pyme.

Quarterly periodicity.

Edition 42, Volume 11, Issue 2 (August - December 2022).

National and internacional circulation.

Articles reviewed by the double blind peer evaluation method.

ISSN: 2254 - 4143
Legal: A 268 - 2012
DOI: https://doi.org/10.17993/3ctecno.2022.v11n2e42

Edita:
Área de Innovación y Desarrollo by UP4 Institute of Sciences, S.L.
info@3ciencias.com _ www.3ciencias.com

https://doi.org/10.17993/3ctecno/2022.v11n2e42

https://doi.org/10.17993/3ctecno/2022.v11n2e42

EDITORIAL BOARD

https://doi.org/10.17993/3ctecno/2022.v11n2e42

AIMS AND SCOPE

PUBLISHING GOAL

3Ciencias wants to transmit to society innovative projects and ideas. This goal is reached thought the publication of original articles which are subdue to peer review or thorough the publication of scientific books.

TEMATIC COVERAGE

3C Empresa is a scientific - social journal, where original works are spread, written in English, for dissemination with empirical and theoretical analyzes on financial markets, leadership, human resources, market microestructure, public accounting and bussines management.

OUR TARGET

- Research staff.
- PhD students.
- Professors.
- Research Results Transfer Office.
- Companies that develop research and want to publish some of their works.

SUBMISSION GUIDELINES

3C Empresa is an arbitrated journal that uses the double-blind peer review system, where external experts in the field on which a paper deals evaluate it, always maintaining the anonymity of both the authors and of the reviewers. The journal follows the standards of publication of the APA (American Psychological Association) for indexing in the main international databases.

Each issue of the journal is published in electronic version (e-ISSN: 2254-3376), each work being identified with its respective DOI (Digital Object Identifier System) code.

STRUCTURE

The original works will tend to respect the following structure: introduction, methods, results, discussion/conclusions, notes, acknowledgments and bibliographical references.

The inclusion of references is mandatory, while notes and acknowledgments are optional. The correct citation will be assessed according to the 7th edition of the APA standards.

https://doi.org/10.17993/3ctecno/2022.v11n2e42

PRESENTATION WORK

All the information, as well as the templates to which the works must adhere, can be found at:

https://www.3ciencias.com/en/journals/infromation-for-authors/

https://www.3ciencias.com/en/regulations/templates/

ETHICAL RESPONSIBILITIES

Previously published material is not accepted (they must be unpublished works). The list of signatory authors should include only and exclusively those who have contributed intellectually (authorship), with a maximum of 4 authors per work. Articles that do not strictly comply with the standards are not accepted.

STATISTICAL INFORMATION ON ACCEPTANCE AND INTERNATIONALIZATION FEES

- Number of accepted papers published: 8.
- Level of acceptance of manuscripts in this number: 66,7%.
- Level of rejection of manuscripts: 33,3%.
- Internationalization of authors: 3 countries (India, Spain, China).

Guidelines for authors: https://www.3ciencias.com/en/regulations/instructions/

https://doi.org/10.17993/3ctecno/2022.v11n2e42

INDEXATIONS

https://doi.org/10.17993/3ctecno/2022.v11n2e42

INDEXATIONS

https://doi.org/10.17993/3ctecno/2022.v11n2e42

/SUMMARY/

https://doi.org/10.17993/3ctecno/2022.v11n2e42

https://doi.org/10.17993/3ctecno/2022.v11n2e42

/01/

DYNAMICS OF SOFIC SHIFTS

ALI AKBAR K.
Department of Mathematics, Central University of Kerala, Kasaragod (India).
E-mail: aliakbar.pkd@gmail.com, aliakbar@cukerala.ac.in
ORCID: https://orcid.org/0000-0003-3542-3727

Reception: 13/08/2022 **Acceptance:** 28/08/2022 **Publication:** 29/12/2022

Suggested citation:

Ali A. K. (2022). Dynamics of Sofic Shifts. *3C Tecnología. Glosas de innovación aplicada a la pyme,11*(2), 13-23. https://doi.org/10.17993/3ctecno.2022.v11n2e42.13-23

ABSTRACT

In this paper, we provide a characterization for the subshifts of finite type (SFT) in terms of Cellular automata (CA). In addition, we prove that

1. *The following are equivalent for a non-singleton subshift of finite type $X_{\mathcal{F}}$.*
    a) *$X_{\mathcal{F}}$ is transitive and $Per(X_{\mathcal{F}})$, the set of periodic points of $X_{\mathcal{F}}$, is cofinite*
    b) *$X_{\mathcal{F}}$ is weak mixing*
    c) *$X_{\mathcal{F}}$ is mixing.*
2. *For non-singleton sofic shifts, only the statements (a) and (b) are equivalent.*

KEYWORDS

subshift of finite type, sofic shifts, mixing, strongly connected digraph, labeled digraph, cellular automata

https://doi.org/10.17993/3ctecno.2022.v11n2e42.13-23

1 INTRODUCTION AND PRELIMINARIES

A dynamical system is a pair (X, f), where X is a metric space and f is a continuous self map. For each dynamical system (X, f), the period set $\text{Per}(f) = \{n \in \mathbb{N} : \exists\ x \in X$ such that $f^n(x) = x \neq f^m(x)\ \forall m < n\}$ consisting of the lengths of the cycles there, is a subset of the set $\mathbb{N}$ of positive integers. We say that a point $x \in X$ is periodic if $f^n x = x$ for some $n \in \mathbb{N}$, where f^n is the composition of f with itself n times. The smallest such positive integer n is called the period of x. Two dynamical systems (X, f), (Y, g) are said to be topological conjugate if there exists a homeomorphism $h : X \to Y$ such that $h \circ f = g \circ h$. If there is a continuous surjection $h : X \to Y$ such that $h \circ f = g \circ h$ then we say that (Y, g) is a factor of (X, f). A dynamical system (X, f) is said to be transitive if for any non-empty open sets U, V in X there exists $n \in \mathbb{N}$ such that $f^n(U) \cap V \neq \emptyset$ and is said to be mixing if for any non-empty open sets U, V in X there exists $n \in \mathbb{N}$ such that $f^m(U) \cap V \neq \emptyset$ for all $m \geq n$. A dynamical system (X, f) is said to be weak mixing, if given any four nonempty open sets U_1, V_1, U_2, V_2 in X there exists $m \in \mathbb{N}$ such that $f^m(U_1) \cap V_1$ and $f^m(U_2) \cap V_2$ are non-empty.

The subshifts form an important class of dynamical systems, because almost all dynamical systems are factor of some subshifts. There are plenty of books that explain how their study would throw light on still larger classes of dynamical systems (see [7], [10] and [14]). There are some dynamical systems such that the notions transitivity together with cofiniteness, weak mixing, and mixing which are equivalent (See [5], [8] for interval maps, See [2] for topological graph maps). It is natural to ask on which spaces a similar result will be true. We find that the same result is true in the class of non-singleton SFTs, and in the class of continuous 2-dimensional toral automorphisms. Note that SFTs, continuous 2-dimensional toral automorphisms and topological graph maps are different kinds of dynamical systems, and we cannot hope to have a similarity of proofs. In this paper, we concentrate on two-sided shifts. The case of one-sided shifts is similar.

Let $\mathcal{A}$ be a non-empty finite set (called alphabet) with discrete topology and consider the set $\mathcal{A}^{\mathbb{Z}}$, which denotes the set of doubly-infinite sequences $(x_i)_{i\in\mathbb{Z}}$ where each $x_i \in \mathcal{A}$, with product topology. It is compact and metrizable. The shift is the homeomorphism $\sigma : \mathcal{A}^{\mathbb{Z}} \to \mathcal{A}^{\mathbb{Z}}$ given by $\sigma(x)_i = x_{i+1}$ for all $i \in \mathbb{Z}$. A subset $A \subset \mathcal{A}^{\mathbb{Z}}$ is called σ-invariant if $\sigma(A) \subset A$. The pair $(\mathcal{A}^{\mathbb{Z}}, \sigma)$ forms a dynamical system called a full shift. A subshift is a σ- invariant non-empty closed subset X of a full shift, together with the restriction of σ to X. We denote the set of periods of all periodic points of σ in X by $Per(X)$. We call $Per(X)$ the period set of X. A word w on $\mathcal{A}$ is a concatenation $w_1w_2...w_k$, where each $w_i \in \mathcal{A}$ and $(\overline{w})_n = w_r$ whenever $n \equiv r(\textbf{mod}\ k)$. A subshift X is said to be a subshift of finite type (SFT) if $X = X_{\mathcal{F}} = \{x \in \mathcal{A}^{\mathbb{Z}} :$ no word in $\mathcal{F}$ occurs in $x\}$ for some finite set of words $\mathcal{F}$. A subshift $X \subset \mathcal{A}^{\mathbb{Z}}$ is called sofic if it is a factor of an SFT.

The notion of strongly connected digraphs is well known. For every SFT, there is an associated digraph and an associated matrix as described in [7]. This may or may not be strongly connected. Let $G = (V, E)$ be any directed graph (digraph) with vertex set V and edge set E. A subgraph $G' = (V', E')$ of G is said to be a full subgraph if $E' = E \cap \{(v_1, v_2) : v_1, v_2 \in V'\}$. A digraph is said to be simple if from every vertex v to a vertex w there is atmost one edge and it is said to be strongly connected if for every pair of vertices there exists a directed path. It is to be noted that a connected digraph may not be strongly connected. The SFT associated for a digraph G is denoted as X_G and the SFT associated for an $m \times m$ matrix A with entries 0 or 1 is denoted as X_A. Let $V' = \{v \in V :$ there exists a cycle through this $v\}$. Consider a full subgraph of a simple digraph G with vertex set V', say $G' = (V', E')$. Define a relation R on V' in such a way that xRy if there is a directed path from x to y and from y to x. Then R is an equivalence relation on the set of vertices V'. Let G'_x be the full subgraph of G' with $[x]$, equivalence class of x, as the vertex set. This G'_x is strongly connected simple digraph and G' can be written as a finite union of such strongly connected simple digraphs, say $\bigcup_{i=1}^{n} G_i$. The SFT associated for a simple digraph G is denoted as X_G. Note that $Per(X_G) = Per(X_{G'})$.

Let $\mathcal{A}$ be an alphabet having atleast two elements. Let $r \in \mathbb{N}_0$. A function $f : \mathcal{A}^{2r+1} \to \mathcal{A}$ is called a local rule. It induces a function $F : \mathcal{A}^{\mathbb{Z}} \to \mathcal{A}^{\mathbb{Z}}$ by the rule

$(F(x))_n = f(x_{n-r}, x_{n-r-1}, ..., x_{n-1}, x_n, x_{n+1}, ..., x_{n+r-1}, x_{n+r})$ for all $n \in \mathbb{Z}$. The pair $(A^{\mathbb{Z}}, F)$ (simply the map $F : \mathcal{A}^{\mathbb{Z}} \to \mathcal{A}^{\mathbb{Z}}$) is called a cellular automaton (abbreviated as CA). A map $F : \mathcal{A}^{\mathbb{Z}} \to \mathcal{A}^{\mathbb{Z}}$ is

https://doi.org/10.17993/3ctecno.2022.v11n2e42.13-23

a cellular automaton if and only if it is continuous and commutes with the shift (see [13]).

Our main results prove that:

1. Let $(\mathcal{A}^{\mathbb{Z}}, F)$ be any CA. Then $Fix(F)$ is an SFT or empty set. Conversely given any SFT X there exists a CA F such that $Fix(F) = X$.
2. The following are equivalent for a subset S of $\mathbb{N}$.
   a) $S = \mathrm{Per}(X)$ for some mixing subshift of finite type X.
   b) Either $S = \{1\}$ or $\mathbb{N} \setminus F$ for some finite subset F of $\mathbb{N}$.
3. a) The following are equivalent for a non-singleton SFT X.
      i. X is transitive and $Per(X)$ is cofinite
      ii. X is weak mixing
      iii. X is mixing.
   b) In general, in the case of non-singleton sofic shifts, only the statements 3(a)ii and 3(a)iii are equivalent.

The results are intuitive in nature and provide a basic understanding of the dynamics of shift spaces. This review article will be useful to any reader interested in understanding basics of dynamics of shift spaces.

2 SUBSHIFTS OF FINITE TYPE AND SOFIC SHIFTS: TRANSITIVITY, WEAK MIXING, MIXING

One of the result in this paper is motivated by the following two known theorems.

Theorem 1. *The following are equivalent for a topological graph map $f : G \to G$ (See [5], [8] for interval maps, See [2] for topological graph maps).*

1. *f is transitive and $Per(f)$ is cofinite (ie., $\mathbb{N} \setminus Per(f)$ is finite)*
2. *f is weak mixing*
3. *f is mixing.*

Theorem 2. *The following are equivalent for a continuous toral automorphism $T : \mathbb{T}^2 \to \mathbb{T}^2$.*

1. *T is transitive and $Per(T)$ is cofinite (ie., $\mathbb{N} \setminus Per(T)$ is finite)*
2. *T is weak mixing*
3. *T is mixing.*

Proof. Proof follows from the main results of [16] and [17].

2.1 SUBSHIFTS OF FINITE TYPE

Let A be a $k \times k$ adjacency matrix (i.e., the matrix with entries 0 or 1). We call the matrix primitive if there exists $N \in \mathbb{N}$ such that $A^N > 0$. Now we consider the following known proposition.

Proposition 1. *[7] An SFT induced by a matrix A with non-zero rows and columns is mixing if and only if A is primitive.*

https://doi.org/10.17993/3ctecno.2022.v11n2e42.13-23

Next we state the following known theorem. We denote any finite subset A of $\mathbb{N}$ as $A \subset\subset \mathbb{N}$, and *gcd* for the greatest common divisor.

Theorem 3. *[1] The following are equivalent for a subset S of $\mathbb{N}$.*

1. *$S = Per(X_G)$ for some strongly connected simple digraph G containing cycles of lengths $m_1, ..., m_k$ such that $gcd(m_1, m_2, ..., m_k) = 1$.*
2. *Either $S = \{1\}$ or $S = \mathbb{N} \setminus F$ for some $F \subset\subset \mathbb{N}$.*

Next we have:

Theorem 4. *A strongly connected simple digraph G induced by an adjacency matrix $A_{k\times k}$ with non zero rows and columns contains cycles of lengths $m_1, m_2, ..., m_k$ such that $gcd(m_1, m_2, ..., m_k) = 1$ if and only if A is primitive.*

Proof. Suppose that G is a strongly connected simple digraph, and contains cycles of lengths $m_1, m_2, ..., m_k$ such that $\gcd(m_1, m_2, ..., m_k) = 1$. Without loss of generality we can assume that these are simple cycles of G that contain all vertices. By a basic number theory result, there exists $n_0 \in \mathbb{N}$, $F \subset\subset \mathbb{N}$ such that for all $n \geq n_0$, $n \in \mathbb{N} \setminus F$ there exist $a_1, a_2, ..., a_k \in \mathbb{N}$ such that $n = a_1m_1 + a_2m_2 + ... + a_km_k$. Therefore, given any vertex x there exists a cycle of length n for all $n \geq n_0$. Let $m = diam(G) = Max\{l(x, y) : x, y \in V(G)\}$ where $l(x, y)$ denotes the length of a directed path from x to y. Let $N = n_0 + m$. Hence $A^N > 0$ since for every $x, y \in V(G)$ there exists a path of length p for all $p \leq m$ and for every $x \in V(G)$ there exists a cycle of length n for all $n \geq n_0$. Write $N = n_0 + m - p + p$. Hence A is primitive.

Conversely, suppose that A is primitive and $\gcd(m_1, m_2, ..., m_l) = p > 1$ for all cycles of length m_i, $1 \leq i \leq p$, $p \in \mathbb{N}$. Let $k =$ gcd of lengths of all cycles of G. Then there exist cycles of length $m_1, m_2, ..., m_l$ such that $\gcd(m_1, m_2, ..., m_l) = k$. Then k divides the lengths of all cycles. Also, there exists $s \in \mathbb{N}$ such that $A^s > 0$, and for every $x, y \in V(G)$ there exists a path of length s from x to y since A is primitive and G is strongly connected. Therefore k divides s and $s + 1$, which implies $k = 1$. A contradiction. Hence the proof.

Corollary 1. *A strongly connected simple digraph G contains cycles of length $m_1, ..., m_k$ such that $gcd(m_1, m_2, ..., m_n) = 1$ if and only if X_G is mixing.*

Proof. This follows from Proposition 1, Theorems 3 and 4.

Corollary 2. *The following are equivalent for a subset S of $\mathbb{N}$.*

1. *$S = Per(X)$ for some mixing subshift of finite type X.*
2. *Either $S = \{1\}$ or $\mathbb{N} \setminus F$ for some finite subset F of $\mathbb{N}$.*

Proof. Proof follows from Theorems 3, 4, and Corollary 1.

The proof of the following theorem relies mostly on the proof of Proposition 1, as given in [7].

Lemma 1. *An SFT X_A is weak mixing if and only if for every $1 \leq i_1, j_1, i_2, j_2 \leq k$ there exists $n \in \mathbb{N}$ such that $A^n(i_1, j_1) > 0$ and $A^n(i_2, j_2) > 0$ where A denotes a $k \times k$ adjacency matrix.*

Proof. Assume that X_A is weak mixing. Let $U_1 = \{(x_n)_{n\in\mathbb{Z}} \in X_A : x_0 = i_1\}$, $V_1 = \{(x_n)_{n\in\mathbb{Z}} \in X_A : x_0 = j_1\}$, $U_2 = \{(y_n)_{n\in\mathbb{Z}} \in X_A : y_0 = i_2\}$ and $V_2 = \{(y_n)_{n\in\mathbb{Z}} \in X_A : y_0 = j_2\}$ where $1 \leq i_1, j_1, i_2, j_2 \leq k$. These sets are open. Then there exists $n \in \mathbb{N}$ such that $\sigma^n(U_i) \cap V_i \neq \emptyset$, $i = 1, 2$. Hence $x_0 = i_1$, $y_0 = i_2$, $x_n = j_1$ and $y_n = j_2$. Note that $A^N(i, j) = \sum_{r_1=1}^{k} ... \sum_{r_{N-1}=1}^{k} A(i, r_1)A(r_1, r_2)...A(r_{N-2}, r_{N-1})A(r_{N-1}, j)$ for all $N \in \mathbb{N}$. But $A(i_1, x_1) = A(x_1, x_2) = A(x_2, x_3) = ... = A(x_{n-1}, j_1) = 1$ and $A(i_2, y_1) = A(y_1, y_2) = A(y_2, y_3) = ... = A(y_{n-1}, j_2) = 1$. Therefore $A^n(i_1, j_1) > 0$ and $A^n(i_2, j_2) > 0$.

https://doi.org/10.17993/3ctecno.2022.v11n2e42.13-23

Conversely, assume that for every $1 \leq i_1, j_1, i_2, j_2 \leq k$ there exists $N \in \mathbb{N}$ such that $A^N(i_1, j_1) > 0$ and $A^N(i_2, j_2) > 0$. Given non-empty open sets U_1, V_1, U_2, V_2 we can choose $(i_n^{(l)})_{n\in\mathbb{Z}} \in U_l$ and $(j_n^{(l)})_{n\in\mathbb{Z}} \in V_l$ such that for $M > 0$ sufficiently large; and $U_l \supset \{(x_n)_{n\in\mathbb{Z}} \in X_A : x_k = i_k^{(l)}, -M \leq k \leq M\}$, $V_l \supset \{(x_n)_{n\in\mathbb{Z}} \in X_A : x_k = j_k^{(l)}, -M \leq k \leq M\}$ for $l = 1, 2$ (It is possible since the set of symmetric cylinders form a base for the topology on $\mathcal{A}^{\mathbb{Z}}$).

By hypothesis, there exists $N > 0$ such that $A^N(i_M^{(l)}, j_{-M}^{(l)}) > 0$ for $l = 1, 2$. This means we can find a word $x_1^l ... x_{N-1}^l$ such that $A(i_M^{(l)}, x_1^l) = A(x_1^l, x_2^l) = ... = A(x_{N-1}^l, j_{-M}^{(l)}) = 1$.

Define $x_n^{(l)} = \begin{cases} i_n^{(l)} & \text{if } n \leq M \\ x_{n-M}^l & \text{if } M+1 \leq n \leq M+N-1 \\ j_{n-(2M+N)}^{(l)} & \text{if } M+N \leq n \end{cases}$

Then $\sigma^{2M+N}(U_l) \cap V_l \neq \emptyset$ for $l = 1, 2$. Hence X_A is weak mixing.

Next we have:

Theorem 5. *An SFT is weak mixing if and only if it is mixing.*

Proof. Let A be an adjacency matrix of order k. Assume that X_A is weak mixing. We have to prove that there exist cycles of lengths $m_1, m_2, ..., m_p$ such that $\gcd(m_1, m_2, ..., m_p) = 1$. Suppose not. Then there exists $s \in \mathbb{N} \setminus \{1\}$ such that s divides the lengths of all cycles (let $s =$ gcd of lengths all cycles). Let $1 \leq v_1, w_1, v_2 \leq k$ be such that $v_1 w_1$ is a block in x for some $x \in X_A$. Then there exist a cycle of length n through v_2 and a path of length n from w_1 to v_1, which implies s divides n and $n+1$. Hence $s = 1$. A contradiction. Hence X_A is mixing. Converse part is easy.

Hence we have:

Theorem 6. *The following are equivalent for a non-singleton SFT $X_{\mathcal{F}}$.*

(i) $X_{\mathcal{F}}$ is transitive and $Per(X_{\mathcal{F}})$ is cofinite.

1. *$X_{\mathcal{F}}$ is weak mixing.*
2. *$X_{\mathcal{F}}$ is mixing.*

Proof. We first observe that the period set $\mathrm{Per}(X_{\mathcal{F}})$ of a finite SFT $X_{\mathcal{F}}$ is finite. So $\mathrm{Per}(X_{\mathcal{F}})$ is not cofinite. Except singleton SFTs all other finite SFTs are not weak mixing and hence not mixing. Hence the theorem follows from Theorems 3, 4 and 5, and Proposition 1.

Remark 1. *Suppose some rows of A or columns of A is of full of zeros, say i th row and j th column. Then remove ith row and j th column. Doing this for all such i and j, we obtain another matrix $\tilde{A}$ of smaller size. Then X_A and $X_{\tilde{A}}$ are in a sense one and the same. Therefore the equivalence of* (2) *and* (3) *is true for all subshifts induced by adjacency matrices.*

Next we consider:

Theorem 7. *(see [15]) (Blokh, Barge-Martin) Let $f : I \to I$ be an interval map such that the periodic points are dense in I. Then the interval I decomposes into transitive components C_n in the following way.*

1. *C_n is a closed non-degenerate interval or C_n is the union of two disjoint closed non degenerate intervals,*
2. *$f|_{C_n}$ is transitive,*
3. *the complement set of $\bigcup C_n$ is included in $\{x \in X : f^2(x) = x\}$.*

In addition, the number of transitive components C_n is finite or countable and their interiors are pairwise disjoint.

https://doi.org/10.17993/3ctecno.2022.v11n2e42.13-23

As similar to Theorem 7, now we have:

Theorem 8. *Let $X_{\mathcal{F}}$ be an SFT for some finite set of words $\mathcal{F}$ over an alphabet $\mathcal{A}$ with dense set of periodic points. Then there exists some finite set of words $\mathcal{G} \supset \mathcal{F}$, and an SFT $X_{\mathcal{G}}$ with dense set of periodic points and it is a finite union of transitive SFTs, and $Per(X_{\mathcal{F}}) = Per(X_{\mathcal{G}})$.*

Proof. Let X^G denotes the subshift of finite type associated for a simple digraph G such that $X^G = X_{\mathcal{F}}$. Let V be the set of all vertices of G. For $v_1, v_2 \in V$, we say that $v_1 \sim v_2$ whenever there is a path from v_1 to v_2 and vice-versa. Then $\sim$ forms an equivalence relation on V. Each equivalence class corresponds to a strongly connected simple digraphs. Let G' be the union of all such strongly connected simple digraphs. Observe that $Per(X^G) = Per(X^{G'})$. Now consider $\mathcal{G} \supset \mathcal{F}$ such that $X_{\mathcal{G}} = X^{G'}$. Hence the proof.

Consider a countable set $\{1, 2, ...\}$. With the discrete topology it is a non-compact metrizable space. Let $\sum = \{1, 2, ...\}^{\mathbb{Z}}$. With product topology $\sum$ is a totally disconnected, perfect and non-compact metric space. As in the finite case, the cylinder sets form a countable basis of clopen sets. The shift, σ, is a homeomorphism of the space to itself. The dynamical system $(\sum, \sigma)$ is the full shift on the symbols. If A is a countable, zero-one matrix, then as in the finite case, we use transition rules to define a shift-invariant subset of the full shift on countably many symbols, denoted by $\sum_A$. Then the subspace $\sum_A$ of $\sum$ is non-compact, metrizable and $\sigma : \sum_A \to \sum_A$ is the countable state Markov shift defined by A.

Next consider the following two known propositions.

Proposition 2. *[12] A countable state Markov shift $\sum_A$ is topologically transitive if and only if A is irreducible.*

Proposition 3. *[12] A countable state Markov shift $\sum_A$ is topologically mixing if and only if A is primitive.*

Now we have:

Theorem 9. *[12] The following are equivalent for countable Markov shift $\sigma : \sum_A \to \sum_A$.*

(i) $\sigma : \sum_A \to \sum_A$ is transitive and $Per(\sigma)$ is cofinite.

(ii) $\sigma : \sum_A \to \sum_A$ is weak mixing.

(iii) $\sigma : \sum_A \to \sum_A$ is mixing.

Proof. The proof follows from Propositions 2 and 3.

2.2 SOFIC SHIFTS

The notion of labeled digraph is well known (see [14], [7]). For every sofic shift there is a labeled digraph and vice versa (see [7]). As similar to digraphs, we can define simple labeled digraph and strongly connected labeled digraph. First we have to define it for corresponding digraphs. Then consider the corresponding labeled digraphs. As similar to digraphs, for every labeled digraph Γ there exists another labeled digraph Γ' such that $\mathrm{Per}(X_\Gamma) = \mathrm{Per}(X_{\Gamma'})$ and Γ' is a finite union of strongly connected simple labeled digraphs where X_Γ denotes the subshift induced by Γ. Let Γ be a finite labeled digraph, the edges of Γ are labeled by an alphabet $\mathcal{A}_m = \{1, 2, ..., m\}$. Note that we do not assume that the different edges of Γ are labeled differently. Let $E(\Gamma)$ denotes the set of all edges of Γ. The subset $X_\Gamma \subset \mathcal{A}_m^{\mathbb{Z}}$ consisting of all infinite directed paths in Γ is closed and shift invariant. If a subshift X is topologically conjugate to X_Γ for some labeled digraph Γ, then we say that Γ is a presentation of X.

Proposition 4. *[7] A subshift $X \subset \mathcal{A}^{\mathbb{Z}}$ is sofic if and only if it admits a presentation by a finite labeled digraph.*

https://doi.org/10.17993/3ctecno.2022.v11n2e42.13-23

Theorem 10. *[1] The following are equivalent for a subset S of $\mathbb{N}$.*

(1) *$S = Per(X_\Gamma)$ for some strongly connected labeled digraph Γ containing cycles of length $m_1, m_2, ..., m_k$ such that $gcd(m_1, m_2, ..., m_k) = 1$.*

(2) *Either $S = \{1\}$ or $S = \mathbb{N} \setminus F$ for some $F \subset\subset \mathbb{N}$.*

From the definition of transitivity, mixing, weak mixing and by using some ideas from Lemma 1, we can prove the following lemma for any directed labeled graph Γ. Recall that for every non-empty open set U in X_Γ we can choose $(i_n)_{n\in\mathbb{Z}} \in U$ such that for $M > 0$ sufficiently large; $U \supset \{(x_n)_{n\in\mathbb{Z}} : x_k = i_k, -M \leq k \leq M\}$.

Lemma 2. *Let Γ be a labeled digraph. Then the following are true.*

1. *X_Γ is transitive if and only if for every $i, j \in E(\Gamma)$ there exists a directed path of length n from i to j for some $n \in \mathbb{N}$.*
2. *X_Γ is weak mixing if and only if for every $i_1, j_1, i_2, j_2 \in E(\Gamma)$ there exist directed paths of length n from i_1 to j_1 and from i_2 to j_2 for some $n \in \mathbb{N}$.*
3. *X_Γ is mixing if and only if for every $i, j \in E(\Gamma)$ there exists $N \in \mathbb{N}$ such that for all $n \geq N$ there is a directed path of length n from i to j.*

Theorem 11. *Let Γ be a strongly connected labeled digraph. Then Γ contains cycles of lengths $m_1, m_2, ..., m_k$ such that $gcd(m_1, m_2, ..., m_k) = 1$ if and only if X_Γ is mixing.*

Proof. We can provide a proof similar to that of Theorem 4. Here while proceeding the proof without loss of generality it is not possible to assume the cycles are simple. Still the conclusion is true.

Corollary 3. *The period set of a mixing SFT is*

either $\{1\}$ or $\mathbb{N} \setminus F$ for some $F \subset\subset \mathbb{N}$.

Proof. Proof follows from Theorems 10 and 11.

Theorem 12. *A sofic shift is weak mixing if and only if it is mixing.*

Proof. Because of Lemma 2 and Theorem 11, we can provide a proof similar to that of Theorem 5.

Remark 2. *There exists a sofic shift X_Γ which is transitive and its period set is cofinite, but it is not Mixing.*

Proof. Let X_Γ be the sofic shift based on the directed graph Γ with vertices 0 and 1, arcs labeled a, b, c from 0 to 1, and arcs labeled a, b, d from 1 to 0. Then X_Γ is the image of the topologically transitive subshift of finite type, based on Γ but with distinctly labeled edges. The period set of X_Γ is $\mathbb{N}$. But X_Γ is not topologically mixing by Theorems 11. Hence the remark follows.

Remark 3. *If X_Γ is a transitive non-singleton sofic shift, then the set of periodic points of σ in X_Γ is dense in X_Γ. But a compact dynamical system which is totally transitive and has a dense set of periodic points is weak mixing (See [4]). Therefore X_Γ is totally transitive if and only if X_Γ is weak mixing. In general, for a subshift, the conclusion of Theorem 12 need not be true. There is a subshift which is weak mixing but not mixing (Chacon shift, See [11]).*

https://doi.org/10.17993/3ctecno.2022.v11n2e42.13-23

3 A CHARACTERIZATION OF AN SFT

The cellular automata play an important role in various contexts such as computer graphics, parallel computing and cell biology. It is natural to ask for a neat description of the sets of periodic points of cellular automata, unfortunately we do not have a complete answer. There have been some papers that discussed about the sets of periodic points for continuous self maps (See [3], [7], [9]). It is natural to ask: Which sets will arise as the set of all periodic points of continuous self maps? This question is too abstract. If we ask the same question in the class of some nice class of maps then we can expect a nice answer. In this section, we consider in the case of CA. Characterization of the sets of periodic points for a continuous self map of an interval is incomplete. J.-P. Delahaye gave partial results in this context (see Propositions 5, 6). This is our first motivation for considering CA. We completely solved in the case of a continuous 2-dimensional toral automorphism in [16] (see Theorem 13). This is our second motivation for considering CA. In this section we give a partial answer in the case CA. Our result is similar to the following propositions 5 and 6, and Theorem 13. It characterizes an SFT in terms of a CA.

Proposition 5. *[9] (i) The set of fixed points of a continuous function from* $[0,1]$ *to* $[0,1]$ *is a closed subset of* $[0,1]$.

(ii) For every closed subset F *of* $[0,1]$ *there exists a continuous function* f *whose fixed point set is* F .

Definition 1. *A subset* F *of* $[0,1]$ *is symmetric if for* $x \in [0,1]$, $\frac{1}{2}+x \in F \Leftrightarrow \frac{1}{2}-x \in F$.

Proposition 6. *[9]* (i) *The set of periodic points of period* 1 *or* 2 *of a continuous function from* $[0,1]$ *to* $[0,1]$ *is a closed subset of* $[0,1]$.

(ii) *For every symmetric closed subset of* $[0,1]$ *there exists a continuous function from* $[0,1] \to [0,1]$ *whose set of periodic points period* 1 *or* 2 *is* $F \cup \{\frac{1}{2}\}$.

Theorem 13. *[16]*

For any continuous toral automorphism T*, the set* $P(T)$ *of periodic points of* T *is one of the following:*

1. $\mathbb{Q}_1 \times \mathbb{Q}_1$*, where* $\mathbb{Q}_1$ *denotes the set of all rational points in* $[0,1)$.

2. S_r *for some* $r \in \mathbb{Q} \cup \{\infty\}$*; where* $S_r = \{(x,y) \in \mathbb{T}^2 \ : \ rx+y \text{ is rational }\}$.

3. $\mathbb{T}^2$.

Definition 2. *A dynamical system* (X,f) *has the shadowing property, if for any* $\epsilon > 0$ *there exists* $\delta > 0$ *such that any finite* δ*-chain is* ϵ*-shadowed by some point. A point* $x \in X$ ϵ*-shadows a finite sequence* $x_0, x_1, ..., x_n$*, if for all* $i \leq n$*,* $d(F^i(x), x_i) < \epsilon$*. A (finite or infinite) sequence* $(x_n)_{n\geq 0}$ *is a* δ*-chain, if* $d(F(x_n), x_{n+1}) < \epsilon$ *for all* n.

ie., $\forall \epsilon > 0$, $\exists \delta > 0, \forall x_0, ..., x_n$, $(\forall i, d(F(x_i), x_{i+1}) < \delta \implies \exists x, \forall i, d(F^i(x), x_i) < \epsilon)$.

Definition 3. *A dynamical system* (X,f) *is open, if* $f(U)$ *is open for any open* $U \subset X$.

There are two distinct topological characterization of SFT known in literature as follows.

Theorem 14. *[13] A subset* $X \subset \mathcal{A}^{\mathbb{N}}$ *is an SFT if and only if* X *has the shadowing property.*

Theorem 15. *[13] A subset* $X \subset \mathcal{A}^{\mathbb{N}}$ *is an SFT if and only if* X *is an open subset of* $\mathcal{A}^{\mathbb{N}}$.

Next we have:

Lemma 3. *For every SFT* X*, there exists a finite set of words* $\mathcal{G}$ *having odd length such that* $X = X_{\mathcal{G}}$.

Proof. Let X be a k-step SFT. Then there exists a finite set of words $\mathcal{F}$ having length atmost k such that $X = X_{\mathcal{F}}$. If k is odd then consider $\mathcal{G} = \{x \in W_k(\mathcal{A}^{\mathbb{Z}}) : y \text{ is a subword of } x \text{ for some } y \in \mathcal{F}\}$. If k is even then consider $\mathcal{G} = \{x \in W_{k+1}(\mathcal{A}^{\mathbb{Z}}) : y \text{ is a subword of } x \text{ for some } y \in \mathcal{F}\}$.

https://doi.org/10.17993/3ctecno.2022.v11n2e42.13-23

Claim: $X_{\mathcal{F}} = X_{\mathcal{G}}$.

Let $x \in X_{\mathcal{F}}$. Suppose $x \notin X_{\mathcal{G}}$. Then for some $y \in \mathcal{F}$, y is a subword of x. A contradiction. Therefore $x \in X_{\mathcal{G}}$. Next, let $x \in X_{\mathcal{G}}$. Which implies y is not a subword of x for all $y \in \mathcal{F}$. Then $x \in X_{\mathcal{F}}$. Hence the claim.

Next we have:

Theorem 16. *Let $(\mathcal{A}^{\mathbb{Z}}, F)$ be any CA. Then $Fix(F)$ is an SFT or an empty set. Conversely given any SFT X there exists a CA F such that $Fix(F) = X$.*

Proof. Let $(\mathcal{A}^{\mathbb{Z}}, F)$ be a CA defined by the local rule $f : \mathcal{A}^{2r+1} \to \mathcal{A}$. Let $\mathcal{F} = \{w \in \mathcal{A}^{2r+1} : f(w) \neq \text{the middle term of } w\}$. Note that $\mathcal{F}$ is finite (it may be empty or $\mathcal{A}^{2r+1}$). First, let $x \in X_{\mathcal{F}}$. Which implies $(F(x))_i = x_i$ for all i. ie., $F(x) = x$. Next, let $x \in \mathcal{A}^{\mathbb{Z}}$ such that $F(x) = x$. Then $f(x_{i-r}x_{i-r+1}...x_0...x_{i+r-1}x_{i+r}) = x_i$ for all i. ie., $x \in X_{\mathcal{F}}$. Hence $Fix(F) = X_{\mathcal{F}}$.

Conversely, given any SFT $X_{\mathcal{F}}$ without loss of generality assume that $\mathcal{F}$ contains words of same length (odd length) because of Lemma 3.

Define $f : A^{2r+1} \to A$ such that

$$f(w) = \begin{cases} \textit{the middle term of } w & \text{if } w \textit{ is forbidden} \\ \textit{some other alphabet} & \textit{otherwise} \end{cases}$$

Then $Fix(F) = X_{\mathcal{F}}$.

Remark 4. *In the statement of Theorem 16, we can replace $Fix(F)$ by $Fix(F^n)$.*

Proof. Let $f : A^{2r+1} \to A$ be the local rule of a CA $F : \mathcal{A}^{\mathbb{Z}} \to \mathcal{A}^{\mathbb{Z}}$. The local rule $f : \mathcal{A}^{2r+1} \to \mathcal{A}$ induces a function $\tilde{f} : \mathcal{A}^{2s+2r+1} \to \mathcal{A}^{2s+1}$ for all s. Then by inductively, define $f_n : \mathcal{A}^{2nr+1} \to \mathcal{A}$ such that $f_n(w) = f(\tilde{f}_{n-1}(w))$ where $\tilde{f}_m : \mathcal{A}^{2r+2(m-1)r+1} \to \mathcal{A}^{2r+1}$ denotes the induced function of f_m for $s = r$. Note that the length of $\tilde{f}(w)$ is equal to the difference between the length of w and $2r$. Let $\mathcal{F}_n = \{w : f_n(w) \neq \text{the middle term of } w\}$. Then $Fix(F^n) = X_{\mathcal{F}_n}$.

Converse part follows easily.

Remark 5. *Let $(\mathcal{A}^{\mathbb{Z}}, F)$ be any CA. Then $Fix(F^n)$ is an SFT for each $n \in \mathbb{N}$. Conversely, given any SFT X there exists CA $F_n : \mathcal{A}^{\mathbb{Z}} \to \mathcal{A}^{\mathbb{Z}}$ such that $Fix(F_n^n) = X$.*

4 CONCLUSIONS

For each self-map f on a set X, we associate a subset of $\mathbb{N}$ namely, $Per(f)$. If f belongs to a certain nice class of functions, then not all subsets of $\mathbb{N}$ may arise as the set of periods. Which subsets of N will come in this class? We answer this question for mixing SFT?s, and for mixing sofic shifts.
It is natural to ask: On which class of dynamical systems the following statements are equivalent?

1. f is transitive and $Per(f)$ is cofinite.
2. f is weak mixing
3. f is mixing.

We have proved that the above statements are equivalent in the case of non-singleton SFT's but not true in the case of sofic shifts. Also we have obtained a characterization for SFT's in terms of Cellular automata.

ACKNOWLEDGMENT

The author is very thankful to the referee for giving valuable suggestions.

https://doi.org/10.17993/3ctecno.2022.v11n2e42.13-23

REFERENCES

[1] **K. Ali Akbar** and **V. Kannan** (2018), Set of periods of subshifts, *Pro. Indian Acad. Sci. (Math. Sci.)*, 128:63.

[2] **LL. Alseda**, **M.A. Del Rio** and **J. A. Rodrigues** (2003), A survey on the Relation Between Transitivity and Dense periodicity for graph maps, *Journal of Difference equations and Applications, Vol.9(3/4)*, 281-288.

[3] **I.N. Baker** (1964), Fixpoints of polynomials and rational functions, *J. London Math. Soc., 39*, 615-622.

[4] **J. Banks** (1997), Regular Periodic decomposition for topologically transitive maps, *Ergodic Theory and Dynamical Systems, 17*, 505-529.

[5] **L.S. Block** and **W.A. Coppel** (1992), Dynamics in One Dimension, *Springer-Verlag, Berline, Volume 1513 of Lecture Notes in Mathematics.*

[6] **J.A. Bondy** and **U.S.R. Murty** (1982), Graph theory with application, *Elsevier science publishing Co., Inc, New York.*

[7] **M. Brin** and **G. Stuck** (2002), Introduction to Dynamical Systems, *Cambridge University Press.*

[8] **E.M. Coven** and **M.C. Hidalgo** (1991), On the topological entropy of transitive maps of the interval, *Bull. Aust. Math. Soc., 44*, 207-213.

[9] **J.-P. Delahaye** (1981), The set of periodic points, *Amer. Math. Monthly., 88*, 646-651.

[10] **R.L. Devaney**(1989), An Introduction to Chaotic Dynamical Systems, *Addison-wesley Publishing Company Advanced Book Program., Redwood City, CA, second edition.*

[11] **Eli Glasner** (2003), Ergodic Theory Via Joinigs, *American Mathematical Society, Mathematical surveys and monographs, Vol 101.*

[12] **B.P. Kitchens** (1997), Symbolic Dynamics, *Springer.*

[13] **P. Kurka** (2003), Topological and symbolic dynamics, *Societe Mathematique de France, Paris.*

[14] **D.A. Lind** and **B. Marcus** (1995), An introduction to symbolic dynamics and coding, *Cambridge University Press., New York, NY, USA.*

[15] **Sylvie Ruette** (2003), Chaos for continuous interval maps, *A survey of relationship between the various forms of chaos.*

[16] **I. Subramania Pillai**, **K. Ali Akbar**, **V. Kannan** and **B. Sankararao** (2010), The set of periodic points of a toral automorphism, *Journal of Mathematical Analysis and Applications., 366*, 367-371.

[17] **I. Subramania Pillai**, **K. Ali Akbar**, **V. Kannan** and **B. Sankararao** (2011), The set of periods of periodic points of a toral automorphism, *Topology Procedings, Volume 37*, 1-14.

https://doi.org/10.17993/3ctecno.2022.v11n2e42.13-23

/02/

LIMIT CYCLES OF PERTURBED GLOBAL ISOCHRONOUS CENTER

Zouhair Diab
Department of Mathematics and Computer Science, Larbi Tebessi University, 12002 Tebessa, Algeria.
E-mail:zouhair.diab@univ-tebessa.dz
ORCID:

Maria Teresa de Bustos
Department of Applied Mathematics. University of Salamanca, Casas del Parque, 2, 37008-Salamanca, Spain.
E-mail:tbustos@usal.es
ORCID:

Miguel Ángel López
SIDIS Research Group, Department of Mathematics, Institute of Applied Mathematics in Science and Engineering (IMACI), Polytechnic School of Cuenca, University of Castilla-La Mancha, 16071 Cuenca, Spain.
E-mail:mangel.lopez@uclm.es
ORCID:

Raquel Martínez
SIDIS Research Group, Department of Mathematics, Institute of Applied Mathematics in Science and Engineering (IMACI), Polytechnic School of Cuenca, University of Castilla-La Mancha, 16071 Cuenca, Spain.
E-mail:Raquel.Martinez@uclm.es
ORCID:

Reception: 29/08/2022 **Acceptance:** 13/09/2022 **Publication:** 29/12/2022

Suggested citation:

Zouhair D., Maria Teresa B. , Miguel Ángel L. and Raquel M.(2022). Limit cycles of perturbed global isochronous center. *3C Tecnología. Glosas de innovación aplicada a la pyme,11*(2), 25-36. https://doi.org/10.17993/3ctecno.2022.v11n2e42.25-36

https://doi.org/10.17993/3ctecno.2022.v11n2e42.25-36

ABSTRACT

We apply the averaging method of first order to study the maximum number of limit cycles of the ordinary differential systems of the form

$$\begin{cases} \ddot{x} + x = \varepsilon \left(f_1(x, y)y + f_2 \left(x, y \right) \right), \\ \ddot{y} + y = \varepsilon \left(g_1(x, y)x + g_2 \left(x, y \right) \right), \end{cases}$$

where $f_1(x, y)$ and $g_1(x, y)$ are real cubic polynomials; $f_2(x, y)$ and $g_2(x, y)$ are real quadratic polynomials. Furthermore ε is a small parameter.

KEYWORDS

Limit Cycles, Averaging Method, Ordinary Differential Systems

https://doi.org/10.17993/3ctecno.2022.v11n2e42.25-36

1 INTRODUCTION AND STATEMENT OF THE MAIN RESULT

At the Paris International Congress of Mathematics in 1900, Hilbert presented twenty-three problems in mathematics. Some problems are still unsolved so far, they were a challenge for all mathematicians of that era. The second part of the well-known Hilbert's 16th problem is to find the maximum number of limit cycles and their position for an ordinary differential planar system of degree n of the form

$$\begin{cases} \dot{x} = \psi(x, y), \\ \dot{y} = \eta(x, y), \end{cases} \tag{1}$$

where n is a positive integer, the dot above the variables represents the first derivative with respect to the variable t, $\psi(x, y)$ and $\eta(x, y)$ are real polynomials, see for instance [13, 14, 17]. This problem has so far remained unresolved, for $n \geq 2$. Let us denote by $\mathcal{H}(n)$ the maximum number of limit cycles of differential system (1) which is usually called a Hilbert number. For example, Chen and Wang in [3], Shi in [22] gave the best result up to now about the lower bounds of $\mathcal{H}(2)$, which is $\mathcal{H}(2) \geq 4$. Li, Liu, and Yang in [15] proved $\mathcal{H}(3) \geq 13$, Li and Li in [16] proved $\mathcal{H}(3) \geq 11$, also Han, Wu and Bi in [10] and Han, Zhang and Zang in [12] proved $\mathcal{H}(3) \geq 11$. For more results about the Hilbert number, see, for example, the paper [9] and the references therein.

There are many papers that studied number of limit cycles using several methods, including the Poincaré–Melnikov integrals, see for instance [11]; the Poincaré return map, see for example [1]; the Abelian integrals, see for example [4]; the averaging method, see [5, 6]; the inverse integrating factor, see for instance [8].

In [19], Llibre and Teixeira used the averaging method of first-order for study the existence of limit cycles of the system of second-order differential equations

$$\begin{cases} \ddot{x} + x = \varepsilon f(x, y), \\ \ddot{y} + y = \varepsilon g(x, y), \end{cases}$$

where $f(x, y)$ and $g\,(x, y)$ are real cubic polynomials and ε is a small parameter.

In this paper, we apply the averaging method of first-order for study the existence of limit cycles of system of second-order differential equations

$$\begin{cases} \ddot{x} + x = \varepsilon\left(f_1(x, y)y + f_2\,(x, y)\right), \\ \ddot{y} + y = \varepsilon\left(g_1(x, y)x + g_2\,(x, y)\right), \end{cases} \tag{2}$$

where $f_1(x, y)$ and $g_1(x, y)$ are real cubic polynomials, $f_2(x, y)$ and $g_2(x, y)$ are real quadratic polynomials such that $f_i(0, 0) = g_i(0, 0) = 0$, for $i = 1, 2$, and ε is a small parameter. These polynomials are expressions of the form

$$\begin{aligned} f_1(x, y) &= a_1x + a_2y + a_3x^2 + a_4xy + a_5y^2 + a_6x^3 + a_7x^2y + a_8xy^2 + a_9y^3, \\ f_2(x, y) &= A_1x + A_2y + A_3x^2 + A_4xy + A_5y^2, \\ g_1(x, y) &= b_1x + b_2y + b_3x^2 + b_4xy + b_5y^2 + b_6x^3 + b_7x^2y + b_8xy^2 + b_9y^3, \\ g_2(x, y) &= B_1x + B_2y + B_3x^2 + B_4xy + B_5y^2. \end{aligned}$$

The system of second order differential equations (2) can be expressed as the following system of first-order differential equations in the usual way:

$$\begin{cases} \dot{x} = u, \\ \dot{u} = -x + \varepsilon\left(f_1(x, y)y + f_2\,(x, y)\right), \\ \dot{y} = v, \\ \dot{v} = -y + \varepsilon\left(g_1(x, y)x + g_2\,(x, y)\right). \end{cases} \tag{3}$$

https://doi.org/10.17993/3ctecno.2022.v11n2e42.25-36

Note that system (3) when $\varepsilon = 0$, is

$$\begin{cases} \dot{x} = u, \\ \dot{u} = -x, \\ \dot{y} = v, \\ \dot{v} = -y. \end{cases} \tag{4}$$

We notice that the system (4) have a global isochronous center at the the origin, i.e. all orbits different from the origin are 2π-periodic, for more detail see [18].

The main result of our work is the following.

Theorem 1. *Using the first-order averaging method, system of second-order differential equations* (3)*, where* $f_1(x, y)$ *and* $g_1(x, y)$ *are real cubic polynomials;* $f_2(x, y)$ *and* $g_2(x, y)$ *are real quadratic polynomials, has at most four limit cycles bifurcating from the periodic orbits of the linear center* $\dot{x} = u, \dot{u} = -x, \dot{y} = v, \dot{v} = -y$*. Here* ε *is a small parameter. Moreover if* $a_4 = 0$ *and* $a_3 = 0$*, the system* (3) *has at most two periodic solutions.*

The first-order averaging method theory, that we summarize in the sequel, can be found in a more extended way in [2]. Similar works where the perturbations via polynomials play an important role are for instance [7] and [20].

2 THE FIRST-ORDER AVERAGING METHOD FOR COMPUTING PERIODIC ORBITS

Theorem 2. *We consider the following two problems*

$$\dot{x}(t) = \varepsilon F(t, x(t)) + \varepsilon^2 R(t, x(t), \varepsilon), \tag{5}$$

and

$$\dot{y}(t) = \varepsilon \mathrm{f}(y(t)), \tag{6}$$

where $t \in [0, +\infty)$*,* x *and* y *in some open* D *of* $\mathbb{R}^n$ *and* $\varepsilon \in (-\varepsilon_0, \varepsilon_0)$ *is a small parameter. Moreover, we suppose that the vector functions* $F(t, x)$ *and* $R(t, x, \varepsilon)$ *are* $T-$*periodic in the first variable and we consider the first-order averaging function*

$$\mathrm{f}(y) = \frac{1}{T} \int_0^T F(s, y) ds.$$

Suppose that F*,* R*,* $\mathrm{D}_x F$*, and* $\mathrm{D}_x^2 F$ *are continuous and bounded by a constant* M *in* $[0, \infty) \times D \times (-\varepsilon_0, \varepsilon_0)$ *where* M *is independent of* ε*. Then, the statements* (I) *and* (II) *satisfied:*

(I) *If there exists an equilibrium point* $\alpha \in D$ *of* (6) *such that*

$$\det \left. \frac{\partial (\mathrm{f}(y))}{\partial y} \right|_{y=p} \neq 0,$$

then, for $\varepsilon > 0$ *sufficiently small, there exists an isolated* $T-$*periodic solution* $\phi_\varepsilon(t)$ *of system* (5) *such that* $\phi_\varepsilon(t) \to 0$ *when* $\varepsilon \to 0$*.*

(II) *If* $y = \alpha$ *(the equilibrium point) of* (6) *is hyperbolic. Then, for* $\varepsilon > 0$ *sufficiently small, the corresponding periodic solution of system* (5) *is unique, hyperbolic and of the same stability type as* α*.*

The proof of this theorem can be seen in [21, 23].

https://doi.org/10.17993/3ctecno.2022.v11n2e42.25-36

3 PROOF OF THEOREM 1

In this work, we consider $\rho > 0$, $s > 0$ and writing differential system (3) in the new variables $(\theta, \rho, s, \omega)$ given by

$$\begin{aligned} x &= \rho\cos(\theta), \\ u &= \rho\sin(\theta), \\ y &= s\cos(\theta+\omega), \\ v &= s\sin(\theta+\omega). \end{aligned}$$

we get

$$\begin{cases} \dot{\theta} = -1 + \varepsilon \mathrm{G}(\theta, \rho, s, \omega), \\ \dot{\rho} = \varepsilon \mathrm{F}_1(\theta, \rho, s, \omega), \\ \dot{s} = \varepsilon \mathrm{F}_2(\theta, \rho, s, \omega), \\ \dot{\omega} = \varepsilon \mathrm{F}_3(\theta, \rho, s, \omega), \end{cases}$$

where

$$\begin{aligned} \mathrm{G}(\theta,\rho,s,\omega) =& \frac{1}{\rho}\cos(\theta)\Big[A_1\rho\cos(\theta) + A_3\rho^2\cos^2(\theta) \\ &+ s\cos(\theta+\omega)\Big(A_2 + (a_1+A_4)\rho\cos(\theta) + a_3\rho^2\cos^2(\theta) + a_6\rho^3\cos^3(\theta)\Big) \\ &+ s^2\cos^2(\theta+\omega)\Big(a_2 + A_5 + a_4\rho\cos(\theta) + a_7\rho^2\cos^2(\theta)\Big) \\ &+ s^3\cos^3(\theta+\omega)\Big(a_5 + a_8\rho\cos(\theta)\Big) \\ &+ s^4\cos^4(\theta+\omega)a_9\Big] \end{aligned}$$

$$\begin{aligned} \mathrm{F}_1(\theta,\rho,s,\omega) =& \sin(\theta)\Big[A_1\rho\cos(\theta) + A_3\rho^2\cos^2(\theta) \\ &+ s\cos(\theta+\omega)\Big(A_2 + (a_1+A_4)\rho\cos(\theta) + a_3\rho^2\cos^2(\theta) + a_6\rho^3\cos^3(\theta)\Big) \\ &+ s^2\cos^2(\theta+\omega)\Big(a_2 + A_5 + a_4\rho\cos(\theta) + a_7\rho^2\cos^2(\theta)\Big) \\ &+ s^3\cos^3(\theta+\omega)\Big(a_5 + a_8\rho\cos(\theta)\Big) \\ &+ s^4\cos^4(\theta+\omega)a_9\Big] \end{aligned}$$

$$\begin{aligned} \mathrm{F}_2(\theta,\rho,s,\omega) =& \sin(\theta+\omega)\Big[B_1\rho\cos(\theta) + (b_1+B_3)\rho^2\cos^2(\theta) + b_3\rho^3\cos^3(\theta) + b_6\rho^4\cos^4(\theta) \\ &+ s\cos(\theta+\omega)\Big(B_2 + (b_2+B_4)\rho\cos(\theta) + b_4\rho^2\cos^2(\theta) + b_7\rho^3\cos^3(\theta)\Big) \\ &+ s^2\cos^2(\theta+\omega)\Big(B_5 + b_5\rho\cos(\theta) + b_8\rho^2\cos^2(\theta)\Big) \\ &+ s^3\cos^3(\theta+\omega)b_9\rho\cos(\theta)\Big] \end{aligned}$$

https://doi.org/10.17993/3ctecno.2022.v11n2e42.25-36

$$
\begin{aligned}
\mathrm{F}_3(\theta,\rho,s,\omega) = -\frac{\cos(\theta)}{\rho}\Big[& A_1\rho\cos(\theta) + A_3\rho^2\cos^2(\theta) \\
& + s\cos(\theta+\omega)\Big(A_2 + (a_1+A_4)\rho\cos(\theta) + a_3\rho^2\cos^2(\theta) + a_6\rho^3\cos^3(\theta)\Big) \\
& + s^2\cos^2(\theta+\omega)\Big(a_2 + A_5 + a_4\rho\cos(\theta) + a_7\rho^2\cos^2(\theta)\Big) \\
& + s^3\cos^3(\theta+\omega)\Big(a_5 + a_8\rho\cos(\theta)\Big) \\
& + s^4\cos^4(\theta+\omega)a_9\Big] \\
+\frac{\cos(\theta+\omega)}{s}\Big[& B_1\rho\cos(\theta) + (b_1+B_3)\rho^2\cos^2(\theta) + b_3\rho^3\cos^3(\theta) + b_6\rho^4\cos^4(\theta) \\
& + s\cos(\theta+\omega)\Big(B_2 + (b_2+B_4)\rho\cos(\theta) \\
& \qquad + b_4\rho^2\cos^2(\theta) + b_7\rho^3\cos^3(\theta)\Big) \\
& + s^2\cos^2(\theta+\omega)\Big(B_5 + b_5\rho\cos(\theta) + b_8\rho^2\cos^2(\theta)\Big) \\
& + s^3\cos^3(\theta+\omega)b_9\rho\cos(\theta)\Big]
\end{aligned}
$$

The previous differential system in the new independent variable θ becomes as follows

$$
\begin{cases}
\dfrac{d\rho}{d\theta} = -\varepsilon \mathrm{F}_1(\theta,\rho,s,\omega) + \varepsilon^2 \mathrm{R}_1(\theta,\rho,s,\omega,\varepsilon), \\
\dfrac{ds}{d\theta} = -\varepsilon \mathrm{F}_2(\theta,\rho,s,\omega) + \varepsilon^2 \mathrm{R}_2(\theta,\rho,s,\omega,\varepsilon), \\
\dfrac{d\omega}{d\theta} = -\varepsilon \mathrm{F}_3(\theta,\rho,s,\omega) + \varepsilon^2 \mathrm{R}_3(\theta,\rho,s,\omega,\varepsilon),
\end{cases} \tag{7}
$$

We observe that this system is into the normal form of the averaging method (5), with $t = \theta$ and $x = (\rho, s, \omega)$ that the all assumptions of the Theorem 2 are satisfied for the system (7). We compute the average functions of the first-order associated with the system (7)

$$
\mathrm{f}_i(\rho,s,\omega) = \frac{1}{2\pi}\int_0^{2\pi} \mathrm{F}_i(\theta,\rho,s,\omega)d\theta,
$$

for $i = 1, 2, 3$, we obtain

$$
\begin{cases}
\mathrm{f}_1(\rho,s,\omega) = \dfrac{s\sin(\omega)}{8}\Big(3\,s^2a_5 + 4\,A_2 + 2\,sa_4\rho\,\cos(\omega) + a_3\rho^2\Big), \\
\mathrm{f}_2(\rho,s,\omega) = -\dfrac{\rho\sin(\omega)}{8}\Big(2\,\rho\,b_4 s\cos(\omega) + 4\,B_1 + 3\,\rho^2 b_3 + b_5 s^2\Big), \\
\mathrm{f}_3(\rho,s,\omega) = -\dfrac{1}{8\rho s}\Big(- 2\,s^3a_4\rho\,\cos^2(\omega) + \rho^3 b_4 s - 3\,s^4a_5\cos(\omega) \\
\qquad + 4\,\rho^2 B_1\cos(\omega) + 2\,\rho^3 b_4 s\cos^2(\omega) - 4\,s^2A_2\cos(\omega) \\
\qquad + 3\,\rho^2 b_5 s^2\cos(\omega) - 3\,s^2a_3\rho^2\cos(\omega) + 3\,\rho^4 b_3\cos(\omega) \\
\qquad + 4\,\rho\,B_2 s - 4\,sA_1\rho - s^3a_4\rho\Big).
\end{cases}
$$

If (ρ_0, s_0, ω_0) is a zero of the system

$$
\mathrm{f}_i(\rho,s,\omega) = 0, \text{ for } i = 1,2,3, \tag{8}
$$

such that

$$
\det \left.\frac{\partial(\mathrm{f}_1,\mathrm{f}_2,\mathrm{f}_3)}{\partial(\rho,s,\omega)}\right|_{(\rho_0,s_0,\omega_0)} \neq 0, \tag{9}
$$

https://doi.org/10.17993/3ctecno.2022.v11n2e42.25-36

then Theorem 2 assures that the system (3) has a periodic solutions. So, in particular a zero of (8) must be isolated in the set of all zeros of (8). We note that the zeros of (8) having $\sin(\omega) = 0$ are non-isolated, so we cannot apply to them the averaging theory for obtaining limit cycles. Moreover, since the differential system (7) is only well defined when $s > 0$ and $\rho > 0$, in the rest of this section we will assume that $\rho > 0$, $s > 0$ and $\sin(\omega) \neq 0$, and consequently we can restrict to look for the zeros of

$$\begin{cases} \xi_1(\rho, s, \omega) = 0, \\ \xi_2(\rho, s, \omega) = 0, \\ \xi_3(\rho, s, \omega) = 0, \end{cases} \tag{10}$$

satisfying (9), where

$$\begin{cases} \xi_1(\rho, s, \omega) = \dfrac{8\mathrm{f}_1}{s\sin(\omega)}, \\ \xi_2(\rho, s, \omega) = \dfrac{-8\mathrm{f}_2}{\rho\sin(\omega)}, \\ \xi_3(\rho, s, \omega) = -8\rho s\mathrm{f}_3. \end{cases}$$

The rest of the proof of Theorem 1 is divided into the following cases and subcases.

Case 1 If $a_4 \neq 0$. Then, by solving the first equation $\xi_1 = 0$ with respect to $\cos(\omega)$ we get

$$\cos(\omega) = -\frac{a_3\rho^2 + 4\,A_2 + 3\,s^2 a_5}{2sa_4\rho}.$$

Substituting the expression of $\cos(\omega)$ in the second equation, $\xi_2 = 0$, we obtain

$$-b_4a_3\rho^2 - 4\,b_4A_2 - 3\,b_4s^2a_5 + 4\,B_1a_4 + 3\,b_3\rho^2a_4 + b_5s^2a_4 = 0. \tag{11}$$

Subcase 1.1 If $b_4a_3 - 3\,b_3a_4 \neq 0$. Then, from (11) we get

$$\rho = \sqrt{\frac{4\,B_1a_4 - 4\,b_4A_2 - 3\,b_4s^2a_5 + b_5s^2a_4}{b_4a_3 - 3\,b_3a_4}}.$$

Substituting the expressions of ρ and $\cos(\omega)$ in the third equation, $\xi_3 = 0$, we obtain an equation of the form

$$\frac{s(\mathbf{A} + \mathbf{B}s^2 + \mathbf{C}s^4)}{\sqrt{(b_4a_3 - 3b_3a_4)^2\big((b_5a_4 - 3b_4a_5)s^2 - 4b_4A_2 + 4B_1a_4\big)}} = 0,$$

where $\mathbf{A}, \mathbf{B}, \mathbf{C}$ are constants. From now onwards, we are going to denote by $\mathbf{A}, \mathbf{B}, \mathbf{C}$ this kind of generic constants. As $\mathbf{A} + \mathbf{B}s^2 + \mathbf{C}s^4$ is a quadratic polynomial in s^2, which can have at most two positive solutions for s, in this subcase we get two values for ρ, s and $\cos(\omega)$. Observe that each value of (ρ, s) provides at most two solutions for ω. Hence, assuming that in these four solutions the determinant (9) is not zero, by Theorem 2, it follows that in this subcase we have at most four periodic solutions of system (3).

Example 1. *Let us consider the system of differential equations:*

$$\begin{cases} \dot{x} = u, \\ \dot{u} = -x + \varepsilon\left(\left(\dfrac{5}{2}x + x^2 + \dfrac{1}{2}xy - \dfrac{1}{2}y^2 + 5x^3 - \dfrac{3}{2}x^2y + y^3\right)y \right. \\ \qquad\qquad \left. + x + x^2 + \dfrac{1}{2}y^2\right), \\ \dot{y} = v, \\ \dot{v} = -y + \varepsilon\left(\left(\dfrac{3}{4}y + x^2 - \dfrac{1}{2}xy - \dfrac{3}{2}y^2 + x^3 - xy^2 - y^3\right)x \right. \\ \qquad\qquad \left. + 2y + x^2 - xy + y^2\right). \end{cases} \tag{12}$$

https://doi.org/10.17993/3ctecno.2022.v11n2e42.25-36

Then, it can be checked that

$$(\rho, s, \omega) = \left(2\sqrt{\frac{6}{37}}, 4\sqrt{\frac{2}{37}}, \frac{\pi}{6}\right)$$
$$(\rho, s, \omega) = \left(2\sqrt{\frac{6}{37}}, 4\sqrt{\frac{2}{37}}, \frac{11\pi}{6}\right)$$

are zeros of system (12) *with determinant* (9) *equals to* $\pm\dfrac{6\sqrt{3}}{1369}$, *respectively. So, this system has two periodic solutions coming from periodic orbits of the center* (4) .

Subcase 1.2 If $b_4a_3 - 3\,b_3a_4 = 0$, then $b_3 = a_3b_4/(3a_4)$, and we need to consider the following subcases.

Subcase 1.2.1 If $b_5a_4 - 3\,b_4a_5 \neq 0$, then, from (11) we obtain that

$$s = 2\sqrt{\frac{-B_1a_4 + b_4A_2}{b_5a_4 - 3\,b_4a_5}}.$$

We must consider that $-B_1a_4 + b_4A_2 \neq 0$, otherwise $s = 0$ and we cannot get periodic solutions. If we substitute the expressions of $\cos(\omega)$ and s in $\xi_3 = 0$, we get an equation of the form $\rho(\mathbf{A} + \mathbf{B}\rho^2 + \mathbf{C}\rho^4) = 0$. Since ρ must be positive, again in this subcase we get two values for ρ, s and $\cos(\omega)$; and consequently at most four periodic solutions of system (3).

Subcase 1.2.2 $b_5a_4 - 3\,b_4a_5 = 0$. Therefore, from (11) we must have that $-B_1a_4 + b_4A_2 = 0$, otherwise we do not have solutions. That is, $b_5 = 3\,b_4a_5/a_4$. Substituting now $\cos(\omega)$ in $\xi_3 = 0$, we get a continum of solutions for ρ and s. So, in this case we cannot apply Theorem 2.

Case 2 $a_4 = 0$. Again we need to consider the following subcases.

Subcase 2.1 $a_3 \neq 0$. Therefore, from the first equation, $\xi_1 = 0$, we get

$$\rho = \frac{\sqrt{-a_3\,(3\,s^2a_5 + 4\,A_2)}}{a_3}.$$

Of course we suppose $-a_3\left(3\,s^2a_5 + 4\,A_2\right) \neq 0$, otherwise $\rho = 0$. Now, we substitute the expression of ρ in the second equation $\xi_2 = 0$.

Subcase 2.1.1 $b_4 \neq 0$. Therefore, from the second equation, $\xi_2 = 0$, we get that

$$\cos(\omega) = -\frac{(b_5a_3 - 9\,b_3a_5)\,s^2 - 12\,b_3A_2 + 4\,B_1a_3}{2b_4s\sqrt{-a_3\,(3\,s^2a_5 + 4\,A_2)}}.$$

Substituting the expressions of ρ and $\cos(\omega)$ in $\xi_3 = 0$, we get an equation of the form

$$\frac{s}{a_3b_4\sqrt{-a_3\,(3\,s^2a_5 + 4\,A_2)}}(\mathbf{A} + \mathbf{B}s^2 + \mathbf{C}s^4) = 0.$$

Since the first factor cannot be zero, as in the previous subcases, we can get at most four periodic solutions of system (3).

Subcase 2.1.2 $b_4 = 0$.

Subcase 2.1.2.1 If $b_5a_3 - 9\,a_5b_3 \neq 0$, then, from the second equation, $\xi_2 = 0$, we obtain

$$s = 2\sqrt{\frac{3\,b_3A_2 - B_1a_3}{b_5a_3 - 9\,a_5b_3}},$$

substituting the expressions of ρ and s in $\xi_3 = 0$, we arrive to an equation of the form $\mathbf{A} + \mathbf{B}\cos(\omega) + \mathbf{C}\cos^2(\omega) = 0$. So, once again, we can obtain at most four solutions for ρ, s and ω, and, consequently, we obtains at most four periodic solutions for system (3).

https://doi.org/10.17993/3ctecno.2022.v11n2e42.25-36

Subcase 2.1.2.2 If $b_5a_3 - 9\,a_5b_3 = 0$, then, $b_5 = \dfrac{9\,a_5b_3}{a_3}$. Now, from $\xi_2 = 0$, it follows that $B_1a_3 - 3\,b_3A_2 = 0$, otherwise we have no solutions. Therefore, $B_1 = \dfrac{3b_3A_2}{a_3}$. Substituting the expression of ρ in $\xi_3 = 0$, we get a continuum of solutions. So, again, we are not in the assumptions of Theorem 2.

Subcase 2.2 $a_3 = 0$. Looking at equation $\xi_1 = 0$, we see that a_5 cannot be zero, otherwise $\xi_1 = 0$ reduces to $A_2 = 0$, and either we do not have solutions or we have a continuum of solutions. Then, from $\xi_1 = 0$ we get

$$s = 2\sqrt{-\frac{A_2}{3a_5}}.$$

Substituting the expression of s in the second equation $\xi_2 = 0$, we must consider the subcases:

Subcase 2.2.1 If $b_4 \neq 0$, then, by solving the equation $\xi_2 = 0$ with respect to $\cos(\omega)$ we get

$$\cos(\omega) = -\frac{12\,B_1a_5 + 9\,\rho^2b_3a_5 - 4\,b_5A_2}{4\rho\,b_4\sqrt{-3\,a_5A_2}}.$$

Substituting the expressions of $\cos(\omega)$ and s in $\xi_3 = 0$, we obtain an equation of the form $\rho(\mathbf{A} + \mathbf{B}\rho^2) = 0$. Hence, as in previous subcases, system (3) has at most two periodic solutions.

Subcase 2.2.2 Assume $b_4 = 0$. Then, the second equation $\xi_2 = 0$ is of the form $\mathbf{A} + \mathbf{B}\rho^2 = 0$, so, there is at most one positive solution for ρ. Hence, by substituting the value of s and ρ in $\xi_3 = 0$, we obtain an equation of the form $\mathbf{A} + \mathbf{B}\cos(\omega) = 0$. Therefore, we get at most one solution for ρ and $\cos(\omega)$. In short, putting aside those subcases where we obtain a continuum of solutions, there is at most one solution for s, ρ and $\cos(\omega)$ and so, there are at most two periodic solutions for system (3).

In the previous case, we gave a particular solution obtained from the subcase 1.1, that is the most general one. Now we are going to see the general solution of subcase 2.2.2, characterized by $a_3 = a_4 = b_4 = 0$.

Corollary 1. *If $a_3 = a_4 = b_4 = 0$ then*

a) If $b_5 = 0$ the system (10) has no solution or it has a continuum of solutions.

b) If $b_5 \neq 0$, the solutions of system (10) are given by:

$$\begin{aligned} \rho^2 &= -\frac{4B_1 + b_5s^2}{3b_3} \\ s^2 &= -\frac{4A_2}{3a_5} \\ \cos(\omega) &= \frac{2(A_1 - B_2)}{b_5\rho s} \end{aligned} \quad .$$

Demonstração. a) If $b_5 = 0$, the system (10) reduces to

$$\begin{aligned} 4A_2 + 3a_5s^2 &= 0, \\ 4B_1 + 3b_3\rho^2 &= 0, \\ 4\rho s(B_2 - A_1) + \cos(\omega)\Big(s^2(-4A_2 - 3a_5s^2) + \rho^2(4B_1 + 3b_3\rho^2)\Big) &= 0 \end{aligned}$$

that is

$$\begin{aligned} 4A_2 + 3a_5s^2 &= 0, \\ 4B_1 + 3b_3\rho^2 &= 0, \\ 4\rho s(B_2 - A_1) &= 0. \end{aligned}$$

https://doi.org/10.17993/3ctecno.2022.v11n2e42.25-36

This system of equations does not depend on ω, hence either has no solution or has a continuum of solutions.

b) If $b_5 \neq 0$, we have the system:

$$\begin{aligned} 4A_2 + 3a_5 s^2 &= 0 \\ 4B_1 + 3b_3\rho^2 + b_5 s^2 &= 0 \\ 4\rho s(B_2 - A_1) + \cos(\omega)\Big(s^2(-4A_2 - 3a_5 s^2) + \rho^2\left(4B_1 + 3b_3\rho^2 + 3b_5 s^2\right)\Big) &= 0. \end{aligned}$$

From the first equation, $\xi_1 = 0$, we obtain that $s^2 = -\frac{4A_2}{3a_5}$, and, by substituting this value in the second equation, $\xi_2 = 0$, it follows that $\rho^2 = -\frac{4B_1 + b_5 s^2}{3b_3}$.

Finally, the equation $\xi_3 = 0$ reduces to

$$\rho s\Big(2(B_2 - A_1) + b_5\rho s\cos(\omega)\Big) = 0,$$

hence,

$$\cos(\omega) = \frac{2(A_1 - B_2)}{b_5\rho s}.$$

This three equalities provides all the possible solutions of this subcase. □

Example 2. *In the previous corollary, if we take $A_1 = B_2$, we have that $\omega = \frac{\pi}{2}$ or $\omega = \frac{3\pi}{2}$, and if we take the values $a_5 = -1, b_3 = -1, b_5 = 1, A_2 = 9, B_1 = 1$, we obtain the following two solutions:*

$$(\rho, s, \omega) = \left(\frac{4}{\sqrt{3}}, 2\sqrt{3}, \frac{\pi}{2}\right),$$

$$(\rho, s, \omega) = \left(\frac{4}{\sqrt{3}}, 2\sqrt{3}, \frac{3\pi}{2}\right).$$

Observe that this subcase does not depend on the constants not listed in this example, so, we can choose any value for them.

4 CONCLUSIONS

This paper shows that the application of averaging method of first-order it is useful for study the existence of limit cycles of perturbated system of second-order differential equations.

We have proved that, using Theorem 2, we can obtain at most four periodic solutions of system (3) when $f_1(x, y)$ and $g_1(x, y)$ are real cubic polynomials, and $f_2(x, y)$ and $g_2(x, y)$ are real quadratic polynomials. Moreover, if $a_4 = 0$ and $a_3 = 0$, the system (3) has at most two periodic solutions. We have also obtained the general solution in the case $a_3 = a_4 = b_4 = 0$.

FUNDING

This paper is partially supported by the FEDER OP2014-2020 and the University of Castilla-La Mancha under Grant 2021-GRIN-31241, and by the Junta de Comunidades de Castilla-La Mancha under grant SBPLY/21/180501/000174.

DATA STATEMENT

This paper is not related with any data.

https://doi.org/10.17993/3ctecno.2022.v11n2e42.25-36

REFERENCES

[1] TR Blows and Lawrence M Perko. Bifurcation of limit cycles from centers and separatrix cycles of planar analytic systems. *Siam Review*, 36(3):341–376, 1994.

[2] Adriana Buică and Jaume Llibre. Averaging methods for finding periodic orbits via brouwer degree. *Bulletin des sciences mathematiques*, 128(1):7–22, 2004.

[3] Lan Sun Chen and Ming Shu Wang. The relative position, and the number, of limit cycles of a quadratic differential system. *Acta Math. Sinica*, 22(6):751–758, 1979.

[4] Colin Christopher and Chengzhi Li. *Limit cycles of differential equations*. Springer Science & Business Media, 2007.

[5] Zouhair Diab, Juan LG Guirao, and Juan A Vera. On the limit cycles for a class of generalized liénard differential systems. *Dynamical Systems*, 37(1):1–8, 2022.

[6] Zouhair Diab and Amar Makhlouf. Limit cycles for the class of-dimensional polynomial differential systems. *Journal of Applied Mathematics*, 2016, 2016.

[7] Amina Feddaoui, Jaume Llibre, Chemseddine Berhail, and Amar Makhlouf. Periodic solutions for differential systems in $\mathbb{R}^3$ and $\mathbb{R}^4$. *Applied Mathematics and Nonlinear Sciences*, 6(1):373–380, 2021.

[8] Hector Giacomini, Jaume Llibre, and Mireille Viano. On the shape of limit cycles that bifurcate from hamiltonian centers. *Nonlinear Analysis, Theory, Methods and Applications*, 41:523–537, 2000.

[9] Maoan Han and Jibin Li. Lower bounds for the Hilbert number of polynomial systems. *Journal of Differential Equations*, 252(4):3278–3304, 2012.

[10] Maoan Han, Yuhai Wu, and Ping Bi. A new cubic system having eleven limit cycles. *Discrete & Continuous Dynamical Systems*, 12(4):675, 2005.

[11] Maoan Han, Junmin Yang, and Pei Yu. Hopf bifurcations for near-hamiltonian systems. *International Journal of Bifurcation and Chaos*, 19(12):4117–4130, 2009.

[12] Maoan Han, Tonghua Zhang, and Hong Zang. On the number and distribution of limit cycles in a cubic system. *International Journal of Bifurcation and Chaos*, 14(12):4285–4292, 2004.

[13] David Hilbert. Mathematische probleme, lecture, second internat. congr. math. (paris, 1900), nachr. ges. wiss. göttingen math. phys. kl. (1900), 253-297; english transl., bull. amer. math. soc. 8 (1902), 437-479.

[14] Yu Ilyashenko. Centennial history of Hilbert's 16th problem. *Bulletin of the American Mathematical Society*, 39(3):301–354, 2002.

[15] Chengzhi Li, Changjian Liu, and Jiazhong Yang. A cubic system with thirteen limit cycles. *Journal of Differential Equations*, 246(9):3609–3619, 2009.

[16] JB Li and CF Li. Distribution of limit cycles for planar cubic hamiltonian systems. *Acta Math Sinica*, 28:509–521, 1985.

[17] Jibin Li. Hilbert's 16th problem and bifurcations of planar polynomial vector fields. *International Journal of Bifurcation and Chaos*, 13(01):47–106, 2003.

[18] Jaume Llibre. Centers: their integrability and relations with the divergence. *Applied Mathematics and Nonlinear Sciences*, 1(1):79–86, 2016.

https://doi.org/10.17993/3ctecno.2022.v11n2e42.25-36

[19] Jaume Llibre and Marco Antonio Teixeira. Limit cycles for a mechanical system coming from the perturbation of a four–dimensional linear center. *Journal of Dynamics and Differential Equations*, 18(4):931–941, 2006.

[20] Jaume Llibre and Xiang Zhang. On the integrability of the hamiltonian systems with homogeneous polynomial potentials. *Applied Mathematics and Nonlinear Sciences*, 3(2):527–536, 2018.

[21] Jan A Sanders and Ferdinand Verhulst. *Averaging Methods in Nonlinear Dynamical Systems*, volume 59. Springer. Berlin, 1985.

[22] Songling Shi. A concrete example of the existence of four limit cycles for plane quadratic systems. *Scientia Sinica*, 23(2):153–158, 1980.

[23] Ferdinand Verhulst. *Nonlinear differential equations and dynamical systems*. Universitext, Springer. Berlin, 1991.

https://doi.org/10.17993/3ctecno.2022.v11n2e42.25-36

/03/

VERIFICATION OF ROLE OF DATA SCANNING DIRECTION IN IMAGE COMPRESSION USING FUZZY COMPOSITION OPERATIONS

Prashant Paikrao
SGGSIET, Nanded, Maharashtra, (India).
E-mail: plpaikrao@gmail.com

Dharmapal Doye
SGGSIET, Nanded, Maharashtra, (India).

Milind Bhalerao
SGGSIET, Nanded, Maharashtra, (India).

Madhav Vaidya
SGGSIET, Nanded, Maharashtra, (India).

Reception: 07/09/2022 **Acceptance**: 22/09/2022 **Publication**: 29/12/2022

Suggested citation:

Paikrao, P., Doye, D., Bhalerao, M., and Vaidya, M. (2022). Verification of role of data scanning direction in image compression using fuzzy composition operations. *3C Tecnología. Glosas de innovación aplicadas a la pyme, 11*(2), 38-49. https://doi.org/10.17993/3ctecno.2022.v11n2e42.38-49

ABSTRACT

A digital image is a numerical representation of visual perception that can be manipulated according to specifications. In order to reduce the cost of storage and transmission, digital images are compressed. Depending upon the quality of reconstruction, compression methods are categorized as Lossy and Lossless compression. The lossless image compression techniques, where the exact recovery of data is possible, is the most challenging task considering the tradeoff between the compression ratio achieved and the quality of reconstruction. The inherent data redundancies like interpixel redundancy and coding redundancy in the image are exploited for this purpose. The interpixel redundancy is treated by decorrelation using Run-length Encoding, Predictive Coding, and other Transformation Coding techniques. While entropy-based coding can be achieved using Huffman codes, arithmetic codes, and the LZW algorithm, which eliminates the coding redundancy. During the implementation of these sequential coding algorithms, the direction used for data scanning plays an important role. A study of various image compression techniques using sequential coding schemes is presented in this paper. The experimentation on 100 gray-level images comprising 10 different classes is carried out to understand the effect of the direction of scanning of data on its compressibility. Depending upon this study the interrelation between the maximum length of the Run and compression achieved similarly the resultant number of Tuples and compression achieved is reported. Considering the fuzzy nature of these relations, fuzzy composition operations like max-min, min-max, and max-mean compositions are used for decision-making. In this way, a rational comment on which data scanning direction is suitable for a particular class of images is made in the conclusion.

KEYWORDS

Image Compression, Data Scanning Direction, Sequential Coding, Fuzzy Composition.

https://doi.org/10.17993/3ctecno.2022.v11n2e42.38-49

1. INTRODUCTION

The digital image is a function of brightness that corresponds to the intensity of pixels. This representation involves large data associated so that the requirements of storage space, computing power and the related communication bandwidth are very high. The technique involved is called image compression to minimize these requirements, so that information can be depicted in a reduced form (Gonzalez, 2004). The capacity of the compression technique to decrease the data size is called the compression ratio. To attain lossless and lossy compression respectively, the redundant and irrelevant data is removed (Holtz, 1993). The techniques of lossy compression have relatively higher compression ratios than that of lossless compression. Compression ratio and reconstructed image quality is always a tradeoff.

Nowadays, with the rise in mobile phone popularity, images are becoming an important record form. Image compression is required for storing and processing large numbers of such images. Depending upon the requirement of data preservation and accuracy reconstructed data quality, DC techniques can be divided into lossless and lossy compression. Compressing the data without sacrificing its originality is the main objective of lossless image compression, the reconstructed data is identical to original data in lossless compression, and it is suitable primarily for applications in compression of Text, medical imaging, law forensics, military imagery, satellite imaging, etc. In lossy compression the reconstructed data is an acceptable approximation of original data, here higher compression ratio can be achieved its applicable in compression of natural images, audio, video, etc. (Hosseini, 2012).

There is always a limit to the compression ratio that can be achieved in Lossless Compression (Rehman, 1952). According to Shannon, on the other hand, in lossless compression techniques, the measure of the amount of information content (Entropy) in the data that can be used to find the theoretical maximum compression ratio for lossless compression techniques, data can be compressed into as small as 10 percent of its actual size, and as the compression techniques require less-complex encoders and decoders as compared to lossless techniques.

The Shannon Entropy concept is explored in the paper to point out different possibilities to increase the compression ratio to its maximum extent. The paper discusses the different concepts related to compression techniques. One alternative to deal with the tradeoff between image quality and compression ratio is to opt for Near-Lossless compression, where difference between the original and reconstructed data is within user-specified amount called as maximum absolute distortion (MAD). This may be suitable for compression of medical images, hyper spectral images, videos, etc.

In addition to the storage space requirements and the overhead of processing time, all users on a specific network are suggested to minimize the size of the data and use the network resources optimally (Kavitha, 2016). Since compression is both time-effective and cost-effective, it helps to share network resources to enhance network performance.

2. MACHINE LEARNING METHODS AND FEATURE IMPORTANCE

In 1999, Holtz gave a review of lossless image compression techniques, saying," Theories are usually the starting point of any new technology.' There are some lossless compression methods explained, namely Shannon's theory, Huffman code, Lempel-Ziv (LZ) code and data trees for Self-Learning Autopsy. Hosseini submitted another review in 2012, which discussed many algorithms with their performances and applications. It includes Huffman algorithm, Run Length Encoding (RLE) algorithm, LZ algorithm, Arithmetic coding algorithm, JPEG and MPEG with their applications.

https://doi.org/10.17993/3ctecno.2022.v11n2e42.38-49

Image Compression deals with the ways in which the data and space needed to represent and store the digital image are reduced. The elimination of data redundancy may be one of the strategies for achieving compression. Human Visual System Redundancy is categorized into three categories: Spatial Redundancy, Spectral Redundancy, and Temporal Redundancy. Spatial redundancy, which is the correlation of neighborhood image pixels. Spectral redundancy is a correlation measure of an image between different color planes (Spectral Bands). The Temporal Redundancy deals with the correlation between a video's consecutive image frames.

In lossless data compression, the removal of data redundancy is the key process, and the data redundancy (Rd) is given by equation 2.1.

$$Rd = 1 - \left(\frac{1}{CR}\right) \tag{2.1}$$

Where,

CR (Compression Ratio) = n1/n2,

n1: Size of compressed data, n2: Size of uncompressed data

Types of data redundancy are as follows,

1. Coding Redundancy
2. Inter-pixel Redundancy
3. Psycho-visual Redundancy

2.1 CODING REDUNDANCY

A code is a system of symbols used for information representation. The pieces of information are represented by a combination of symbols called a codeword, and their length is called the number of symbols in a codeword. The available grey levels in an image are assigned to various codewords. If the grey levels are coded by using longer codewords than needed, an image is said to have coding redundancy. An image's gray-level histogram is created to construct codes with reduced coding redundancy. It is suggested that the most frequent grey levels should be represented by shorter codewords and vice versa to achieve the shortest representation, i.e., to avoid coding redundancy in the data. This variable length coding process may result in an image being shorter overall than the representation of the fixed length code. And when probability-based method(s) are used to design the code, it guarantees the shortest representation. The present coding redundancy is less than optimal, meaning codewords are used for representation, not as short as possible. Below is the average number of bits required to represent each pixel, given by equation 2.2 and 2.3.

$$L_{avg} = \sum_{n=1}^{N} l(g_n).p(g_n) \tag{2.2}$$

Where,

n – Total number of pixels

$l(g_n)$ – Number of bits used to represent gray level of individual pixel

$p(g_n)$ – Probability of occurrence of gray level g_n.

$$p(g_n) = \frac{N}{n}, n = 1,2, \ldots\ldots L \tag{2.3}$$

Where,

N – Number of times the nth gray level appears in image

L – Number of gray levels

https://doi.org/10.17993/3ctecno.2022.v11n2e42.38-49

Total number of bits: The total number of bits required to code an R X C image is given by equation 2.4,

$$L_{RXC} = R.C.L_{avg} \quad (2.4)$$

2.2 INTER-PIXEL REDUNDANCY

There is some connection between the pixel image data represented by the respective grey levels. It is possible to identify this inter-pixel relation of a particular pixel in terms of its neighborhood pixel. These inter-pixel relationships are responsible for the structural and geometric features of objects present in the image. In other words, by means of an Interpixel Redundancy, the intensity value of a particular pixel can be predicted by knowing the intensity value of its neighborhood pixels. An image's spatial resolution is directly proportional to the redundancy of the neighboring pixels. As this increases the likelihood of two adjacent pixels having the same intensity value, the spatial resolution of an image increases. By transforming the 2-D image matrix into a more efficient representation, this redundancy may be taken care of. Mapping is called the operation involved in this process. If it is possible to reconstruct the original image from the mapped data, the operation is called reversible mapping.

Autocorrelation Coefficient:

The autocorrelation coefficients can be computed using equation 2.5,

$$\gamma(\Delta n) = \frac{A(\Delta n)}{A(0)} \quad (2.5)$$

Where,

$A(\Delta n)$ – Scaling factor given by equation 2.6,

$$A(\Delta n) = \frac{1}{N-\Delta n}\sum_{y=0}^{N-1-\Delta n} f(x,y).f(x,y+\Delta n) \quad (2.6)$$

Where,

n - number of pixels on a line.

N- number of sum terms.

x - coordinate of the line used in the computation

2.3 PSYCHO-VISUAL REDUNDANCY

Some information is given more importance than others in normal visual processing and this is how the human visual system does not respond with equal sensitivity to all exposed information. This ignored data is viewed as redundant psycho-visual data. By means of a quantization method, this redundancy is minimized, but as quantization itself is a lossy process, we cannot precisely reconstruct the original image. The method of exploring psycho-visual redundancy is therefore classified under lossy data compression techniques.

3. VARIOUS COMPRESSION TECHNIQUES

Several ways can be employed to compress the images which are further divided into two major categories or compression techniques.

3.1 LOSSY COMPRESSION

https://doi.org/10.17993/3ctecno.2022.v11n2e42.38-49

Here, some of the finer details in an image are compromised and an approximate representation of an input image is the resulting image. The psycho-visual capacities of human eyes should be restricted by this degradation. JPEG (Joint Photographic Experts Group), MPEG (Moving Photographic Experts Group) and MP3 (MPEG Audio Layer 3) are some of the algorithms for lossy image compression.

3.2 LOSSLESS COMPRESSION

The objective of this method is to reduce the compressed representation bit rate without any distortion in the input image signal. The entire set of values is the same as the input. PNG (Portable Network Graphics), TIFF (Tagged Image File Format) and JBIG (Joint Bi-level Image Experts Group) are some lossless picture compression algorithms.

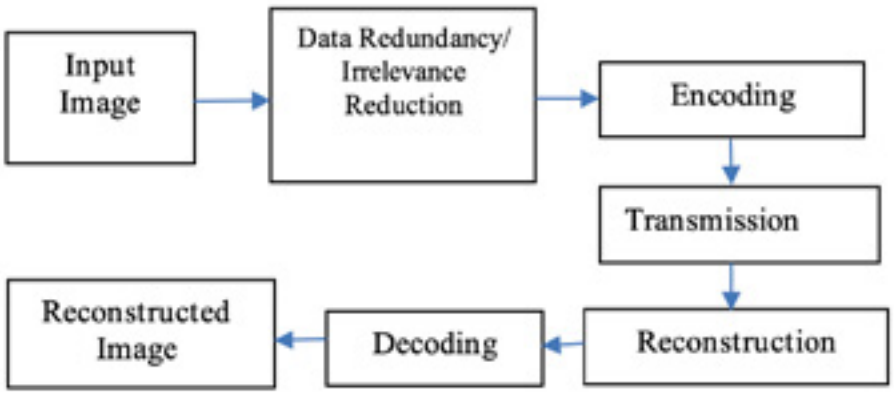

Fig. 1. Image compression model.

The modified representation of data compression is a kind of coding and therefore consists of two separate functional components; an encoder and a decoder, as shown in Fig. 1. The encoder encodes the data in a compressed form, while the decoder decodes it in a decompression form called the original form.

The image signal f (x, y) is used as input of the encoder. The encoder compresses the f (x, y) data to a g (r, c) compressed representation. This information may be stored locally or sent for a specific purpose to some remote location. This compressed representation is used as an input to the decoder whenever necessary, which decompresses this data to f'(x, y). If f (x, y) and f'(x, y) are identical, the compression process used is otherwise referred to as a lossless compression.

4. SEQUENTIAL CODING SCHEMES

The lossy compression technique is used in certain image processing applications involving large image sizes, high resolutions such as satellite images and video processing to achieve a good compression ratio (Vaidya, 2017). Lossless image compression is used in other applications where every data component is important, such as medical imaging and document images. We're going to discuss a few of the techniques for lossless image processing here.

https://doi.org/10.17993/3ctecno.2022.v11n2e42.38-49

4.1 RUN LENGTH CODING (RLE)

Run length coding is based on sequential pixel redundancy. The number of adjacent pixels with the same grey levels are counted here, which is called Run of that grey level and the grey level snippet / tuple {gi, ri} and its run count are formed to represent the whole image. Since the run value can vary from a minimum of 1 pixel to a maximum of m X n (total number of pixels in the image; m: number of rows, n: number of columns), this number will be very large and will require many bits to be represented. The highest size of a run is therefore considered to be multiple components in a row, i.e., n. It is obvious that in the images where the size of runs will be maximum, such kind of coding will be applicable. The kind of images suitable for RLE are graphs, plots, line works, facsimile data, icons, and basic animation images.

Some researchers also perform the RLE on bit planes of an image and perform two-dimensional (2D) RLE.

The image is processed row wise in 1-D RLE as pixel arrays, its grey levels are regarded as source symbols, and its runs are considered to be computed. But in 2-D, some characteristic pixel blocks are treated as source symbols, and for encoding, runs of those symbols are considered.

4.2 ENTROPY CODING

The good coding with entropy encoding results in the information in the message being represented in just enough bits. If an unlikely symbol appears rather than the appearance of a probable symbol, more information will be obtained. The entropy of information, or Entropy of Shannon, is given by equation 4.1.

$$I = p_i . log_2 \left(\frac{1}{p_i}\right) \quad (4.1)$$

Where,

p_i: Probability of occurrence of i^{th} symbol.

N: Number of symbols in a particular message/codebook.

The base2 of the logarithmic function gives an idea here that the symbol's occurrence is represented by means of 0 and 1.

Before encoding the image data using variable length codes that obtain no-prefix condition, the probabilities need to be known. So, these algorithms are generally two-pass and consume more time. Compression of data results from representing more likely symbols with shorter codewords and less likely symbols with longer codewords.

4.3 DICTIONARY-BASED ALGORITHMS

Symbol sub-strings are repeated in a file; these instances are recorded in a string table and referred to for encoding and decoding processes instead of repeating each time their position in the record. To prepare the dictionary, these string table techniques work on various approaches and LZW (Lempel-Ziv-Welch), LZ77 and LZ78 variants are created. In the data sequence, LZ77 uses a sliding window that generates a (position, length) tuple to point back to pre-existing substrings or symbols. LZ78 creates a string table dynamically and only replaces the substring in the message with the position index in the string table. Lossless coding systems are these coding schemes. Since some entries in the dictionary may not be referred to as frequently as others, the system is not optimal and the carrying of the dictionary in files is an overhead.

4.4 ARITHMETIC CODING

Arithmetic coding is a variable length coding scheme that performs better than Huffman coding with skewed probabilities for data with small alphabets (Langdon, 1984). Its implementation is a bit

https://doi.org/10.17993/3ctecno.2022.v11n2e42.38-49

complex, but it is possible to segregate the modelling and coding features of the compression technique. It has two forms, Adaptive Arithmetic Coding, which is a method of lossy coding, and Binary Arithmetic Coding, which is a technique of lossless coding. The real number line is split into smaller intervals corresponding to the probabilities of source symbols in this encoding. The first symbol that appears in the message then selects its corresponding interval, which is further divided into the same number of smaller proportional intervals. The successive symbol selects the corresponding interval from the message and this process of further splitting the smaller intervals continues until the last symbol in the message. This way the entire message is coded most efficiently according to the source symbol probability.

4.5 HUFFMAN CODING

Huffman code is a well-known technique that is efficiently suited to almost all file formats (Huffman, 1952). This probability-based, variable length, optimally coded non-prefix code is used in lossless compression. For more likely codes, this minimum redundancy code uses shorter codes and vice-versa. Using a code tree, the symbols are encoded; the codeword starts from the root node and traverses until the leaf node, where the encoded symbol is placed. The codes of leaf nodes that are closer to the root node are shorter in length and more likely to occur in the given message. If the number of symbols and their probabilities are very close, then the achieved compression ratio is less and far from the entropy of the source. In this case, it is possible to create symbol pairs / group of larger size and to codify these meta-symbols using their joint probabilities. This is a two-pass algorithm that works faster if probabilities are previously known, providing excellent average codeword length otherwise the two-pass procedure is followed. Faller and Gallapher have proposed one-pass adaptive Huffman codes and Knuth and Vitter have further developed them. If we want to code the $(i+1)^{th}$ symbol using earlier ith symbol statistics, the two binary tree parameter procedure is proposed and later developed as adaptive Huffman Code.

5. SCANNING OF DATA

An image is a function of space f (x, y) that is two-dimensional (2D). For sequential data, the coding schemes discussed in the following section are appropriate. To convert the 2D images to one-dimensional (1D) sequential data, a scanning process should be used. Local and global redundancies are represented in an image. In order to deal with the coherence and correlation of image pixels (Vemuri, 2014), local redundancies need to be more explored. The pixels in any direction may be related to each other. The schemes are sensitive to the direction of scanning of the image which is nothing but the direction of scanning the pixels of an image. Horizontal, vertical, and diagonal directions of scanning can be achieved by padding row-after row, column-after-column and pixel intensity scanning in a zig-zag manner.

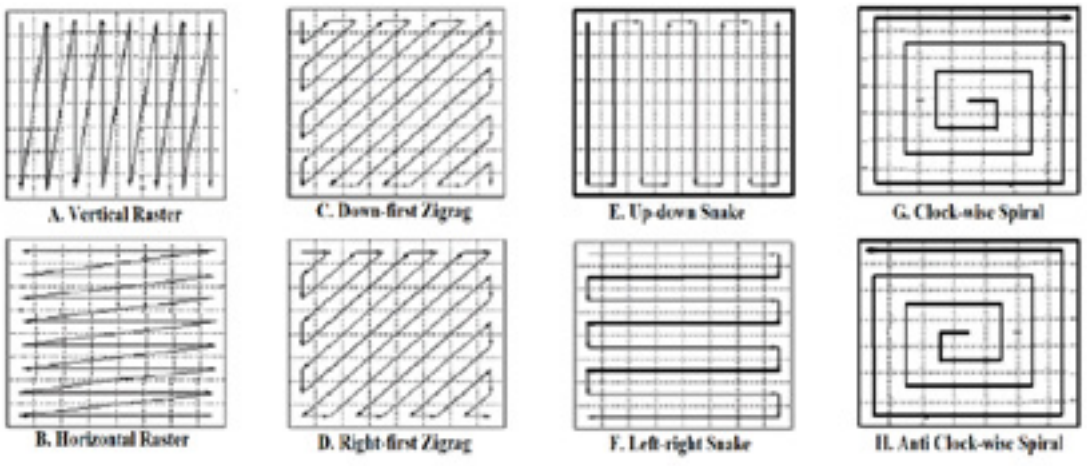

Fig. 2. Directions of Data Scanning.

https://doi.org/10.17993/3ctecno.2022.v11n2e42.38-49

In fig. 2 Directions of Data Scanning are shown, where A. is Vertical Raster direction, B. is Horizontal Raster direction, C. shows the Down-first Zigzag direction, D. shows the Right-first Zigzag direction, E. represents Up-down Snake, F. shows Left-right Snakes, G. is Clockwise Spiral, and H. is Antilock-wise Spiral. Which will be stored in a 1D vector representing image as well as suitable for below discussed coding schemes. Depending upon the nature of input image and the chosen direction of data scanning, variations may be observed in incident data redundancies. So, choosing this direction of scanning is a crucial task before feeding it to subsequent sequential compression algorithms mentioned in the next section.

In Table I, the effect of choosing different directions of data scanning on the interpixel redundancy is visible. Here, the preloaded image in Matlab 'cameraman.tif' is read, then its 2D intensity matrix is converted to 1D vector, by using mentioned data scanning methods one by one. Then the maximum, minimum Runs in the data, and number of resultant tuples are observed in each case. It may be seen that the Horizontal Scanning direction can be more suitable for this image over other methods as the Max. Run observed is longer and the number of tuples generated are less. Further it may be noted that there is certain variation in the compression ratios achieved by applying the Huffman's encoding over the results of RLE algorithm, applied over different vectors resulted from the different scanning directions. This variation ranges from -37.66% to 60.40%, that means the CR achieved can approximately double of one direction scanning to the other. This underlines the importance of data scanning direction applied.

Table I. Effect of choosing different Direction of Scanning.

Name of Image	Direction of Scanning	Max. RUN	No. of resultant Tuples	CR using Huffman's code	Percentage variation in CR
cameraman.tif	Vertical Raster	13	56112	0.2920	--
	Horizontal Raster	15	55387	0.3323	13.89
	Down-first Zigzag	9	57548	0.1820	-37.66
	Right-first Zigzag	9	57550	0.2952	1.10
	Up-down Snake	15	55385	0.4684	60.40
	Left-right Snake	14	56110	0.2761	-5.44
	Clockwise Spiral	15	56104	0.3128	7.13
	Anticlockwise Spiral	15	56114	0.2921	0.02

The distribution of Runs using the mentioned data scanning directions is also shown in the Fig. 3. below.

https://doi.org/10.17993/3ctecno.2022.v11n2e42.38-49

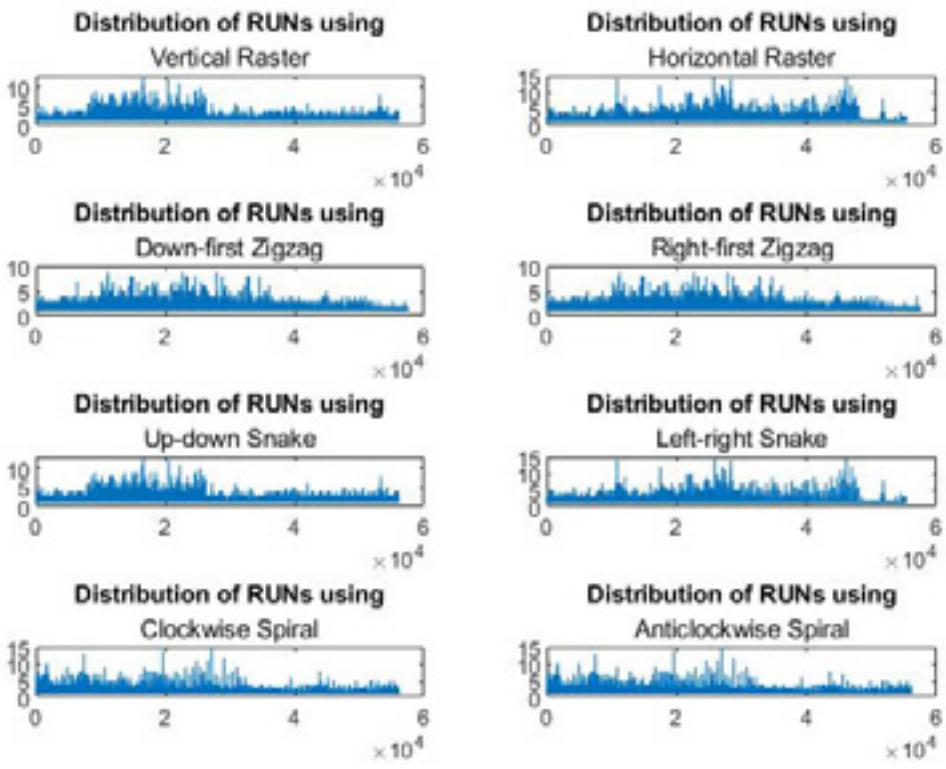

Fig 3. The distribution of Runs using various data scanning directions.

6. LENGTH OF THE RUN, NUMBER OF TUPLES AND CODABLE COMPRESSION ACHIEVED

Here inter-relation between Length of the Run and Number of Tuples generated in the compression procedures involving RLE is discussed. A situation where, when one thing increases, the other thing is supposed to decrease.

If the length of the Run achieved is higher, then the number of resulting Tuples will be less, and

If the length of the Run achieved is smaller, then the number of resulting Tuples will be more.

For achieving a good compression, the first situation should occur, that the maximum size Runs should be registered with smaller number of resultant Tuples. But, in this case, number of bits required to represent the Run count will grow in terms of 8-bits and the overall representation will require more data. On the other hand, if the Runs are smaller and they are representable in lesser number of bits, the number of Tuples generated will be high in number and to represent those greater number of Tuples again the data required will be more. So, to achieve good codable compression it is suggested that those parameters should be evaluated carefully. As there may not be any clear-cut range or threshold limits for length of Runs and the Tuple length. But a vague, imprecise boundary can be thought of which would separate the 'Good' length of Run and 'Average' number of Tuples from the results to achieve better codable compression. Considering this fuzzy nature of the variables it will be more significant if the methods of Fuzzy Composition are employed to form the Relation between them.

7. FUZZY COMPOSITION FOR FINDING THE RELATION BETWEEN VARIABLES

The experimentation is carried on 100 gray scale images of 256 X 256 size, involving 10 images each of 10 classes like Text, Person, Flower, Animal, Bird, Object, Vegetable, Pet, Graph and Diagram.

Table II. Result of choosing different direction of data scanning.

Sr. No.	Linearisation Direction	Min Run	Max Run	No. of Tuples

https://doi.org/10.17993/3ctecno.2022.v11n2e42.38-49

1	Vertical Raster	1	1780	36321
2	Horizontal Raster	1	2282	36767
3	Down-first Zigzag	1	1297	39681
4	Right-first Zigzag	1	1297	39681
5	Up-down Snake	1	1806	36251
6	Left-right Snake	1	2294	36702
7	Clockwise Spiral	1	922	36043
8	Anticlockwise Spiral	1	938	36040

The length of the Run and the number of Tuples for the mentioned eight different data scanning directions are calculated. The inter-relation between the length of the maximum Run and compression achieved, similarly the resultant number of Tuples and compression achieved are formed. Composition of fuzzy relations is used to find interaction of fuzzy variables across different fuzzy relations (Ross, 2010). So, compositions of these relations are computed to find the most suitable direction for data scanning. The composition operations studied here are max-min, min-max, and max-mean. The results of applying them is shown in Table III.

Table III. Suggested direction of data scanning, considering Fuzzy Compositions.

Sr. No.	Name of Class	Run Length			No. of Tuples			Suggested Data Scanning Direction
		Min-max	Max-min	Max-mean	Min-max	Max-min	Max-mean	
1	Text	1089	8260	11669	17994	5931	18222	L-R Snake
2	Person	42	15	51	59515	37489	59682	Both zigzag
3	Flower	1661	12	5215	57382	23755	57809	L-R Snake
4	Animal	2584	14	9937	62639	12925	61170	Both Spiral
5	Bird	212	11	326	50581	25577	53817	R F zigzag
6	Object	4704	12	10686	56746	27120	55686	U-D Snake
7	Vegetable	239	37	2780	62499	27242	57826	R F zigzag
8	Pet	70	21	83	56202	43821	57572	A Spiral
9	Graph	2764	246	5665	13003	4742	17477	U-D Snake
10	Diagram	1457	23	5272	54948	8186	52815	L-R Snake

7. RESULTS AND DISCUSSION

The experimentation on 100 gray level images comprising of 10 different classes is carried out. Depending upon this study the inter-relation between the maximum length of the Run and compression achieved is studied. Similarly, relation between resultant number of Tuples and compression achieved is also underlined. The fuzzy compositions have application in this type of scenarios, where the inter-relation between various experiment parameters is vague.

8. CONCLUSIONS

There is difference between the compressibility of the resultant data vector, i.e., 1D equivalent of 2D input image signal, if different data scanning directions are employed. Estimating the most suitable data scanning direction for a particular image in view of compression should result in higher compression ratio. The scanning directions suggested for a particular dataset in this study are very

https://doi.org/10.17993/3ctecno.2022.v11n2e42.38-49

specific about these datasets. Generally, a spiral direction should be suitable for the images having object at the center. The raster and snake scanning directions are suitable for document images. The Zigzag scanning directions are suitable for the images in which the information is scattered overspread.

REFERENCES

[1] D.A. Huffman, “A Method for the Construction of Minimum-Redundancy Codes.”, (1952), pp. 1098–1102.

[2] G. G. Langdon, “An Introduction to Arithmetic Coding.” IBM Journal of Research and Development”, (1984), 28(2): pp. 135–149.

[3] Holtz, Klaus. "The evolution of lossless data compression techniques" In Proceedings of WESCON'93, (1993), IEEE, pp. 140-145.

[4] M. Hosseini, "A survey of data compression algorithms and their applications", (2012), Network Systems Laboratory, School of Computing Science, Simon Fraser University, BC, Canada.

[5] M. Rehman, M. Sharif, M. Raza, “Image Compression: a survey”, (2014), Res. I. Appl. Sci. Eng. Technol. 7, pp. 656-672.

[6] M. V. Vaidya, Y. V. Joshi, and M. V. Bhalerao. "Marathi numeral identification system in Devanagari script using discrete cosine transform.", (2017), IJIES 10, no. 6.

[7] M. V. Vaidya, Y. V. Joshi. "Marathi numeral recognition using statistical distribution features.", (2015), International Conference on Information Processing (ICIP), pp. 586-591.

[8] M. V. Bhalerao, S. V. Bonde, A. V. Nandedkar, and S. D. Pilawan. "Combined classifier approach for offline handwritten Devanagari character recognition using multiple features.", (2018) In Computational Vision and Bio Inspired Computing, pp. 45-54. Springer, Cham.

[9] P. Kavitha, “A Survey on Lossless and Lossy Data Compression Methods”, (2016), 7: pp. 110-114, 2016.

[10] Vemuri, BABA C., S. Sahni, F. Chen, C. Kapoor, C. Leonard, and J. Fitzsimmons. "Lossless image compression.", (2014), Igarss 2014 45, no. 1, pp: 78-86.

[11] R. C. Gonzalez and R. E. Woods, "Digital Image Processing", (2004), 2nd edition, Prentice Hall.

[12] T. J. Ross, “Fuzzy Logic with Engineering Applications”, (2010), 3rd edition, John Wiley and Sons.

https://doi.org/10.17993/3ctecno.2022.v11n2e42.38-49

/04/

DEEP LEARNING BASED MISSING OBJECT DETECTION AND PERSON IDENTIFICATION AND APPLICATION FOR SMART CCTV

R. C. Dharmik
Assistant Professor, Department of Information Technology Yeshwantrao Chavan College of Engineering, Nagpur, Maharashtra, (India).

Sushilkumar Chavhan
Assistant Professor, Department of Information Technology Yeshwantrao Chavan College of Engineering, Nagpur, Maharashtra, (India).

S. R. Sathe
Professor, Department of CSE, VNIT Nagpur, (India).

Reception: 10/09/2022 **Acceptance**: 25/09/2022 **Publication**: 29/12/2022

Suggested citation:

Dharmik, R. C., Chavhan, S., y Sathe, S. R. (2022). Deep learning based missing object detection and person identification: an application for smart CCTV. *3C Tecnología. Glosas de innovación aplicadas a la pyme, 11*(2), 51-57. https://doi.org/10.17993/3ctecno.2022.v11n2e42.51-57

ABSTRACT

Security and protection are the most crucial concerns in today's quickly developing world. Deep Learning methods and computer vision assist in resolving both problems. One of the computer vision subtasks that allows us to recognise things is object detection. Videos are a source that is taken into account for detection, and image processing technology helps to increase the effectiveness of state-of-the-art techniques. With all of these technologies, CCTV is recognised as a key element. Using a deep convolutional neural network, we accept CCTV data in real time in this article. The main objective is to make content the centre of things. Using the YOLO technique, we were able to detect the missing item with an improvement of 10% sparsity over the current state-of-the-art algorithm in the context of surveillance systems, where object detection is a crucial step. It can be utilised to take immediate additional action.

KEYWORDS

Deep Learning, Object Detection, Computer vision

https://doi.org/10.17993/3ctecno.2022.v11n2e42.51-57

1. INTRODUCTION

The method of object detection involves comprehending the entire image, concentrating on proper categorization while focusing on the item in the image. This process is a subtask of computer vision, which also covers face detection and skeleton identification by Zhao, Zheng, Xu, and Wu (2019) ,Felzenszwalb, Girshick, Mcallester, and Ramanan (2010),Sung and Poggio (1998),Doll´ar, Wojek, Schiele, and Perona (2011)and Sampat and Bovik (2003). The development of computational models that offer the most fundamental data required by computer vision applications is the aim of object detection. An industrial revolution changes the face of the computer vision task where identification, surveillance, medical, robotics, self-driving cars can be part of it. In recent era advancement in deep leaning accelerated the object detection task. A specific form of machine learning called ”deep learning” (DL) uses neural networks to learn in phases. It can therefore mimic human thought. Video analytics is closely related with the deep learning which provides application in different fields. Traditional Object detection is complex in complexity and low level features are also leads to saturation to increased complexities (Zhao et al., 2019).

Image classification and detection are the steps for the detection of object for surveillance. Primary task for both the operation to receive the relevant features. Deep Learning is the better solution for it. It learns from previous stages and extracts new features. Deep Network may conventio al neural network or Multilayer Perceptron networks which consist of activation functions and various hidden layers. Image is extracted from the video with fixed size as neural network required for model (Sung and Poggio, 1998). If fully integrated networks are necessary. However, size reduction results in information loss inside the image, reducing accuracy, precision, and sparsity as well as applicability for surveillance system (Zhao et al., 2019). Viola-Jones Detector (Viola and Jones, 2001) and HOG Detector (Dalal and Triggs, 2005) are two examples of conventional object detection algorithms. One-stage and two-stage algorithms based on deep learning are the two main categories. The two-stage algorithms RCNN and SPPNet(Girshick, Donahue, Darrell, and Malik, 2013),(Liu, Anguelov, Erhan, Szegedy, Reed, Fu, and Berg, 2016), Fast RCNN and Faster RCNN(He, Zhang, Ren, and Sun, 2014), Mask R–CNN, Pyramid Networks/FPN(Girshick, 2015), and G–RCNN(Ren, He, Girshick, and Sun, 2015) propose object region utilising deep feature before classification. Without the region suggestion, one-stage algorithms like YOLO (Redmon, Divvala, Girshick, and Farhadi, 2016), SSD (Liu et al., 2016), RetinaNet (Girshick, 2015), YOLOv3, YOLOv4, etc. anticipate bounding boxes over the pictures.

In this paper we created application using CCTV will be helpful to understand whether any object is stolen from the area (room, cabin, etc.) and recognition of the person, thus helping to form the better security infrastructure. This system can be used at official workspaces where there is a crucial need for more secure surveillance than earlier. Analyses frames and find stolen objects by using structural similarities. A deep learning-based object recognition system coupled with YOLO for remote surveillance that can accurately and quickly identify the target inside video frames has been suggested. proposed system has the ability to send data to a localised remote server after automatically detecting a person or item. To detect and transmit the information, a thin coating of YOLO was utilised. We applied filters to the data to keep it clean.

2. LITERATURE REVIEW

Viola and Jones (2001) proposed a machine Learning based object detection which is populary know as Viola-Jones Detector where they calculate new feature, learn by using AdaBoost and able to clasify more complex features. Dalal and Triggs (2005) proposed HOG (Histograms of Oriented Gradient) object detection algorithm which uses dense overlapping grid gives which provides betteer results for person identification, reducing false positive rates with resppect to Haar wavelet based detector. Forsyth (2014) Exnded the above work and proposed the DPM model for object Detection. They

https://doi.org/10.17993/3ctecno.2022.v11n2e42.51-57

modify the SVM algorithm of data mining for the purpose object detection. It uses divide and conqure technology with the root filter and various part filters which make it Multi instance Leaning algorithm. All above traditional methods have far surpassed many algorithm in term of accuracy.

Girshick et al. (2013) proposed RCNN object detection algorithm with mean average precision. As local Search combine with CNN it said to be RCNN. They Combine the CV and Deep Learning for better results as comparre to traditional Methods. He et al. (2014) proposed SPPNet model for object detection. It Detect the object by variriyng the image size. For that they changes the image size as most of object detection algorithms are used the strandard size of 255*255.Girshick (2015) proposed Fast RCNN detector, advanced verison of R-CNN and SPPNet. They suggested Dense boxex and and Parse preposal to acceleate process as it is costly process.

Ren et al. (2015) proposed Faster RCNN detector and target is too reduce the time of RCNN. Which is mostly presented as RPN as it uses more deep learning network.Redmon et al. (2016) proposed Feature Selection framewok inside convonet popurarly know as FPN (Feature Pyramid Network) which is based on Faster RCNN with framework. They suggest multi scale problems with deep learning. Redmon et al. (2016) proposed most popolar and widely used algoritrhm you only looks one (YOLO) one stage detector using deep learning. Insteed of consideration of whole image, it convert image in to region and simulteniously predict the bounding boxes and probability of each region. Also they train the loss function which helps model to detect the images. Further they improved to YOLOv3, YOLOv4.

3. METHODOLOGY

By observing the various literature, we apply the CNN with two layer architecture and different activation function and Filter. Identified Process is as follows.

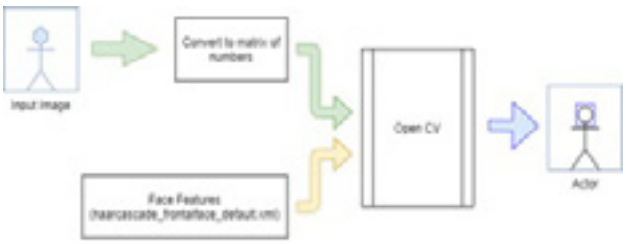

Fig 1: Feature Selection.

https://doi.org/10.17993/3ctecno.2022.v11n2e42.51-57

Fig 2: Flow of Process.

In this process we used real time data capture from CCTV and camera. The images which received which are filter using LBPS parameters. This helps process simpler. Then 2 layer deep neural network with Relu activation functions.

4. RESULTS

Step1: Collection of images: We accept the images from CTTV camera and then we create the slices as shown in bellow figure. Which store in specific folder with less size.

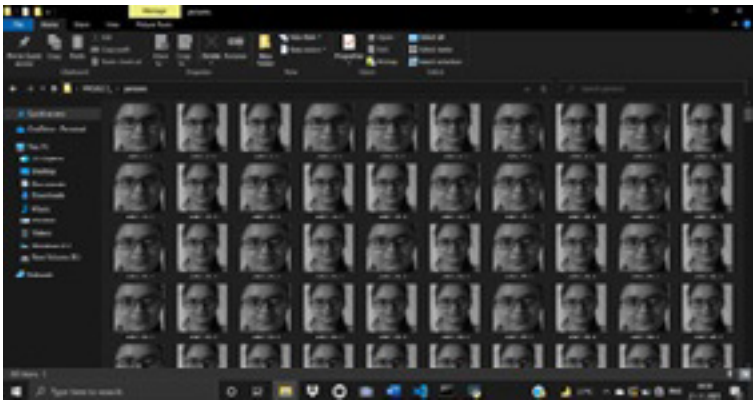

Fig 3: Extraction of images of one frame.

Step2: Extraction of features using specific one layer deep neural Network. The Features are selected as core point of the real time flowing image.

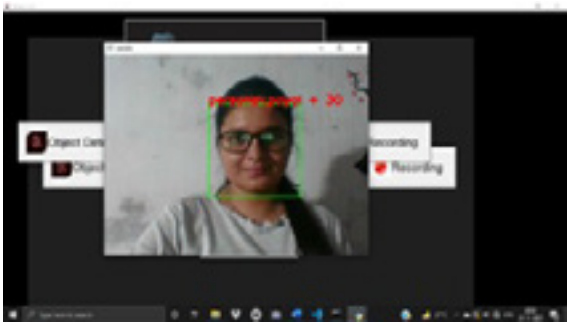

https://doi.org/10.17993/3ctecno.2022.v11n2e42.51-57

Fig 4: Feature Selection

Step3: identification of images using second deep layer where we can identified the images. Following figure demonstrate the detection of images.

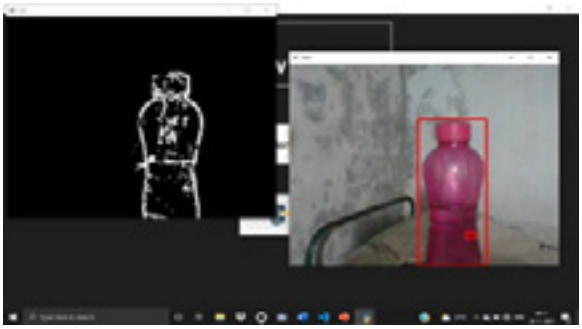

Fig 5: Detection of images.

5. DISCUSSION

The System Developed is shown below:

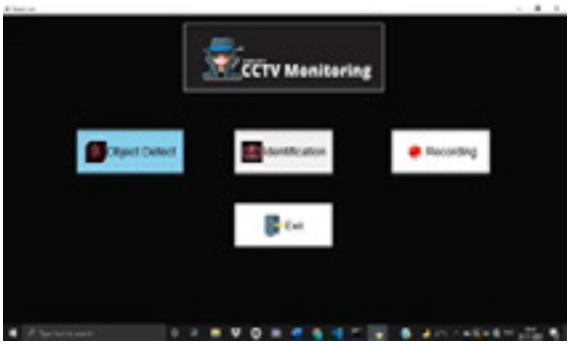

Fig 6: System GUI.

It is application which having Portable CCTV with some in-built night vision capability. In That by using CNN we adding deep learning if having high power device. It consist of feature such as Deadly weapon detection, Accident detection,Fire Detection,much more.. Working of standalone device. As shown in following figure

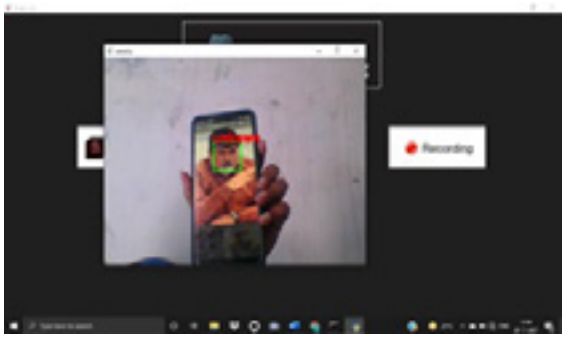

Fig 7: Object Detection.

6. CONCLUSION AND FUTURE SCOPE

In this paper we used two layer deep networks for the object Detection. Using architecture we are able to chive accuracy up to 90%. CNN level are provided the features which helps to make the fast detection of object. In This study it is observed that reduction of image sizes helps to train the networks more faster and deep network can also provide the essentials features. As we implement this

https://doi.org/10.17993/3ctecno.2022.v11n2e42.51-57

study for security purposed we able to detect object and provide suitable alarm messages.as a Future scope we can used high end camera and test the accuracy and speed.

REFERENCES

[1] Dalal, N. and Triggs, B. 2005. Histograms of oriented gradients for human detection. Comput. Vision Pattern Recognit. 1, 886–893.

[2] DollaÅLr, P., Wojek, C., Schiele, B., and Perona, P. 2011. Pedestrian detection: An evaluation of the state of the art. IEEE transactions on pattern analysis and machine intelligence 34, 743–61.

[3] Felzenszwalb, P., Girshick, R., Mcallester, D., and Ramanan, D. 2010. Object detection with discriminatively trained part-based models. IEEE transactions on pattern análisis and machine intelligence 32, 1627–45.

[4] Forsyth, D. 2014. Object detection with discriminatively trained part-based models. Computer 47, 6–7.

[5] Girshick, R. 2015. Fast r-cnn.

[6] Girshick, R., Donahue, J., Darrell, T., and Malik, J. 2013. Rich feature hierarchies for accurate object detection and semantic segmentation. Proceedings of the IEEE Computer Society Conference on Computer Vision and Pattern Recognition.

[7] He, K., Zhang, X., Ren, S., and Sun, J. 2014. Spatial pyramid pooling in deep convolutional networks for visual recognition. IEEE Transactions on Pattern Analysis and Machine Intelligence 37.

[8] Liu, W., Anguelov, D., Erhan, D., Szegedy, C., Reed, S., Fu, C.-Y., and Berg, A. 2016. Ssd: Single shot multibox detector. Vol. 9905. 21–37.

[9] Redmon, J., Divvala, S., Girshick, R., and Farhadi, A. 2016. You only look once: Unified, real-time object detection. 779–788.

[10] Ren, S., He, K., Girshick, R., and Sun, J. 2015. Faster r-cnn: Towards real-time object detection with region proposal networks. IEEE Transactions on Pattern Analysis and Machine Intelligence 39.

[11] Sampat, M. and Bovik, A. 2003. Detection of spiculated lesions in mammograms. Annual International Conference of the IEEE Engineering in Medicine and Biology - Proceedings 1.

[12] Sung, K. and Poggio, T. 1998. Example based learning for view-based human face detection. Pattern Analysis and Machine Intelligence, IEEE Transactions on 20, 39 – 51.

[13] Viola, P. and Jones, M. 2001. Rapid object detection using a boosted cascade of simple features. IEEE Conf Comput Vis Pattern Recognit 1, I–511.

[14] Zhao, Z.-Q., Zheng, P., Xu, S.-T., and Wu, X. 2019. Object detection with deep learning: A review. IEEE Transactions on Neural Networks and Learning Systems PP, 1–21.

https://doi.org/10.17993/3ctecno.2022.v11n2e42.51-57

/05/

IMPLEMENTATION OF ENSEMBLE METHOD ON DNA DATA USING VARIOUS CROSS VALIDATION TECHNIQUES

B. U. Bawankar
G.H. Raisoni University, Amaravati, India, (India).

Kotadi Chinnaiah
G.H. Raisoni University, Amaravati, India, (India).

Reception: 10/09/2022 **Acceptance**: 25/09/2022 **Publication**: 29/12/2022

Suggested citation:

Bawankar, B. U., y Chinnaiah, K. (2022). Implementation of ensemble method on DNA data using various cross validation techniques. *3C Tecnología. Glosas de innovación aplicadas a la pyme, 11*(2), 59-69. https://doi.org/10.17993/3ctecno.2022.v11n2e42.59-69

ABSTRACT

Due to the growing size of datasets, which contain hundreds or thousands of features, feature selection has drawn the interest of many scholars in recent years. Usually, not all columns show important values. As a result, the machine learning models may perform poorly since the noise or unnecessary columns may confound the algorithms. To address this issue, various feature selection methods have been developed to evaluate large dimensional datasets and identify their subsets of pertinent features. The data, however, frequently skews feature selection algorithms. As a result, ensemble approaches have emerged as a substitute that incorporates the benefits of single feature selection algorithms and makes up for their drawbacks. In order to handle feature selection on datasets with large dimensionality, this research aims to grasp the key ideas and links in the process of aggregating feature selection methods. The suggested idea is tested by creating a cross-validation implementation that combines a number of Python packages with functionality to enable the feature selection techniques. By identifying pertinent features in the human, chimpanzee, and dog DNA datasets, the performance of the implementation was demonstrated.

KEYWORDS

Cross-validation, Ensemble methods, Feature selection.

https://doi.org/10.17993/3ctecno.2022.v11n2e42.59-69

1. INTRODUCTION

In recent years, datasets with a lot of attributes have become more common in several fields. Microarray categorization serves as the best illustration. Numerous datasets containing this type of data have been produced as a result of improvements in DNA microarray. The majority of these datasets show that the ratio of instances to features, which range from 6 to 60 genes, is not greater than this. However, most of the genes in these datasets do not represent helpful information to support a machine learning process. In order to efficiently classify microarray data, a pre-processing stage is therefore required. This article will explain how to do so by choosing a representative subset of genes from the original set of genes(Mera-Gaona, LÅLopez, Vargas-Canas, and Neumann, 2021)[16]. The individual success of the ensemble's basis learners
and the independence of the base learners' results due to low error and great diversity are the two major factors that determine how well an ensemble performs. By utilising foundation learners of the same or different types, diverse base learners can be built. When using the same type of base learners, diversity is produced by giving each base learner in the ensemble a different training set. Different training data sets can be created using a variety of techniques, including bagging, boosting, random subspaces, random forests, and rotation forests. In order to créate a superior composite global model with more precise and trustworthy estimates or conclusions than can be produced by utilising a single model, an ensemble methodology combines a group of models, each of which addresses the same original problem. The fact that different classifier types have distinct inductive biases is one of the key reasons why ensemble methods are so successful (Gopika1 and Azhagusundari, 2014)[9]. Finding ways to enhance feature selection on datasets with high dimensionality and few examples is the major goal of this work. Additionally, cross validation is used in the display of ensemble methods to combine the benefits of several feature selection algorithms, avoid their biases, and make up for their shortcomings (Mera-Gaona et al., 2021)[16].

2. ENSEMBLE METHODS

The Ensemble categorization is founded on the idea that several experts can provide more accurate judgments than a single expert. A single composite model with higher accuracy is produced through ensemble modelling, which combines the collection of classifiers. According to research, predictions from a composite model provide better outcomes than predictions from a single model. Since the previous few decades, ensemble technique research has gained popularity. The outputs of many classifiers are combined, which minimises generalisation error, according to a number of experimental tests carried out by machine learning experts. The ensemble approaches are described in this section (Pandey and Taruna, 2014)[10-11].

(1) Bagging

The bagging technique is used to reduce variance, and the bagging ensemble method's goal is to divide the dataset into several subsets for training that are randomly chosen with replacement(Singh and Pal, 2020) [10]. The Bootstrap sampling approach provides the basis for bagging. A distinct set of bootstrap samples is produced for each iteration of the procedure in order to build a unique classifier. During the sample phase of the bootstrap sampling approach, data items are chosen at random with replacement, meaning that some instances may be repeated or some may be omitted from the original dataset. Combining all of the classifiers built in the previous phase is the next stage in the bagging process. To arrive at a final prediction, bagging combines the output of the classifiers with input from the voting process a12[11-12].

(2) Boosting

Another crucial ensemble method is the boosting classifier. It is used to develop a collection of classifiers. By fitting classifiers to data and then assessing mistakes, classifiers are serially trained in the boosting approach (Singh and Pal, 2020) [10]. The weak classifier's performance is improved by boosting to a strong level. With the help of reweighting the data instances, it creates sequential learning classifiers. All the instances are given initial weights that are equal and

https://doi.org/10.17993/3ctecno.2022.v11n2e42.59-69

consistent. Each time a learning phase is completed, a new hypothesis is taught, and the examples are reweighted such that instances that were properly identified during that pase have a lower weight and the system may focus on instances that weren't. Instances that were incorrectly categorised are chosen so they can be correctly categorised in the following learning stage. This procedure keeps on till the final classifier is built. To arrive at the final forecast, the output of each classifier is finally merged using majority voting. The Boosting method has been generalised in AdaBoost(Breiman,)[12].

(3) Random Subspaces

The approach comes in two different types. Each base learner is taught using a distinct feature subspace of the initial training data set at the first form. Only decision trees may be utilised as the base learner at the second form (Gopika1 and Azhagusundari, 2014)[9].

(4) Random Forest

Breiman proposed Random Forest. Bagging plus the second kind of random subspaces can be used to formulate it (Breiman) [12]. The bagging and random subspace methods are combined to induce the tree. Although each model is a random tree rather than a single model, it differs from bagging in that each tree is created in accordance with the bootstrap sample of the training set to N. Each node is divided using yet another random step. Instead of examining all potential splits, a limited subset of features is randomly picked, and the optimum split is determined from this subset. Across all trees, the majority vote determines the final categorization [11].

(5) Rotation Forest

Rotation Forest is a brand-new ensemble approach built on the Principal Component Analysis (PCA) and decision trees. To create a training set for the base classifier using a K axis rotation of the feature subset, the attribute set F is randomly divided into K subgroups, and PCA is then performed separately to each subset. By keeping all of the PCA, Rotation Forest maintains all of the information. The basis classifier for Rotation Forest is the decisión tree(Pandey and Taruna, 2014) [11].

3. CROSS VALIDATION TECHNIQUES

A statistical technique called cross-validation determines how well a trained model will perform on unobserved data. By training the model on a subset of the input data and testing it on a different subset, the model's effectiveness is confirmed. Building a generalised model is assisted by cross-validation. Cross-validation is helpful for both performance estimate and model selection since modelling is an iterative process.

Cross-validation involves the following three steps:

i. Split the dataset into two sections: a training section and a testing section.
ii. Use the training dataset to train the model.
iii. Use the testing set to gauge the model's effectiveness. Check for problems if the model doesn't perform well with the testing set.

If a model can predict accurately for a variety of input data and does well on unknown data, it is stable and consistent. Evaluation of the stability of machine learning models is aided by crossvalidation.

The dataset has to be divided into three separate sections for training and testing the model:

- Training Data: Using the training data, the model is trained to discover the dataset's hidden characteristics and patterns. The model continually assesses the data to better understand its behaviour, and then it modifies itself to achieve its goal. Basically, it's employed to fit the models.
- Validation Data: This is used to confirm that the model's training results were accurate. It aids in adjusting the hyper-parameters and settings of the model appropriately. The prediction error for model selection is estimated using the validation data. Validation data helps prevent over-fitting models.
- Test Data: Following training, the test data confirms that the trained model is capable of making precise predictions. It is used to evaluate the generalisation error of the last model chosen (Hulu and Sihombing, 2020)[1](Jung and A K-Fold, 2015)[7][8](Wu,)[13-14](??,).

https://doi.org/10.17993/3ctecno.2022.v11n2e42.59-69

This paper discusses eight alternative cross-validation approaches, each with advantages and disadvantages that are stated below

(1) Leave p out cross-validation

An exhaustive cross-validation strategy called leave p-out cross-validation uses the p-observation as validation data while utilising the remaining data to train the model. This is repeated in all possible ways on a validation set of p observations and a training set to trim the original sample. In order to estimate the area under the ROC curve of a binary classifier in a virtually unbiased manner, leave-pair-out cross-validation, a variation of Leave p-out with p=2, has been suggested (Kumar, 2020)[14].

(2) Leave one out cross-validation

A thorough cross-validation method is leave-one-out cross-validation. It falls within the leave p-out cross validation category with the instance of p=1. The first row of a dataset of n rows is chosen for validation, and the remaining n-1 rows are utilised to train the model. The second row is chosen for validation and the remainder is used to train the model for the following iteration. Similar to that, the procedure is repeated up to n operations or phases. Cross-validation techniques i.e. leave p-out and leave One-out that learn and test in every conceivable way are known as exhaustive cross-validation techniques. They share the advantages such as straightforward, understandable, and simple to use and disadvantages such as the model might provide a little bias and a lot of computing time is needed[13-14].

(3) Holdout cross-validation

The dataset is randomly divided into training and validation data in holdout cross-validation. In general, training data are split more evenly than test data. The model is created using training data, and validation data is used to assess the model's effectiveness. The model becomes better as more data are used to train it. The holdout cross-validation approach isolates training data from a sizable amount of data. The advantages for this such as straightforward, understandable, and simple to use and disadvantages such as it's not suitable for an unbalanced dataset and a lot of data is not being used to train the model (Raschka, 2020)[5].

(4) Repeated random sub-sampling validation

The dataset is randomly divided into training and validation in repeated random subsampling validation, commonly known as Monte Carlo cross-validation. Unlikely k-fold cross-validation separates the dataset into random splits rather than groups or folds in this. Analysis determines the number of iterations; it is not a set quantity. The outcomes are then multiplied by the divides. Advantage for such validation is i.e. there is no relation exists between the number of iterations or divisions and the fraction of train and validation splits and the disadvantages such as possible that some samples won't be used for either training or validation and not appropriate for a dataset with imbalance [5][14].

(5) k-fold cross-validation

The original dataset is evenly divided into k subparts or folds for k-fold cross-validation. For each iteration, one of the k-folds or groups is chosen as the validation data, while the remaining (k-1) groups are chosen as the training data. Until each group is considered as validation and the rest as training data, the procedure is repeated k times. The mean accuracy of the kmodels validation data is used to calculate the model's final accuracy. The model exhibits little bias, low temporal complexity and both training and validation use the complete dataset is the advantages and the disadvantage is unsuitable for a dataset with imbalance[1-7](Hulu and Sihombing, 2020) (Darapureddy, Karatapu, and Tirumala, 2019)(PAYAM REFAEILZADEH, 2008)(Arumugam, Professor, Department of Statistics, Manonmaniam Sundaranar University, Tirunelveli (Tamil Nadu), India., Kadhirveni, Priya, Manimannan, Research Scholar, Department of Statistics, Manonmaniam Sundaranar University, Tirunelveli (Tamil Nadu), India., Assistant Professor, Department of Statistics, Dr. Ambedkar Government Arts College, Vyasarpadi, Chennai (Tamil Nadu), India., and Assistant Professor. Department of Statistics, TMG College of Arts and Science, Chennai (Tamil Nadu), India., 2021)(Raschka, 2020)(Raschka, 2020).

(6) Stratified k-fold cross-validation

https://doi.org/10.17993/3ctecno.2022.v11n2e42.59-69

All the cross-validation methods mentioned above might not be effective with an unbalanced dataset. Unbalanced dataset issue was resolved by stratified k-fold cross-validation. The dataset is divided into k groups or folds in stratified k-fold cross-validation such that the validation data has an equal number of instances of the target class label. This makes sure that, especially when the dataset is unbalanced, one specific class is not overrepresented in the validation or train data. The average of the scores for each fold is used to get the final score. As a benefit, it performs well for an unbalanced dataset (PAYAM REFAEILZADEH, 2008)[3][14].

(7) Time Series cross-validation

When dealing with problems involving time series, the data's order is crucial. Data divided randomly or in k-folds into train and validation for time-related datasets might not produce the best results. The forward chaining method, also known as rolling cross-validation, is used to divide the time-series dataset's data into train and validation groups. The subsequent instance of train data can be used as validation data for a certain iteration(a13,)[13].

(8) Nested cross-validation

We obtain a subpar estimate of the error in training and test data while using k-fold and stratified k-fold cross-validation. In the prior techniques, hyper-parameter adjustment is done individually. Nested cross-validation is necessary when cross-validation is used to tune the hyper-parameters and generalise the error estimate at the same time. Both the stratified k-fold and k-fold variations can use nested cross validation [14].

4. BASIC PROCESS OF MACHINE LEARNING

The field of machine learning blends traditional statistical methods with computer science techniques. In order to extract knowledge from massive volumes of data for application in science, computing, or industry. We thoroughly discuss the machine-learning process from six angles [2](Darapureddy et al., 2019).

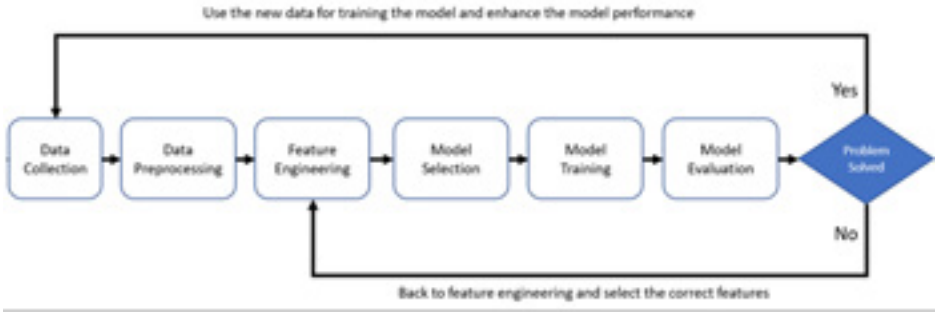

Fig. 1: Basic Process.
Source: datavalley.

1. Data Collection: Gather all the information you need from the many systems that might contribute to your situation.
2. Data Pre-processing: Prior to processing and analysis, raw data must be cleaned and transformed. Prior to processing, it is a crucial phase that frequently entails reformatting data, making adjustments to data, and fusing data sets to enhance data.- Data Cleaning: The initial phase in data mining consists of removing incomplete or inconsistent data since data sets frequently contain missing data and inconsistent data. Low data quality will have a significant negative influence on the information extraction process.- Data Integration: If the data to be examined come from many sources, they must be reliably aggregated.
3. Feature Engineering: This covers all modifications made to the data, from cleaning it up to ingesting it into the machine learning model. You choose and prepare the features that will be used in your machine learning model in this stage, making sure they are in the format required by the model.
4. Selection of Model: Choose the best model for the situation and then make any necessary adjustments.

https://doi.org/10.17993/3ctecno.2022.v11n2e42.59-69

5. Train the Model: A machine learning (ML) model is trained by feeding training data to the learning algorithm. The model artefact produced during training is referred recognised as a ” ML model.”
6. Evaluate the Model: This methodical technique will serve as a guide for evaluating the efficacy and efficiency of training.

5. RESULTS AND DISCUSSIONS

Data Selection: We provide three sorts of data sets i.e. human, chimpanzee and dog DNA for insights which represent DNA sequences that contain seven gene classes. Representation of gene family with seven gene classes and class label as G-protein coupled receptors(0), tyrosine kinase(1), tyrosine phosphate(2), synthetase(3), synthase(4), ion channel(5) and transcription factor(6). Data Processing: The dataset is processed and check how many DNA sequences in each class with class distribution graph by using tools VS code and streamlit through python.

```
#read dataset files and put it in dataframes



def setdna(data):
    human_dna = data
    #lets descripe one dna sequence of human
    import numpy as np
    one_dna = np.array(human_dna)
    one_dna = str(one_dna).split(' ')
    seq = one_dna[0].replace("[['",'')
    seq = seq.replace("'",'')

    #display how many DNA sequences in each class?
    st.write()
    st.write()
    st.write("Class distribution graph:")
    st.bar_chart(human_dna['class'].value_counts())
```

Fig 2: Python code for DNA sequence.

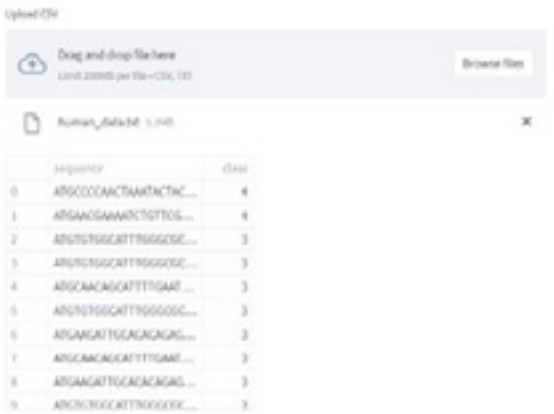

Fig 3 DNA Sequence with class.

https://doi.org/10.17993/3ctecno.2022.v11n2e42.59-69

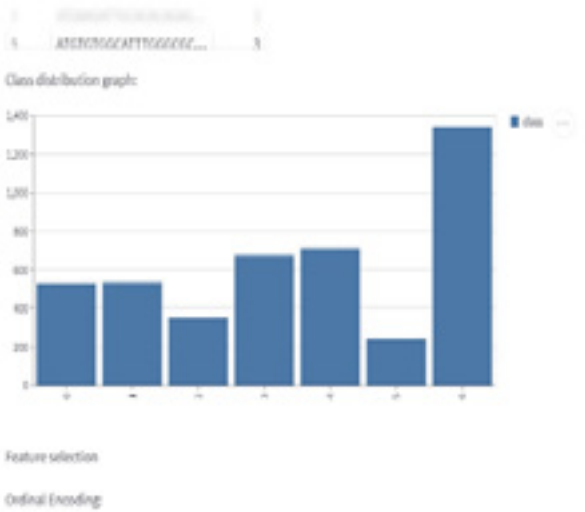

Fig 4 Class distribution graph.

Feature Selection: Although the DNA sequence in a show is represented by characters, machine learning algorithms need numerical values or feature matrices. In order to convert these characters into values, we use three general approaches such as ordinal encoding, one hot encoding and kmers counting. Ordinal Encoding: With this method, each nitrogen base must be encoded as an ordinal value. ”A, T, G, and C,” for instance, becomes [0.25, 0.5, 0.75, and 1.0]. Any additional base, like ”Z,” may be a 0.

```
from sklearn import preprocessing
def ordinal_encoder(my_array):
    label_encoder = preprocessing.LabelEncoder()
    label_encoder.fit(np.array(['a','c','g','t','z']))
    integer_encoded = label_encoder.transform(my_array)
    #print(integer_encoded)
    float_encoded = integer_encoded.astype(float)
    float_encoded[float_encoded == 0] = 0.25 # A
    float_encoded[float_encoded == 1] = 0.50 # C
    float_encoded[float_encoded == 2] = 0.75 # G
    float_encoded[float_encoded == 3] = 1.00 # T
    float_encoded[float_encoded == 4] = 0.00 # anything else, lets say z
    return float_encoded


#Let's try it out a simple short sequence:
seq_test = 'attcgxffgtg'
ord = ordinal_encoder(string_to_array(seq))
```

Fig 5 Python Code for ordinal encoding.

Feature selection

Ordinal Encoding:

	0
0	0.2500
1	1.0000
2	0.7500
3	0.5000
4	0.5000
5	0.5000
6	0.5000
7	0.2500
8	0.2500
9	0.5000

Fig 6 Feature Selection through ordinal encoding.

https://doi.org/10.17993/3ctecno.2022.v11n2e42.59-69

One-hot Encoding: “A,C,G,T,Z” would become [1,0,0,0,0], [0,1,0,0,0], [0,0,1,0,0], [0,0,0,1,0], [0,0,0,0,1], and these one-hot encoded vectors can either be concatenated or turned into 2- dimensional arrays.

```
    def one_hot_encoder(seq_string):
        label_encoder = preprocessing.LabelEncoder()
        label_encoder.fit(np.array(['a','c','g','t','z']))
        int_encoded = label_encoder.transform(seq_string)
        onehot_encoder = preprocessing.OneHotEncoder(sparse=False, dtype=int)
        int_encoded = int_encoded.reshape(len(int_encoded), 1)
        onehot_encoded = onehot_encoder.fit_transform(int_encoded)
        return onehot_encoded
#So let's try it out with a simple short sequence:
    seq_test = 'attcgxffgtg'
    ohe = one_hot_encoder(string_to_array(seq))
```

Fig 7 Python code for One-hot encoder.

One-Hot Encoding:

	0	1	2	3	4
0	1	0	0	0	0
1	0	0	0	1	0
2	0	0	1	0	0
3	0	1	0	0	0
4	0	1	0	0	0
5	0	1	0	0	0
6	0	1	0	0	0
7	1	0	0	0	0
8	1	0	0	0	0
9	0	1	0	0	0

Fig 8 Feature Selection through One-hot encoding.

K-mers counting: The approach we take here is simple and manageable. We first divide the lengthy biological sequence into overlapping k-mer length ”words”. If we use ”words” of length 6 (hexamers), for instance, ”ATGCATGCA” becomes ”ATGCAT,” ”TGCATG,” ”GCATGC,” and ”CATGCA.” In light of this, our example sequence is divided into 6 hexamer words.

```
    def Kmers_funct(seq, size=6):
        return [seq[x:x+size].lower() for x in range(len(seq) - size + 1)]


#So let's try it out with a simple sequence:
    mySeq = 'GTGCCCAGGTTCAGTGAGTGACACAGGCAG'
    #size of each sub-seq = 6
    words = Kmers_funct(seq, size=6)
    print(words)

    joined_sentence = ' '.join(words)
    joined_sentence

##
    #apply kmers function to all datasets & join all words to list
#then add words column & drop sequence column
    human_dna['words'] = human_dna.apply(lambda x: Kmers_funct(x['sequence']), axis=1)
    human_dna = human_dna.drop('sequence', axis=1)
```

Fig 9 Python code for K-mers counting.

https://doi.org/10.17993/3ctecno.2022.v11n2e42.59-69

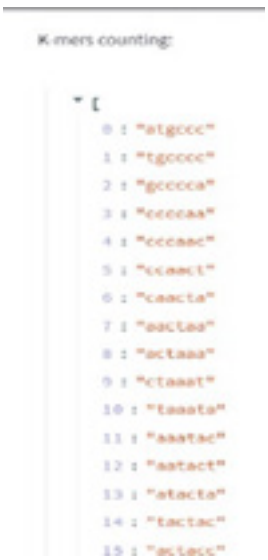

Fig 10 Feature Selection through k-mers counting.

6. CONCLUSION AND FUTURE WORK

This method of feature selection and feature extraction from DNA data sequence was successfully completed. Here, we employed K-mer counting, one-hot encoding, and ordinal encoding as the language for choosing DNA sequence features in python libraries. We have demonstrated the result using these libraries in the forms of a matrix, vector, and graph. In future, we also retrieved K-mers to use in the classifier process.

REFERENCES

https://devopedia.org/cross-validation. Accessed: 2022-12-13.

[1] Arumugam, P., Professor, Department of Statistics, Manonmaniam Sundaranar University, Tirunelveli (Tamil Nadu), India., Kadhirveni, V., Priya, R. L., Manimannan, Research Scholar, Department of Statistics, Manonmaniam Sundaranar University, Tirunelveli (Tamil Nadu), India., Assistant Professor, Department of Statistics, Dr. Ambedkar Government Arts College, Vyasarpadi, Chennai (Tamil Nadu), India., and Assistant Professor. Department of Statistics, TMG College of Arts and Science, Chennai (Tamil Nadu), India. 2021. Prediction, cross validation and classification in the presence COVID-19 of indian states and union territories using machine learning algorithms. International Journal of Recent Technology and Engineering (IJRTE) 10, 1 (May), 16–20.

[2] Breiman, L. Bagging predictors". Boston. Manufactured in The Netherlands.

[3] Darapureddy, N., Karatapu, N., and Tirumala, K. 2019. Research of machine learning algorithms using K-Fold cross validation". International Journal of Engineering and Advanced Technology (IJEAT).

[4] Gopika, D. and Azhagusundari, B. 2014. An analysis on ensemble methods in classification tasks". International Journal of Advanced Research in Computer and Communication Engineering 3, 7.

[5] Hulu, S. and Sihombing, P. 2020. Analysis of performance cross validation method and K-Nearest neighbor in classification data. International Journal of Research and Review 7.

[6] Jung, Y. and A K-Fold. 2015. Averaging cross-validation procedure". Journal of Nonparametric Statistics.

[7] Kumar, S. 2020. Understanding 8 types of cross-validation. https://towardsdatascience.com/understanding-8-types-of-cross-validation-80c935a4976d. Accessed: 2022-12-13.

[8] Mera-Gaona, M., LÅLopez, D. M., Vargas-Canas, R., and Neumann, U. 2021. Framework for the ensemble of feature selection methods. Appl. Sci. (Basel) 11, 17 (Sept.), 8122.

[9] Pandey, M. and Taruna, S. 2014. A comparative study of ensemble methods for students' performance modeling". International Journal of Computer Applications 103, 8, 975–8887.

https://doi.org/10.17993/3ctecno.2022.v11n2e42.59-69

[10] PAYAM REFAEILZADEH, LEI TANG, H. L. A. S. U. 2008. Cross-validation'. Cross validation Bootstrap.
[11] Raschka, S. 2020. Model Evaluation, Model Selection, and Algorithm Selection in Machine Learning".
[12] Singh, R. and Pal, S. 2020. Machine learning algorithms and ensemble technique to improve prediction of students performance". International Journal of Advanced Trends in Computer Science and Engineering 9, 3, 3970–3976.
[13] Wu, S.-H. Cross Validation & Ensembling. Taiwan.

https://doi.org/10.17993/3ctecno.2022.v11n2e42.59-69

/06/

IMPLEMENTATION OF HAND GESTURE-CONTROLLED MOUSE USING ARTIFICIAL INTELLIGENCE

Piyush Pilare
B.Tech Student, Department of Electronics and Communication Shri Ramdeobaba College of Engineering and Management Nagpur, (India).

Coral Mahato
B.Tech Student, Department of Electronics and Communication Shri Ramdeobaba College of Engineering and Management Nagpur, (India).

Chanchal Khergade
B.Tech Student, Department of Electronics and Communication Shri Ramdeobaba College of Engineering and Management Nagpur, (India).

Shubham Agrawal
B.Tech Student, Department of Electronics and Communication Shri Ramdeobaba College of Engineering and Management Nagpur, (India).

Prasheel Thakre
Assistant Professor, Department of Electronics and Communication Shri Ramdeobaba College of Engineering and Management Nagpur, (India).
E-mail: thakrepn2@rknec.edu

Reception: 16/09/2022 **Acceptance**: 01/10/2022 **Publication**: 29/12/2022

Suggested citation:

Pilare, P., Mahato, C., Khergade, C., Agrawal, S., and Thakre, P. (2022). Implementation of hand gesture-controlled mouse using artificial intelligence. *3C Tecnología. Glosas de innovación aplicadas a la pyme, 11*(2), 71-79. https://doi.org/10.17993/3ctecno.2022.v11n2e42.71-79

ABSTRACT

This article presents a proposed mouse system. In this paper, we discussed the implementation of an artificially intelligent hand gesture-controlled mouse that uses computer vision to execute mouse functions using the Colour detection technique. The virtual mouse uses the current python and computer vision algorithms for the recognition of the Masked/colored region and works seamlessly without any extra hardware requirements. A computer may be controlled remotely using hand motions, and it is capable to perform cursor movement, left-clicking, and right-clicking without the need for a hardware mouse.

KEYWORDS

Hand Gestures, mouse, Image capture, Preprocessing, Masking.

https://doi.org/10.17993/3ctecno.2022.v11n2e42.71-79

1. INTRODUCTION

AI hand control technology is a brand-new development that allows people with limited hand usage to control their computers via hand movement recognition. It works by tracking the movements of a person's hand with a webcam or inbuilt camera. The software recognizes the position of the person's hand in space and replays that movement on the screen as a mouse cursor movement. The result is that users can control their cursor with simple movements of their hands. Many of the current iterations of AI hand control technology have been created for people with conditions like arthritis, carpal tunnel syndrome, or paralysis Ghute et al. [2018]. Such disorders result in limited hand use and often make it impossible for people to use a computer mouse. AI hand-control technology allows such individuals to regain computer control, opening up the world of online information and entertainment once more to people who have been cut off from it. The hand gesture-controlled mouse would surely lead to massive development in the field of technology Pradhan et al. [2015].

1.1. EXISTING SYSTEM

All I/O operations are controlled virtually with the assistance of masking. This implemented system aims to regulate a mouse cursor using the fingertips of the individual. A custom locking algorithm is employed to convert masked region coordinates from a virtual screen into a full-screen one to be accustomed to controlling the mouse Mali et al. [2022]. The suggested mouse system captures images using either a built-in camera or a webcam while evaluating the quality of the camera.

The virtual mouse framework can also get aware of problems with hitting in places like things that don't have room to accommodate an actual mouse and be tailored for those who have issues in gripping and can't handle an actual mouse. Assuming that if something is finished with a mouse, it may also be through with your daily webcam. An electronic device could be a handheld pointing device most ordinarily used for manipulating objects on the pc screen.

1.2. PROPOSED SYSTEM

The virtual space between the web camera and the user is described as the "Virtual Monitor," where a mouse cursor can be moved using a masked object and background subtraction. Grif H. T. et al. [2018]. We have mainly concentrated on the movement of the pointer and basic operation of the mouse like dragging and left-clicking Titlee et al. [2017]. The Python module called OpenCV is a library of programming functions, mostly focused on computer vision in real time. It uses a sampling streaming endpoint to listen to new tweets in real-time and draws them onto a virtual globe according to whatever positional information is included Grif H. T. et al. [2018] Prof. Shital Pawar et al. [2022]. It could be modified to a further extent by introducing some new features and adding hand gestures. Instead of using masking, we can control the mouse with the help of just your hand.

https://doi.org/10.17993/3ctecno.2022.v11n2e42.71-79

1.3. USE OF PROPOSED WORK

In this system, we are controlling the mouse pointer by using colored tape or caps on the fingertips and with the open and Close gestures we are operating the mouse, we are using inbuilt libraries in Python to get the pointer coordinates and match them with the masked region from the camera to screen resolution.

2. METHOD

The methodology of each system component will be covered separately. These are the different sections:

2.1. CAMERA SETUP

The web-cam manages the mouse operations. We need to use a Video Capture object to capture a video. After that, we can capture frame-by-frame. We could apply color detection techniques to any image by making minor algorithm changes.

2.2. PREPROCESSING THE FRAMES

The web camera is continually active and captures the video during the program's duration thanks to an infinite loop. Next, each frame that was gathered in RGB (the default) color system is converted to HSV color format. Grif et al. [2016].

2.3. MASKING TECHNIQUE

We are producing a certain region with the help of a mask by the use of the original image using the threshold image and applying AND operation when we do that the masked region is then highlighted and we get the region we want and we can propose some rules to that area Chienet al. [2015] Grif et al. [2015].

2.4. OPERATION

The detected coordinate is then used to convert camera resolution to actual screen resolution Wen et al. [2012]. The position of the mouse is then set, however, it will take some time to shift the mouse pointer. Once the current mouse position and the designated mouse location are the same, we started a loop.

https://doi.org/10.17993/3ctecno.2022.v11n2e42.71-79

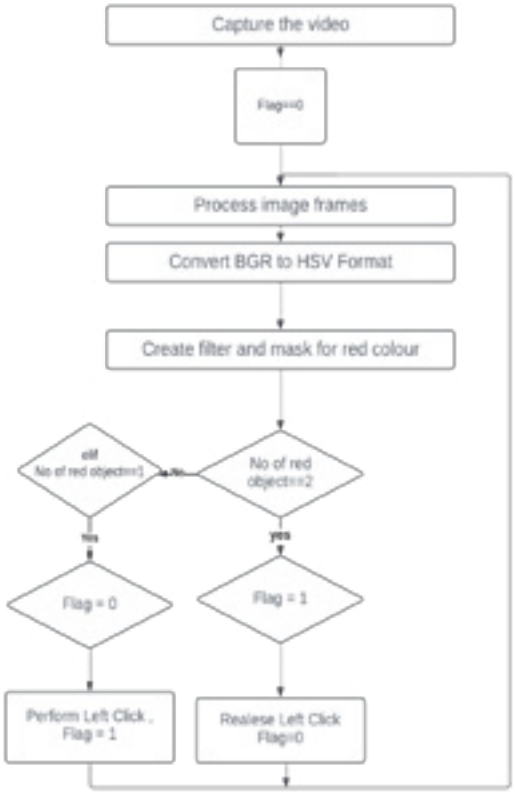

Fig 1. FlowChart of proposed Method.

2.5. CLICKING

In this instance, dragging and clicking the object is used to complete the action. It is comparable to making an open gesture, but since there is only one item, we simply need to determine its center. And we'll position that there where our mouse pointer will be.

2.6. DRAG

We introduce a variable called "flag" to implement dragging. It will be set to 1 if it was clicked in the past. So, after finding the open gesture, we click it and then double-check that the flag is set to 1. If it is set to one, the drag action is performed; if not, the mouse move operation is performed.

3. RESULT AND EVALUATION

Many of the current iterations of AI hand control technology have been created for people with conditions like arthritis, carpal tunnel syndrome, or paralysis. This implemented system aims to regulate a mouse cursor using the fingertips of the individual. AI hand control technology is a brand-new development that allows people with limited hand usage to control their computers via hand movement recognition. A custom locking algorithm is employed to convert masked region coordinates from a virtual screen into a full-screen one to be accustomed to controlling the mouse Suriya et al. [2014]. The software recognizes the position of the person's hand in space and replays that movement on the screen as a mouse cursor movement. The suggested mouse system captures images using either a webcam or a built-in camera while considering the camera quality, allowing us to reduce the number of system components. This creates a greater impact on the Environment by stopping the E-waste generation from keyboard and mouse and their wires.

https://doi.org/10.17993/3ctecno.2022.v11n2e42.71-79

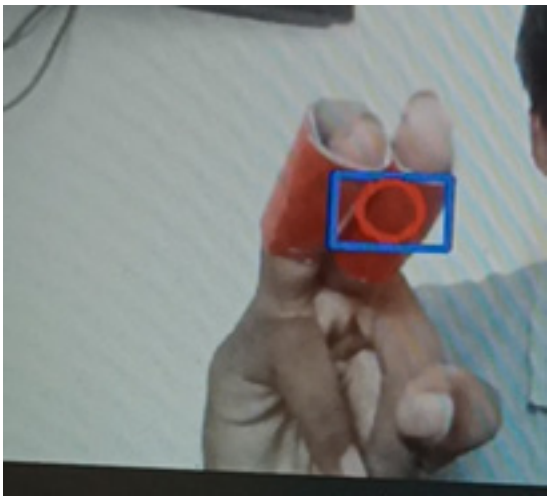

Fig 2. Hand Gesture for clicking and dragging.

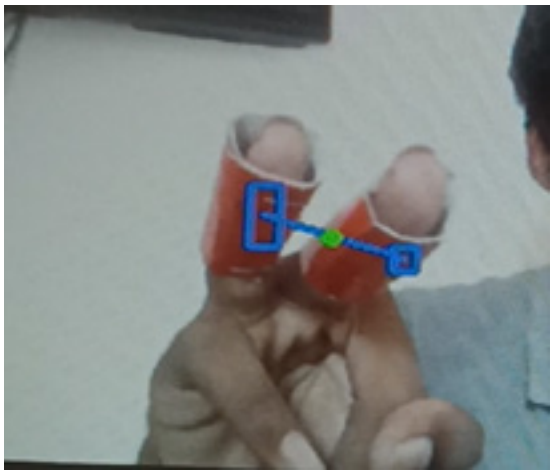

Fig 3. Hand Gesture for Deselecting.

Table I. Performance analysis (Where S-successful and U-unsuccessful).

Mouse operations No.	Detection	Drag	Left-Click	Move
1	S	S	S	S
2	S	S	S	S
3	S	S	S	S
4	S	U	S	S
5	S	S	S	S
6	S	S	S	S
7	S	S	U	S
8	S	U	S	S
9	S	S	S	S
10	S	S	S	S

https://doi.org/10.17993/3ctecno.2022.v11n2e42.71-79

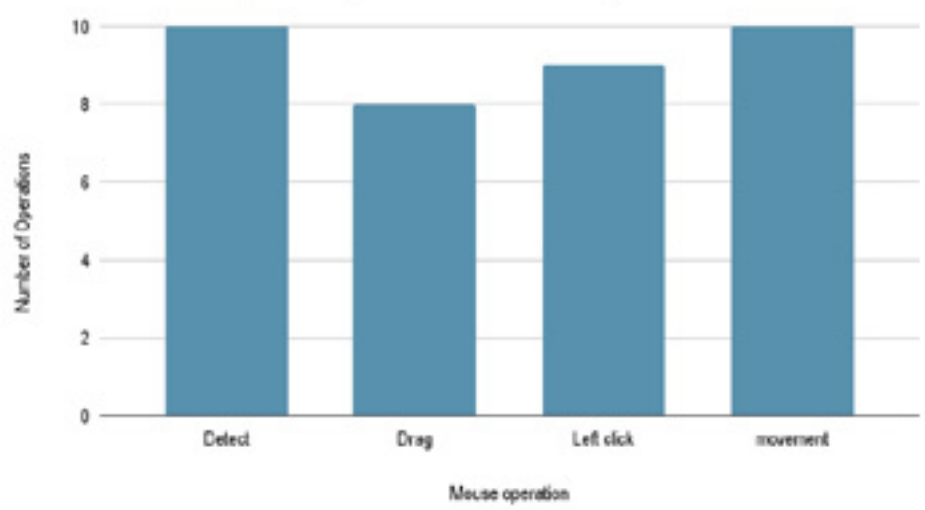

Fig 4. Number of Mouse Operation Performed Successfully.

The Histogram displays how frequently each of the four operations is carried out correctly and accurately.

The correctness of the system was assessed using the below formula to calculate the performance of the system.

$$\text{Accuracy} = \text{DF/TF x } 100$$

Where TF is the total number of operations performed and DF is the number of operations successfully recognized.

Hence, the accuracy of the system is 92.5

4. CONCLUSION

Gesture recognition is used to give the best human-machine interface. Gesture recognition is essential for the creation of new human-computer interface techniques. It facilitates more natural interactions between people and machines Grif etal. [2015]. Many different applications, including robot control and sign language recognition for the deaf and dumb, can use gesture recognition. This technique has applications in many different fields, including augmented reality, prosthetics, computer graphics, gaming, and biomedical devices. Our system's Digital Canvas, becoming increasingly popular among artists, allows them to use the Virtual Mouse technology to create 2D or 3D images while using hands like brushes and a VR headset as a display. Patients who lack control over their limbs can benefit from this device. Modern gaming consoles have incorporated computer visuals and gaming technology to create interactive games that track player actions and translate them into commands Chowdhury et al. [2020].

This work can be further extended to make the system more adaptable to various lighting conditions and background complexity. It is possible to create a user interface that is both efficient and complete in terms of mouse functionality. Additionally, it would be excellent to look into cutting-edge mathematical techniques for image processing and look into other hardware options that would produce more precise hand detections. This study illustrated the possibilities for streamlining user interactions with personal computers and hardware systems in addition to illustrating the various gesture operations that users may perform.

https://doi.org/10.17993/3ctecno.2022.v11n2e42.71-79

REFERENCES

[1] S. R. Chowdhury, S. Pathak and M. D. A. Praveena (2020). Gesture Recognition Based Virtual Mouse and Keyboard. 4th InternationalConference on Trends in Electronics and Informatics (ICOEI). doi: 10.1109/ICOEI48184.2020.9143016.

[2] Horatiu-Stefan Grif, Zoltan German, Adrian Gligor (2015). Hand Posture Mouse. Procedia Technology, 19, 766-771, https://doi.org/10.1016/j.protcy.2015.02.108.

[3] Horatiu-Stefan Grif, Trian Turc (2018). Human Hand gesture based system for Mouse cursor control. Procedia Manufacturing, 22, 1038-1042, https://doi.org/10.1016/j.promfg.2018.03.147.

[4] Horatiu-Stefan Grif, Cornel Cristian Farcas (2016). Mouse Cursor Control System Based on Hand Gesture. Procedia Technology, 22, 657-661, https://doi.org/10.1016/j.protcy.2016.01.137.

[5] M. S. Ghute, M. Anjum and K. P. Kamble (2018). Gesture-Based Mouse Control. Second International Conference on Electronics, Communication, and Aerospace Technology(ICECA), (pp. 710-713). doi:10.1109/ICECA.2018.8474905

[6] Mali, Y., Malani, H., Mahore, N., & Mali, R. (2022). Hand Gesture Controlled Mouse. International Research Journal of Engineering and Technology.

[7] P. -Y. Chien, Y. -H. Miao and J. -I. Guo (2015). A 3D hand tracking design for gesture control in complex environments. VLSI Design, Automation and Test (VLSI-DAT), 1-4. doi:10.1109/VLSI-DAT.2015.7114577

[8] A. Pradhan and B. B. V. L. Deepak (2015). Obtaining hand gesture parameters using image processing. International Conference on Smart Technologies and management for computing, Communnication, Controls, Energy and Materials. IEEE.

[9] Prof. Shital Pawar, S. M. (2022). Virtual Mouse using Hand Gesture. Gradiva Review Journal, 8(1).

[10] R. Suriya and V. Vijayachamundeeswari (2014). A Survey on hand gesture recognition for simple mouse control. International Conference on Information Communication and Embedded Systems (ICICES2014). IEEE.

[11] Titlee, R., Rahman, A. U., Zaman, H. U., & Rahman, H. A. (2017). A novel design of an intangible hand gesture controlled computer mouse using vision based image processing. 3rd International Conference on Electrical Information and Communication Technology (EICT). IEEE.

[12] Y. Wen, C. Hu, G. Yu and C. Wang. (2012). A robust method of detecting hand gestures using depth sensors. IEEE International Workshop on Haptic Audio-Visual Environments and Games (HAVE 2012) Proceedings. IEEE.

https://doi.org/10.17993/3ctecno.2022.v11n2e42.71-79

AUTORS BIOGRAPHY

Mr. Piyush Deorao Pilare is pursuing 4th year B.E. in the department of Electronics and Communication Engineering, at Shri Ramdeobaba College of Engineering and Management, Nagpur.
E-mail: pilarepd@rknec.edu

Ms. Coral Mahato is pursuing 4th year B.E. in the department of Electronics and Communication Engineering, at Shri Ramdeobaba College of Engineering and Management, Nagpur.
E-mail: mahatocr@rknec.edu

Ms. Chanchal Khergade is pursuing 4th year B.E. in the department of Electronics and Communication Engineering, at Shri Ramdeobaba College of Engineering and Management, Nagpur.
E-mail: khergadecs@rknec.edu

Mr. Shubham Agrawal is pursuing 4th year B.E. in the department of Electronics and Communication Engineering, at Shri Ramdeobaba College of Engineering and Management, Nagpur.
E-mail: agrawalsr_10@rknec.edu

P. N. Thakre has received Bachelor's degree in Electronics Engineering from RTM Nagpur University in 2010. He has done M.Tech. in Electronics Engineering from Shri Guru Gobind Singhji Institute of Engineering and Technology, Nanded University in 2013. Presently he is pursuing Ph. D. from Shri Ramdeobaba College of Engineering and Management, RTM Nagpur University, under the fellowship of Visvesvaraya PhD Scheme for Electronics & IT. His research area includes Non-Orthogonal Multiple Access (NOMA) for 5G Wireless Communication Systems and Wireless channel Estimation Algorithms. Presently he is working as Assistant Professor in Electronics & Communication Engineering Department, Shri Ramdeobaba College of Engineering and Management, Nagpur.

https://doi.org/10.17993/3ctecno.2022.v11n2e42.71-79

/07/

ARDUINO BASED INSECT & RODENT REPELLER FOR LIVING & WORKING SPACES

Vishal Ghorse
Department of Industrial Engineering, Shri Ramdeobaba College of Engineering & Management, Nagpur, (India).

Jagdish Kene
Department of Electronics and Communication Engineering and Department of Industrial Engineering, Shri Ramdeobaba College of Engineering & Management, Nagpur, (India).
E-mail: kenejd@rknec.edu

Rakshal Agrawal
Department of Electronics and Communication Engineering and Department of Industrial Engineering, Shri Ramdeobaba College of Engineering & Management, Nagpur, (India).

Reception: 01/10/2022 **Acceptance**: 16/10/2022 **Publication**: 29/12/2022

Suggested citation:

Ghorse, V., Kene, J., y Agrawal, R. (2022). Arduino based insect & rodent repeller for living & working spaces. *3C Tecnología. Glosas de innovación aplicadas a la pyme, 11*(2), 81-88.
https://doi.org/10.17993/3ctecno.2022.v11n2e42.81-88

ABSTRACT

With so many amazing things going on in the world of science and technology, we still don't have an effective solution to ward off pests electronically. Pesticides, insecticides and other repellents are toxic and dangerous to human health. Electronic Pest Repellent (EPR) is a new technology that is cheap, environmentally friendly, effective and poses no risk to humans. Electronic pest repellents are electronic devices that are capable of producing sounds in the ultrasonic frequency range that are inaudible to the human ear but are audible to pests such as rodents, birds and insects. Sounds of this frequency (10-100 kHz) are annoying to pests and leave the place due to severe hearing impairment. The device can be used by the general public to repel mosquitoes, insects, cockroaches and by farmers to repel rodents, insects and other pests.

KEYWORDS

Arduino, Insects, Repellent, Ultrasound, Variable Frequency.

https://doi.org/10.17993/3ctecno.2022.v11n2e42.81-88

1. INTRODUCTION

As Humans, we are conditioned from childhood to fear insects, rodents, pests usually, from a negative or traumatic experience with them in the past. Most of the time we choose from commercially available solutions, like chemical sprays, dead traps, deterrents, fast acting poisons , electromagnetic wave based repellents and many more. For a fact, they aren't as effective as they are advertised. And in itself they are harmful by nature of substances used in them, which makes them not suitable to use at home where toddlers are around. Therefore we aimed to design an electronic repeller which will use ultrasounds of a wide range of frequencies to repel the common hazardous insects and rodents. As it is a variable frequency repeller it makes the targeted insects and rodents to not adapt to the sounds which is the case the traditional electronic repellers fails and makes them inefficient. by using high-frequency pulsed sound waves to attack the pest's nervous system, and finally, the only way for the pest to survive is to leave it. Odorless, non-toxic, smokeless, silent, no side effects on the human body. It can be used continuously and is suitable for home and office use.

2. LITERATURE REVIEW

The authors of this paper [1] focus on the development of electronic composites to produce smarter, safer and more effective alternatives to harmful repellants. This article provides detailed information on ultrasonic pest repellers. This device produces variable ultrasonic frequencies that can repel, block and disrupt the acoustic communication of pests and insects. The desired outcome of this device was to reduce the use of pesticides and insecticides that pollute the soil and pose various environmental, physical and health risks. With this in mind, these chemical fertilizers affect the food chain and all the people who are part of the food chain. You can also interact with electronic repellers that use electromagnetic and ultrasonic waves to repel insects such as mosquitoes, houseflies, and spiders. , insects, fleas and cockroaches. An ultrasonic pest control system repels, not kills, pests with multi-frequency modulation alerts.

These high-intensity ultrasonic waves (25-65 KHz) are beyond the range of human hearing and temporarily disturb most pests. These (in the case of rodents and insects) nervous sounds travel directly to the brain and nervous system, causing abnormal behavior such as severe pain, discomfort, agitation, and radiation sites. This device produces variable ultrasonic frequencies that repel, trap, and block sound communication of pests and insects. By using the GSM module, the device can be controlled from anywhere in the world and can be accessed worldwide. Additionally, the use of power amplifiers, microcontrollers (Arduino UNO) and short diaphragms increase the operating range, efficiency and area of the device. With the help of BLE technology and its mesh networking capabilities, the device can also be used to cover large areas in agriculture while increasing the efficiency of the device. The biggest challenge with this device is reducing the use of pesticides and pesticides. Pesticides and pesticides contaminate the soil and pose environmental, physical, and health risks.

The author of this paper [2] presents a design concept for an automatic ultrasonic animal and insect repellent, consisting of an ultrasonic sensor, a motion sensor, a GSM module and an Arduino Uno board. Identify the sound of the pest by recording the ultrasonic signals emitted by the presence of pests in the products. Then the presence of pests is detected by PIR motion sensors. When both Arduino Uno board sensors confirm the presence of pests, an ultrasonic repeller is activated to drive animals and insects out of the area. A message is sent through the GSM module and farmers are ready to protect themselves with pesticides or pesticides depending on the crop. This project can also be utilized in agricultural functions like cattle monitoring as well.

In this paper [3] Experimental observations have shown that bird activity is extreme early in the morning and decreases regularly throughout the day. Therefore, the field test was four times from 5 am to 8 am and from 5 pm to 6 pm. The test was conducted during both wheat and rice harvest after corn

https://doi.org/10.17993/3ctecno.2022.v11n2e42.81-88

had been planted in the field. The target bird species were pigeons (Spilopelia senegalensis), crows (Corvus cornix), pigeons (Columba livia) and sparrows (Passer Domesticus). The flock averaged dozens of mighty birds. For analysis Stepwise multiple linear regression models involving frequency level, exposure time interval, and field to find the relationship between sound pressure level (SPL), bird departure time, frequency level, exposure time interval, and field measurement distance was used. Distance was measured as the explanatory variable, and (SPL) and bird flight time are considered dependent variables. The regression model results showed a significant association between SPL, bird departure time, and the explanatory variables. This can be inferred from the t-values and associated p-values. The explanatory variables explained 88% and 93% of the variation in SPL and bird departure times, indicating a high strength of the relationship between SPL and bird departure times and the explanatory variables. By looking at the F-value and its p-value, they concluded that the model is valid and that there is a correlation between SPL and bird departure times and explanatory variables.

In this work [4], a scheme was developed that works with fixed blocking frequencies around 26 kHz and between 34 and 44 kHz. To ensure effective performance, the ultrasonic frequency of this ultrasonic oscillator is continuously and automatically changed within a certain range. This was accomplished by changing the clock pulse output of IC1 NE555 (used as a low frequency square wave oscillator in the design) and Results were obtained from the tests performed on the device and from the testers who used the device. The developed device operated within the specified insect repellent frequencies. The results obtained from simulation and experiment , the waveforms obtained using an oscilloscope in the lab were both square waves. When the device was placed in close proximity to a subject (flies or mosquitoes), the device repelled them up to a distance of 3 meters. When placed approximately 4 meters away from the subject, the subject showed no significant reaction. The system was designed, built and tested satisfactorily and successfully executed. The system has been found to be very effective, performing according to design specifications despite minor variations in readings.

This article [5] deals with a brief review of different ways and devices for repelling insects and rodents in agricultural areas and poultry farms. A variety of manual techniques were used in the past, but subsequent advances in electronics gradually led to their use in agriculture to increase yields. Three controls were developed for the new system. The rat repellent works with your phone or a switch. Rats are repelled by the ultrasonic range of frequency produced by the device. The frequency range varies from 60 KHz to 85 KHz. The developed technology was tested on caged rats to see if it could affect the organism. Varying the ultrasound over a frequency range of 60 to 85 kHz exhibited erratic behavior in the rats, proving that the designed system helped repel dangerous rodents and pests from poultry farms. The proposed prototype design allows the device to operate for up to 12-13 hours on a fully charged battery. DTMF is the signal sent to the Arduino Uno by pressing a button on the phone's dial pad. The high and the low frequencies on the keys of the mobile phone keyboard produce two different sounds.. The third control unit uses an LDR connected to an analog pin to detect day and night and activate the night mode.

This paper [6] describes the design and testing of electronic jamming protection. The audio amplifier circuit is designed to produce ultrasound in the frequency range up to 75-80 kHz. A suitable frequency response is used to transmit these sound waves. This device is an effective alternative to pesticides commonly used on farms and homes. Oscilloscope readings indicated that the generated signal was within the repulsion frequency range of 30 to 50kHz of ultrasonic frequencies. ultrasonic signals for different pest species tested in a series of 10 experiments were within the specified range. It was determined to be five times more affordable than the insecticide propoxur, and that simulation and experimental results were consistent within ±5% measurement uncertainty.

The device designed in this study [7] is an automated pest control tool specifically targeted at bird and rodent pests. Control technology is implemented by listening to pests. The device developed is a prototype for repelling rodent and bird pests in rice. In this prototype, two sensors (an ultrasonic sensor and a PIR sensor) were used to detect pests. The dimensions of the prototype to be produced are 40 cm wide and 50 cm long on a 1/100 scale. That means the prototype created could reach an area

https://doi.org/10.17993/3ctecno.2022.v11n2e42.81-88

of 4 x 5 m with respect to the real area. The prototype is expected to develop into a large-scale tool for direct installation and use by farmers and auto tow trucks. Repellent techniques are implemented by making sounds that can stun pests It was hoped that this prototype could be developed into a larger scale tool for direct installation and use by farmers.

[8] An acoustic deterrent that repels birds by emitting bird calls or ultrasonic waves**.** To determine the effectiveness and efficiency of ultrasonic restraint systems. Standard ultrasound equipment has been tested on a variety of animal species. There is ample evidence that researchers have successfully developed ultrasonic devices that repel birds, despite the ineffectiveness of commercial ultrasonic devices as described above. Ezeonu et al. (2012) developed and tested an ultrasonic bird repellent. Ultrasound was generated with varying frequencies between 15 kHz and 25 kHz. The waves were amplified and radiated at high sound pressure levels from a solar-powered electronic device manufactured on site.

The purpose of this paper [9] is to find an achievable way to reduce the impact of traffic on wildlife, a priority for nature conservation. Roadsides are important refuges for small animals and excellent hunting ground for hunters. This makes predators and prey vulnerable to vehicle collisions. Therefore, measures aimed at preventing these animals from approaching the streets are necessary. Here, they test the effectiveness of ultrasonic devices to keep rodents out of the way. We hypothesized that when rodents are exposed to ultrasound, they move away from the device and track.

The author of this article [10] proposed such a system that would also be beneficial in agriculture and households. This should also reduce the losses animals often cause. Here he looks at the Arduino code and uploads it to his Arduino UNO board. The Arduino UNO board connects the board to an LCD display, an ultrasonic sensor, and a DTMF decoder that detects animal frequencies and acts as a repellent. Mode 1 transmits dog and cat frequencies (22 KHZ to 25 KHZ), and mode 2 transmits input frequencies (31 KHZ to 44 KHZ) that repel flies and spiders. Therefore, when installed in these locations, the system is equipped with an ultrasonic sensor and an LCD display that indicates the selected mode of operation. Drive away animals based on the selected mode of operation.

The authors conducted a detailed review of alternative controls for house flies [11]. The house fly is the most widespread commensal pest in the world. It rarely breeds indoors, but it does invade buildings, causing problems and transmitting pathogens. Exclusion means keeping flies away from the structure. Despite the best efforts, flies can invade the human environment. Therefore, air curtains, fans, screened windows and doors are excluded. UV light traps attract and immobilize flies. The window trap invites you to a device that catches flies. Adhesive tubes and tapes rely on the tendency of flies to land on vertical lines and get stuck in the adhesive. Even low-tech fly swatters can play an important role in getting rid of individual flies. Timely-release pyrethrin aerosol dispensers are effective against flies trapped in small spaces. Poison Bait can only be used in urban environments.

This study [12] aims to illustrate the usefulness and effectiveness of automated tools that can repel agricultural pests, especially rats and birds. The tool has a passive infrared-receiving sensor that detects the presence of agricultural pests, and a servo motor activates and pulls a bell, making sounds that scare away birds and rats. This mechanism is controlled by a microcontroller called the Arduino ATmega 2560. This tool is an innovation from traditional technology, so it can easily solve farmers' problems related to agricultural pests.

In the article [13], the author constructed an EMR-generated ultrasound in the frequency range of 20-38 kHz, propagating at an angle of 45° from the source and covering a large radius. These ultrasound focused auditory stresses on mosquitoes either deactivate them or push them out of the vicinity of the device. The device is based on the 555 timer IC and can be used by the public indoors or outdoors to combat the mosquito threat, with an EMR (Electronic Mosquito Repellent) he turns off for 12 seconds, in a famous mosquito hatchery Field experiments were conducted using human chow. minute. Human prey felt the number of mosquitoes on different parts of the body. It was difficult to determine whether ground gnats were of the same species. They turned on the EMR machine and

https://doi.org/10.17993/3ctecno.2022.v11n2e42.81-88

watched for another 12 minutes. In the first 4 minutes, 8 mosquitoes landed on human food. In his last eight minutes of his life, he saw a mosquito land on average every four minutes of his life. It was just the two of him. Mosquito landing rates differ with and without EMR ON. This demonstrates the ability of the EMR device to repel mosquitoes outdoors. Another experiment was conducted with two subjects in a closed classroom. The first human bait was placed in the center of the classroom and the second human bait was placed in each corner of the classroom. The results of these tests provided clear evidence from field observations that this device impacted mosquito landing rates. investigated (because location and environmental conditions can affect ultrasound transmission).

This paper [14] focuses on different pest control methods and also describes frequency variation generation technology based on electronic pest control machines. Using the LM 380 in an audio power amplifier circuit, we have designed a system capable of producing sound in the 75 kHz frequency range. Loudspeakers of suitable frequency ranges are used to transmit these sound waves. E-Pest Repellent is intelligently made with ANN (Artificial Neural Network). ANNs are trained on data collected from the literature to repel different types of pests. ANN output is the amplitude, frequency, and duration of the signal to repel pests. It is said to be highly effective compared to simple E-pest repellents.Comprehensive performance evaluations of e-pest repellents were conducted to determine the effectiveness of the device against a variety of pests. and ANN has received training. Her trained ANN will be used in the development of his intelligent E-Pest Repellent System. This device is intended to repel small birds, mosquitoes, flies, moths, bats and other nocturnal insects, rodents and birds in farm fields.

3. EXISTING METHODOLOGY

The above section details many of the available technologies. Each article discusses different technologies and techniques for proving to be effective repellents. Such as the development of an electronic repeller system in articles [1] [2] [4] [6] and his use of DTMF techniques in [5] [11]. This allows GSM technology to complement existing EPR. Additionally, Powering them for long hours of operation is a big challenge where some used batteries , some tried solar power and many solutions for this situation are detailed in [9][11][12][13]. All the above techniques and technologies are available separately ranging from cheaper solutions to more expensive ones but the scope of them proving to repel, is limited to some specific rodents or insects mainly rats and mosquitoes. These can be combined with each other by improving and working on the existing anomalies by completing these challenges.

4. ACOUSTIC METHODS

Acoustic sensors used in recent research include piezoelectric sensors, accelerometers, microphones, and ultrasonic transducers that are used to detect and identify rodents & insects. The laser doppler vibrometer is a modern sensor that is very useful for detecting and identifying insects.

4.1 Accelerometers - Accelerometers are acoustic sensors that sense vibrations and shocks to measure environmental G-forces. It's a microchip-like device that gently but firmly attaches to the stems and stems of plants. The signals recorded by the accelerator are sent as output signals to a wireless computer for further analysis.

4.2 Piezoelectric sensors - Sensors that work on the principle of piezoelectricity. When the piezo disk deforms, a voltage is generated. Crystals, like crystals, have the ability to conduct electricity. When the crystal is subjected to an external force, it deforms and the negative and positive charges move within the crystal, creating a voltage that helps identify pests. The core of a piezoelectric sensor consists of a piezoelectric crystal that directly converts mechanical stress into electrical charge.

4.3 Acoustic Probes - Integrate acoustic sensors like accelerometers and piezoelectric sound sensors to create acoustic probes. It is usually inserted into the area of the sound field under investigation. Soil,

https://doi.org/10.17993/3ctecno.2022.v11n2e42.81-88

stored grain or wood. Known as the SP-1 probe, the portable device combines a specialized probe and sensor manufactured by Acoustic Emission Consulting (AEC) to detect acoustic emissions produced by burrowing insects and red weevil larvae. It consists of date palms for identification.

4.4 Microphone - a type of sound device that uses IA (Impact Acoustics) to evaluate the quality of production. It helps to identify the damage of insects, scabs and buds on the seeds. It is a non-intrusive and cost-effective alternative to laborious, time-consuming and expensive manual methods.

4.5 Ultrasonic Transducers -An ultrasonic transducer is a system capable of producing and receiving ultrasonic vibrations. This converter consists of a wear plate, an active element and a back. Active elements are piezoelectric or single crystal materials that convert electrical energy into ultrasonic energy. It then recovers the ultrasonic energy and converts it into electrical energy.

4.6 Laser Doppler Vibrometer (LDV) -. Compared to other contact methods for vibration measurements, LDV has the advantage that interference between sensor and sample is actively avoided. We have developed a vibration sensor that can classify flying insect species based on flapping frequency. The sensor consists of a laser light source and a phototransistor connected to an electronic gain and filter board, used as a laser beam to measure the beating frequency of flying insects. When a wing hits a laser beam in flight, the light is partially trapped, creating small light fluctuations. These changes were detected by a phototransistor. As a result, the sensor was able to distinguish between the beneficial species and the species two harmful mosquitoes, yellow fever mosquito and west nile fever, with accuracies ranging from 70.69% to 91.3%.

5. PROPOSED METHODOLOGY

In this proposed technology, smart gadgets are designed to keep rodents away from your home and living spaces around your home. Passive infrared sensors are used to detect the presence of people when entering a room. After a successful detection, the tweeter turns off and starts emitting variable frequencies only when the room is empty. Insects and rodents such as cockroaches, mice and mosquitoes are very annoying when they are there, so prevent them from entering the room. That space not only protects the room from the most common pests, but also minimizes exposure to ultrasound, keeping teenagers and toddlers away from high-frequency sounds that can affect their age. . prefer. Long lasting with solar panel and rechargeable DC battery unit. Ultrasonic tweeters can produce frequencies between 10 and 65 kHz, which is enough to keep pesky insects and rodents away. Currently, prevention coverage is limited to one room, and costs increase with each additional room space.

6. CONCLUSION

Acoustic devices have proven highly effective in trapping, identifying, detecting, and behaviorally manipulating pest species. Acoustic devices have been used since the 1900s, but the use of sonic devices in pest control remains limited and untapped, especially in the field. A major reason for the lack of research on acoustic technology in pest control is the fact that acoustic technology is very expensive compared to other available alternatives. However, advances in technology are definitely developing devices that are cheaper and easier to use. Moreover, the latest technology has the potential to improve the efficiency and effectiveness of these devices. It is generally accepted that certain aspects of insect communication remain undiscovered, and many useful potential applications of acoustics in pest control await investigation. A fully fact-based IPM (Integrated Pest Management) strategy for the ecological control of notorious vertebrate, bird, forest, terrestrial and other pests through preserved plants. Acoustics should be viewed as an effective tool.

REFERENCES

[1] VIJAY GAIKWAD, SAURAV SANAP, RUTURAJ SAWANT, SHAZEB SAYYED, SHOAIB SHAIKH, AAYUSHA SHINGAVI “Smart Ultrasonic Variable Frequency Pest Repeller”

https://doi.org/10.17993/3ctecno.2022.v11n2e42.81-88

International Research Journal of Modernization in Engineering Technology and Science, Volume:03/Issue:05, pp. 797-807. May 2021.

[2] P. SILAKARI, P. SILAKARI, L. BOPCHE AND A.GUPTA, "Smart Ultrasonic Insects & Pets Repeller for Farms & Inventories Purpose," 2018 International Conference on Advanced Computation and Telecommunication (ICACAT),, pp. 1-3. December 2018.

[3] HAMED, A. R. **"**Utilization Sonic Waves for Birds Controlling in Crops Field", Journal of Soil Sciences and Agricultural Engineering, , Vol. 12 (12): pp 919 - 927, December 2021.

[4] MUHAMMAD, Z.Z , KASSIM, A. Y., MIKAIL, S. A. "Design and Implementation of an Ultrasonic Insects Repellent" Journal of Science Technology and Education. pp. 92-102, September, 2020.

[5] HEMA N "Solar powered Smart Ultrasonic Rodent Repellent with DTMF and Manual Control for Poultry farms"' International Journal of Progressive Research in Science and Engineering, Vol.3, No.04, pp. 115-120. April 2022.

[6] HASSAN M. ABDULREHMAN, ABDULLAHI L. AMOO, BUBA U. MUHAMMAD, "Design and Construction of Electronic Pest Repellent for Use in Homes and Farmland", Iconic Research and Engineering Journals, Vol 3 Issue 1 pp. 400-407, July 2019.

[7] S R NINGSIH, AHS BUDI, A T NUGRAHA AND T WINATA, "Automatic farmer pest repellent with Arduino ATmega2560 based on sound displacement technique S R Ningsih", IOP Conf. Series: Materials Science and Engineering, pp. 1- 9, July 2019

[8] OLUWOLE AROWOLO, ADEFEMI ADEKUNLE AND JOSHUA ADE-OMOWAYE "A Real Time Image Processing Bird Repellent System Using Raspberry Pi", FUOYE Journal of Engineering and Technology (FUOYEJET), Vol. 5, Issue 2, pp. 101-108, September 2020.

[9] DIANA SOUSA-GUEDES, HÉLDER RIBEIRO, MARIA TERESA VAZ-FREIRE, ANTÓNIO MIRA & NEFTALÍ SILLERO, "Ultrasonic device effectiveness in keeping rodents off the road" , European Journal of Wildlife Research. pp 1-4, January 2020.

[10] NANCY C. HINKLE AND JEROME A. HOGSETTE , "A Review of Alternative Controls for House Flies", MDPI Journal, November 2021

[11] P. BHAGYA SRI, "Smart Ultrasonic Insects Repellent with DTMF and Manual Control" , JAC : A Journal Of Composition Theory, Volume XIV, Issue VIII pp 355- 361, , August 2021.

[12] KRISNA DWI NURIKHSANI, JONAH MUPITA, "Benefits and Effectiveness of Automatic Farmer Pest Repellent", ASEAN Journal of Science and Engineering, Vol 2. issue 3. pp. 243 - 248. October 2021.

[13] YUSUF, ABDULKAWIYU K, "Design and Implementation of An Electronic Mosquito Repellent", New Trends in Science, Technology, Management and Social Sciences in Africa. pp. 119- 129, June, 2021.

[14] D.K. CHATURVEDI, "Intelligent e- Pest Repellent System", International Journal of Engineering Research and Applications, Vol. 11, Issue 5, (Series-VII) , pp. 21-24, May 2021.

https://doi.org/10.17993/3ctecno.2022.v11n2e42.81-88

/08/

STUDY OF DIFFERENT CODING METHODS OF POLAR CODE IN 5G COMMUNICATION SYSTEM

Atish A. Peshattiwar
Reaserch Scholar Department of Electronics Engineering, Yeshwantrao Chavan College of Engineering, Nagpur, Maharashtra, (India).
E-mail: atishp32@gmail.com

Atish S. Khobragade
Professor, Department of Electronics Engineering, Yeshwantrao Chavan College of Engineering, Nagpur, Maharashtra, (India).
E-mail: atish_khobragade@rediffmail.com

Reception: 01/12/2022 **Acceptance**: 16/12/2022 **Publication**: 29/12/2022

Suggested citation:

Peshattiwar, A. A., y Khobragade, A. S. (2022). Study of different coding methods of polar code in 5G communication system. *3C Tecnología. Glosas de innovación aplicadas a la pyme, 11*(2), 90-99. https://doi.org/10.17993/3ctecno.2022.v11n2e42.90-99

ABSTRACT

Sure, most of you are aware that right now everyone is thinking or at least the industry and researchers are thinking about the next generation, the first generation of what will 5G be, and that a significant part of the 5G telecommunication standard has been finalised, in particular the error control codes that will be used in 5G telecommunication. One of the codes that will be used is called a Low-Density Parity Check code (or LDPC code for short), and the other is called Polar Code. These two famous and celebrated codes have distinct and fascinating histories. Both technologies are now capable of providing near-capacity results, making them formidable competitors in the race to become the 5G communication system's ultimate provider. In this paper, we zeroed in on the 5G Polar codes and their encoding methods.

KEYWORDS

5G Communication System, Channel Coding, LDPC Codes, Polar Codes, Coding Methods.

https://doi.org/10.17993/3ctecno.2022.v11n2e42.90-99

1. INTRODUCTION

The POLAR codes are a new type of capacity-achieving codes developed by Arkan [1]. Since 2008, polar codes have been the subject of increasing study and interest in both the academic and professional worlds. As part of the ongoing standardisation process for 5th generation wireless systems, the 3rd Generation Partnership Project (3GPP) has certified polar codes as the channel coding for uplink and downlink control information for the enhanced mobile broadband (eMBB) communication service (5G). Polar coding is one of the proposed encoding methods for the two new frameworks that 5G expects, namely extremely reliable low-latency communications (URLLC) and massive machine-type communications (mMTC).

Creating a polar code involves determining the values of channel dependability associated with each bit of information to be encoded. This id can be accomplished with a specific signal-to-noise ratio and code length. Due to the expected wide range of code lengths, transmission rates, and channel conditions in the 5G architecture, it is impractical to calculate separate reliability vectors for each possible parameter combination. A lot of work has gone into creating polar codes that are straightforward to implement, require little in the way of descriptive complexity, and provide adequate error-correction across a wide range of code and channel parameters.

In light of their impending widespread deployment, researchers would do well to take into account the one-of-a-kind codes created for 5G and their encoding procedure when evaluating error-correction performance and constructing encoders and decoders. Almost all works of contemporary literature fall short of this goal. Polar code properties have an immediate effect on decoder performance, and there may be substantial time and effort costs associated with encoding and decoding. Publications that focus on hardware and software implementations of the 5G standard may be able to increase their readership if they emphasise compliance with the standard.

An "industry standard" is a set of guidelines for providing a service that has been accepted by a number of different companies. In most cases, an agreement between multiple manufacturers to create products that are compatible with one another leads to a standardisation of details, which is the result of a commercial trade-off. A standard is a compromise between competing goals that ultimately results in a hodgepodge of techniques that, when combined, achieve satisfactory performance.

Here, we zeroed in on one particular 5G coding method—Polar Codes—to see what all the fuss is about. 2014 saw the introduction of new encoding schemes for the polar code [2] developed by kia niu.

The remainder of the paper is organised as follows. Polar code: the basics Section II focuses on encoding, while Section III discusses the more advanced design elements and ideas used in 5G decoding, such as SC, SCF, and SCL. In Section IV, we compare the results of our Latency and Throughput measurements, and in Section V, we draw some conclusions based on our findings.

2. 5G POLAR CODE ENCODING

The method employed by the 5G standard to encode polar codes is discussed at length here. In what follows, I'll be making use of the notation defined by the 3GPP technical specification [2]. Polar codes are used to transmit uplink control data over the physical uplink shared channel and uplink control channel. Both the payload on the physical broadcast channel and the downlink control information (DCI) on the physical down-link control channel (PDCCH) are encrypted using polar codes during the downlink transmission (PBCH). For the upper communication layers in 5G applications, the required rate R = A/E is specified, where A is the amount of information bits.

https://doi.org/10.17993/3ctecno.2022.v11n2e42.90-99

A mother polar code of length N = 2n is required for this purpose. When the code is too long (or too short) for the specified code length E, it is punctured, shortened, or repeated until it is. Depending on the channel, the minimum and maximum code lengths N for the uplink and downlink are 32 and 512, 1024, respectively. An additional cap is imposed by the minimum allowable coding rate of 1/8. Figure 6 depicts the various encoding methods planned for use in the 5G polar codes design. The bits of information contained in vector a, denoted by the G code, will be conveyed using the payload of G code bits. Depending on the parameters of the encoding scheme, the message could be split into two parts, each of which would be encoded separately before being sent. For every AJ-bit segmented vector, a polar code-word of length E will be generated. There is an associated L-bit CRC for each AJ-bit vector. The resulting vector c is fed into an interleave, which requires K = AJ + L bits. To generate a mother polar code of length N, we need to know the expected coding rate R, the expected codeword length E, the relative bit channel reliability sequence, and the frozen set. While the remaining bits of the N-bit u vector are held steady, the interleaved vector cJ and any parity-check bits are added to the information set.

Using the generator matrix of the selected mother code, GN = G2n, we encode the vector u as d = u GN. Sub-block interleaving is then used to divide the encoded d into 32 blocks of the same length. Then, the circular buffer receives these blocks after they have been scrambled to produce y. For rate matching, the N-bit vector y is modified in some way (puncturing, shortening, or repeating) to yield the E-bit vector e. In the event that concatenation is necessary, the computed vector f is then ready to be modulated and transmitted as g.

Having the parameters A and E in play makes it clear that there is a cap on the effectiveness of the channel being used. While A 11 uses many different block codes, the uplink uses 12 A 1706. The agreed upon codeword length range is 18 E 8192, even though G 16384 may cause the payload length G to be longer. Segmentation could be used to do this, dividing the data bits into two polar codewords. . For PDCCH in the downlink, the maximum value of A is 140, but in this case, if A is 11, the message will be zero-padded until A = 12. Although E 8192 is employed for uplink, the presence of the CRC lower limits E to 25. There is only one valid PBCH passcode that utilises the combination of A = 32 and E = 864. These flags are the Input Bits Interleaver Activation (IBIL) signal and the Channel Interleaver Activation (CIA) (IIL). There are two kinds of PC helper bits, and NPC and nwm both provide the total number of them.

Fig. 1. Yellow, red, and orange blocks are used in downlink, uplink, and both, respectively, in the 5G polar codes encoding chain.

3. DECODING CONSIDERATION

Even though the 3GPP does not provide any decoding instructions, the final code structure provides some pointers on how to decode polar codes, which are commonly used in 5G. Figure 1 shows an encoding sequence; flipping the sequence facilitates decoding. The received encoded symbols are then padded and deinterleaved to the length of the mother polar code following a second block segmentation and deinterleaving operation for the uplink. A rate-matching algorithm will be used to determine the type of padding to be used, with punctuation requiring the addition of zeros, shortening requiring the use of saturated symbols, and repetition calling for the merging of symbols. The importance of properly handling the code's helper bits at this stage will be emphasised. After padding,

https://doi.org/10.17993/3ctecno.2022.v11n2e42.90-99

the number of encoded symbols is a power of two, which is readable by common polar code decoders [1]. Next, we consider SCL in light of these repercussions and current needs.

When the check for all active pathways fails, the list decoder triggers its early decoding termination feature; decoding continues when at least one active pathway succeeds. The decoder's BLER performance may, however, depend on how it deals with routes that have become unavailable. Keeping the unsuccessful paths in the list is the simple solution to keeping the number of active paths constant and simplifying the decoder design. After each bit estimate, one strategy is to immediately turn off failed paths. As a result, the BLER performs better, and the computational complexity and energy consumption of the decoder are reduced. However, this causes a variation in the total number of possible courses of action. Last but not least, distributed assistance bits could be thought of as dynamically frozen bits that supply the bit's value for the check. The BLER's efficiency is the same using this method as it was using the ineffective path deactivation. Since all surviving paths are guaranteed to get the work done, assistance bits do not have the same impact on the decoder's computational complexity or power consumption as dynamically frozen bits do. As an added bonus, they do not lead to dismissal in the midst of the work week.

However, the number of viable paths varies based on the computational complexity and power requirements of the decoder. Finally, distributed assistance bits can be viewed as dynamically frozen bits that supply the bit with the value the check requires. The BLER's efficiency is the same using this method as it was using the ineffective path deactivation. However, unlike dynamically frozen bits, which reduce computational complexity and power consumption of the decoder and lead to early termination, assistance bits do not guarantee that all remaining pathways will pass the check.

Native successive cancellation (SC) decoding of polar codes is also recommended in [1]. Like a left-biased depth-first binary tree search, its decoding time is linear in N log N. N bits are approximable at the leaf nodes, while the root node has soft information on the received code bits. Figure 4 depicts the decoding tree for a (8, 4) polar code, where black leaf nodes represent the information bits and white nodes represent the frozen bits. Figure 3 shows how the message flow can be defined recursively with a node at the tth stage as the starting point. The node receives 2t soft inputs from its parent node and uses them to generate 2t1 soft outputs _, which are then sent to the node's left child via the formula I = f I i+2t1); later, the node combines the 2t1 hard decisions it receives from the node's left child with to generate 2t1 soft outputs r for the Finally, it combines the 2t1 hard decisions r it received from its right child with to determine the 2t hard decisions it will send to its parent node, with I = I ri if I 2t1 and I = r i2t1 otherwise. When a leaf node is accessed, the soft information is used to make a hard decision regarding the value of the information bits; frozen bits are always decoded as zeros.

In particular, the channel model affects update rules f and g for left and right child nodes. In BEC, hard decisions can take on any value from 0 to 1, while soft values are limited to 0 and 1.

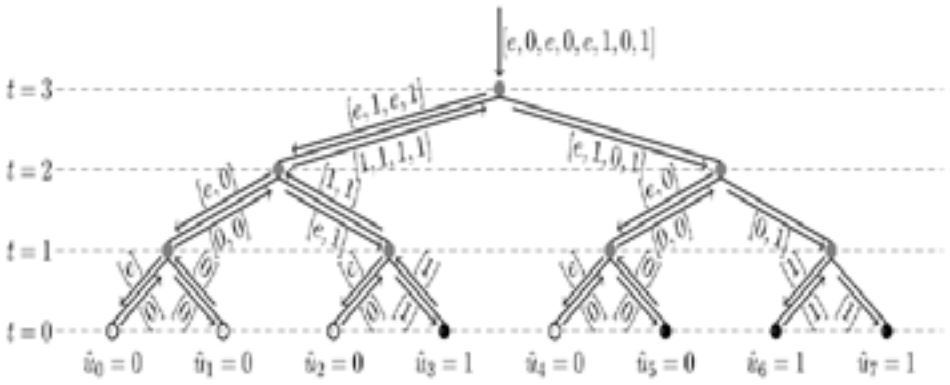

Fig. 2. White and black dots in the SC decoding of a (8, 4) polar code over a BEC stand for frozen and information bits.

https://doi.org/10.17993/3ctecno.2022.v11n2e42.90-99

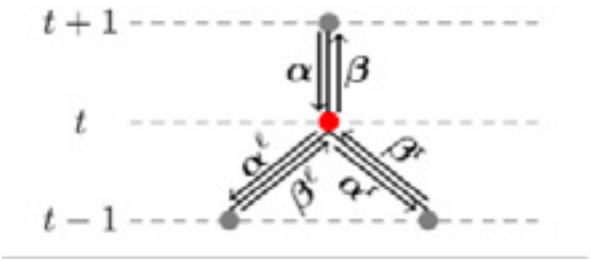

Fig. 3. SC decoding node.

3.1. DECODING FOR SUCCESSIVE-CANCELLATION (SC)

The SC decoding method, as first described [1], operates by sequentially traversing the graph representation of Fig. 2 while iteratively computing u from the noisy channel data. Do this from top to bottom and from right to left. It was first advised to calculate two bits at once in order to decrease time and boost throughput [3]. By utilising specialised, quicker decoding algorithms on selected network nodes [6] or even pruning the graph using a priori knowledge of the locations of the frozen bits [5], the SC technique was further improved. One candidate codeword is always considered, regardless of the SC algorithm version that is being used.

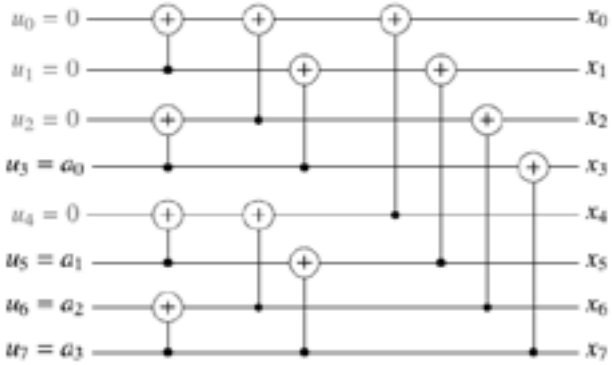

Fig. 4. Graph representation of a (8, 4) polar code.

3.2. PERFORMANCE OF SC DECODING

Fig. 5 compares the (2048, 1723) 10GBASE-T LDPC code's error-correction performance to polar codes running at the same rate. These results were obtained by modulating the binary-input additive white Gaussian noise (AWGN) channel with random codewords and binary phase-shift keying (BPSK). First, it must be stated that the (2048, 1723) polar code performs substantially poorer than the LDPC code. Up until Eb/N0 = 4.25 dB, the LDPC code works better than the PC(32768, 27568) polar code, which was intended to perform best for Eb/N0 = 4.5 dB. There is a growing performance difference over the LDPC code after that. The final polar error-rate curve, abbreviated PC*, is produced by combining the output of two polar codes (32768, 27568). (32768, 27568). The first, which has been in use up until this point, was constructed for 4.25 dB, whereas the second was designed for 4.5 dB. Polar codes can be easily decoded because of their predictable structure, which makes it easy to create a decoder that can decipher any polar code of a specific length. Therefore, polar code changes inside a system are easier than LDPC code modifications.

https://doi.org/10.17993/3ctecno.2022.v11n2e42.90-99

These findings demonstrate that a (32768, 27568) polar code built with an Eb/N0 of 4.5 dB or higher is required to surpass the (2048, 1723) LDPC one in the low error-rate zone and that this may be done even in high error-rate regions by combining numerous polar codes. Even though the polar code is longer than the LDPC code, its decoder is nevertheless built in a simpler manner. The performance difference between the (2048, 1723) code and the LDPC code with a list size of 32 and a 32-bit CRC is reduced by using the list-CRC technique [4], as illustrated in Fig. 2.

The use of some of these strategies to list decoding will need more study. Due to its serial nature, SC decoding has a limited throughput. ASIC decoders for (1024, 512) polar codes currently offer the fastest implementation, processing data at a rate of 48.75 Mbps while operating at 150 MHz [11]. The fastest decoder, on the other hand, can handle data at a rate of 26 Mbps for the (32768, 27568) code and is FPGA-based. Although it may be significantly increased by employing the SSC or ML-SSC decoding algorithms, this poor throughput renders SC decoders unusable for the bulk of systems.

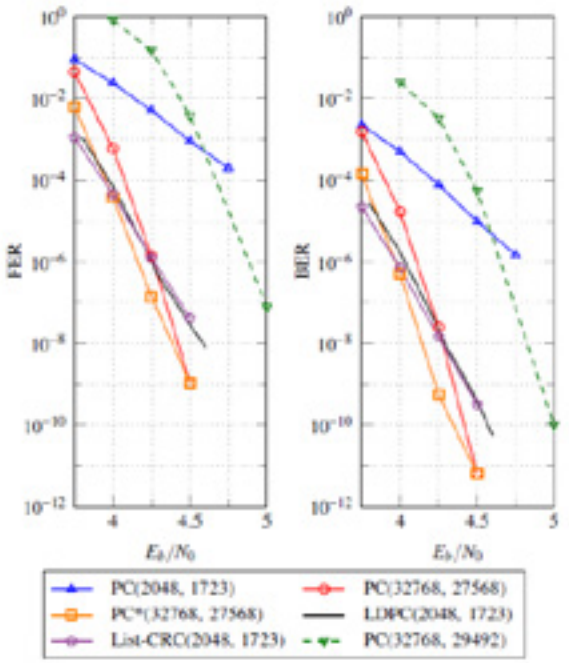

Fig. 5. Polar codes' error-correction performance is contrasted with an LDPC code of the same rate. In addition to a rate 0.9 polar code's functionality.

3.3. DECODING USING SUCCESSIVE-CANCELLATION FLIP (SCF)

Similarities exist between the SC algorithm and the SCF decoding technique [8]. At first, its operation is similar to that of SC decoding; however, in addition to decoding, it also keeps track of the bits that are the least reliable. A cyclic redundancy check must also be used to string together the polar code (CRC). The SCF decoder generates a full codeword candidate and checks if the computed CRC is the same as the expected one. When the CRC verification fails, the SC decoding process continues until the least reliable bit-decision is found. The SCF makes a contrasting conclusion and continues decoding SC. After two tries, if the CRC does not match the expected CRC, the bit-decision with the second-lowest confidence is swapped and the process is repeated. Until the CRC comparison is conclusive or until the maximum number of trials have been conducted, this technique is repeated.

3.4. DECODING OF THE SUCCESSIVE-CANCELLATION LIST (SCL)

As their names imply, the SCL algorithm [7] and the SC algorithm have some similarities. In contrast to SC decoding, the output of the SCL decoding method is a smaller set of up to L possible codewords. It considers both ui options for the locations I where data bits can be found. A path dependability metric computed during the method is used to filter out all but the L best pathways from the final list of survivors. At the end

https://doi.org/10.17993/3ctecno.2022.v11n2e42.90-99

of the decoding process, the estimated codeword is selected from among the L candidates based on which one has the highest route dependability score.

If a polar code and a CRC are paired, the projected CRC and computed CRC for each of the L candidates are compared. Out of all the candidates who pass the CRC, the decoded codeword is selected as the most trustworthy candidate. If all candidates fail the CRC, the technique simply selects the candidate with the highest route dependability.

3.4. LATENCY AND THROUGHPUT

To evaluate the latency boost from the novel algorithm and implementation, we compare two unrolled decoders with an LLR-based SC-list decoder developed in accordance with the technique described in [6] in Table I. The first unrolled decoder, also called the "unrolled SC-list," does not rely on any specific set of constituent decoders. The second is called "unrolled Dec-SPC-4," and it incorporates all of the component decoders we have covered so far while limiting the number of SPC decoders to four. When the SC-list decoder is unrolled, we find that decoding time is cut by more than half. Latency is reduced to between 63% (L = 2) and 18.9% (L = 32) of the unrolled SC-list decoder when the rate-0, rate-1, repetition, and SPC-4 constituent decoders are used. In comparison to SC-list decoding, the suggested decoding strategy and implementation yield a performance boost of between 18.4 and 11.9% for list sizes of 2 and 32, respectively.

The impact of the unrolled decoder is more noticeable for shorter lists, while the impact of the new constituent decoders is greater for longer lists.

When there is no limitation on the length of the individual SPC decoders, as in the case of "Unrolled Dec-SPC-4+" in Table I, the latency for the recommended decoder is also shown. Turning on these longer constituent decoders decreases latency by 14% and 18% for L = 2 and L = 8, respectively. We do not advise using SPC-8+ component decoders because of the drastic decrease in error-correction performance for L >= 8. Consequently, we do not guarantee the lag associated with such a decoder setup. The proposed decoder has a roughly linear decrease in throughput in function of L. At L = 32 and 433 s of latency, the data rate is 4 Mbps. Performance can be improved with adaptive decoding by using a Fast-SSC decoder prior to the list decode. The results of this method's throughput are shown for L = 8 and L = 32 in Table II. According to (17), when the throughput for L = 8 and 32 is equal, the effect of the list decoder on throughput diminishes, and the Fast-SSC performs better at 4.5 dB.

4. COMPARATIVE ANALYSIS

Table 1. Latency (in µsec) for various decoding methods of polar code.

Decoder	L		
	2	8	32
SC-List	558	1450	5145
Unrolled SC-list	193 (2.9×)	564(2.6×)	2294(2.2×)
Unrolled Dec SPC-4	30.4(18.4×)	97.5(14.9×)	433(11.9×)
Unrolled Dec SPC-4+	26.3(21.2×)	80.2(18.1×)	N/A

https://doi.org/10.17993/3ctecno.2022.v11n2e42.90-99

Table 2. When calculating 524,280 information bits, the suggested list decoder's information throughput and latency were compared to those of the ldpc decoders of [32].

Decoder	N	# of N-bit frames	Rate	Latency (ms)		Info. T/P (Mbps)
				Total	Per frame	
[32]	1944	540	1/2	17.4	N/A	30.1
proposed	1024	1024	1/2	13.8	0.014	38.0
[32]	1944	405	2/3	12.7	N/A	41.0
proposed	1024	768	2/3	10.0	0.013	52.4
[32]	1944	360	3/4	11.2	N/A	46.6
proposed	1024	683	3/4	8.78	0.013	59.6
[32]	1944	324	5/6	9.3	N/A	59.4
proposed	1024	615	5/6	6.2	0.010	84.5

5. CONCLUSION

This article will help the reader understand and implement the polar code encoding process in accordance with the 5G wireless systems standard, as well as simulate it for practise. This encoding chain exemplifies the 3GPP standards body's efforts to support a variety of code lengths and speeds while satisfying the various code criteria for the eMBB control channel, such as low description complexity and low encoding complexity. Insights into the consideration given to the receiver side during the standardisation process are provided. So long as cutting-edge hardware and decoders are used, the encoder was designed to allow for the decoder to be generated with a tolerable level of complexity and perform at the required latency. But now it is possible to optimise decoding complexity or improve error-rate performance by developing new decoding structures or principles.

We also investigated potential delays introduced by various decoding strategies, including successive cancellation (SC) decoding, successive cancellation flip (SCF) decoding, and successive cancellation list (SCL) decoding. Additionally, we conducted latency analyses to determine the relative merits of each decoding technique. Decoding algorithms can be tweaked to improve delay and throughput.

REFERENCES

[1] E. Arıkan, “Channel polarization: A method for constructing capacity- achieving codes for symmetric binary-input memoryless channels,” IEEE Trans. Inf. Theory, vol. 55, no. 7, pp. 3051–3073, Jul. 2009 “Multiplexing and channel coding, v.15.3.0,” 3GPP, Sophia Antipolis, France, Rep. 38.212, 2018.

[2] K. Niu, K. Chen, J. Lin, and Q. T. Zhang, “Polar codes: Primary concepts and practical decoding algorithms,” IEEE Commun. Mag., vol. 52, no. 7, pp. 192–203, Jul. 2014.

[3] H. Vangala, E. Viterbo, and Y. Hong, “A comparative study of polar code constructions for the AWGN channel,” Jan. 2015. [Online]. Available: arXiv:1501.02473

https://doi.org/10.17993/3ctecno.2022.v11n2e42.90-99

[4] R. Mori and T. Tanaka, "Performance of polar codes with the con- struction using density evolution," IEEE Commun. Lett., vol. 13, no. 7, pp. 519–521, Jul. 2009.
[5] I. Tal and A. Vardy, "How to construct polar codes," IEEE Trans. Inf. Theory, vol. 59, no. 10, pp. 6562–6582, Oct. 2013.
[6] P. Trifonov, "Efficient design and decoding of polar codes," IEEE Trans. Commun., vol. 60, no. 11, pp. 3221–3227, Nov. 2012.
[7] M. Mondelli, S. H. Hassani, and R. Urbanke, "Construction of polar codes with sublinear complexity," in Proc. IEEE Int. Symp. Inf. Theory (ISIT), Aachen, Germany, Jun. 2017, pp. 1853–1857.
[8] G. He et al., "Beta-expansion: A theoretical framework for fast and recursive construction of polar codes," in Proc. IEEE Glob. Commun. Conf. (GLOBECOM), Singapore, Dec. 2017, pp. 1–6.
[9] C. Condo, S. A. Hashemi, and W. J. Gross, "Efficient bit-channel relia- bility computation for multi-mode polar code encoders and decoders," in Proc. IEEE Int. Workshop Signal Process. Syst. (SiPS), Lorient, France, Oct. 2017, pp. 1–6.
[10] M. Mondelli, S. H. Hassani, and R. L. Urbanke, "From polar to Reed–Muller codes: A technique to improve the finite-length performance," IEEE Trans. Commun., vol. 62, no. 9, pp. 3084–3091, Sep. 2014.
[11] V. Bioglio, F. Gabry, I. Land, and J.-C. Belfiore, "Minimum-distance based construction of multi-kernel polar codes," in Proc. IEEE Glob. Commun. Conf. (GLOBECOM), Singapore, Dec. 2017, pp. 1–6.
[12] M. Mondelli, S. H. Hassani, and R. L. Urbanke, "Scaling exponent of list decoders with applications to polar codes," IEEE Trans. Inf. Theory, vol. 61, no. 9, pp. 4838–4851, Sept. 2015.
[13] J. Guo, M. Qin, A. G. I. Fábregas, and P. H. Siegel, "Enhanced belief propagation decoding of polar codes through concatenation," in Proc. IEEE Int. Symp. Inf. Theory (ISIT), Honolulu, HI, USA, Jun. 2014, pp. 2987–2991.
[14] U. U. Fayyaz and J. R. Barry, "Low-complexity soft-output decoding of polar codes," IEEE J. Sel. Areas Commun., vol. 32, no. 5, pp. 958–966, May 2014.
[15] A. Balatsoukas-Stimming, A. J. Raymond, W. J. Gross, and A. Burg, "Hardware architecture for list successive cancellation decoding of polar codes," IEEE Trans. Circuits Syst. II, Exp. Briefs, vol. 61, no. 8, pp. 609–613, Aug. 2014.
[16] A. Balatsoukas-Stimming, M. B. Parizi, and A. Burg, "LLR-based suc- cessive cancellation list decoding of polar codes," IEEE Trans. Signal Process., vol. 63, no. 19, pp. 5165–5179, Oct. 2015.
[17] C. Leroux, A. J. Raymond, G. Sarkis, and W. J. Gross, "A semi-parallel successive-cancellation decoder for polar codes," IEEE Trans. Signal Process., vol. 61, no. 2, pp. 289–299, Jan. 2013.
[18] B. L. Gal, C. Leroux, and C. Jego, "Software polar decoder on an embed- ded processor," in Proc. IEEE Workshop Signal Process. Syst. (SiPS), Belfast, U.K., Oct. 2014, pp. 180–185.
[19] O. Afisiadis, A. Balatsoukas-Stimming, and A. Burg, "A low-complexity improved successive cancellation decoder for polar codes," in Proc. IEEE Asilomar Conf. Signals Syst. Comput., Pacific Grove, CA, USA, Nov. 2014, pp. 2116–2120.
[20] C. Condo, F. Ercan, and W. J. Gross, "Improved successive cancellation flip decoding of polar codes based on error distribution," in Proc. IEEE Wireless Commun. Netw. Conf. (WCNC), Barcelona, Spain, Apr. 2018, pp. 19–24.
[21] I. Tal and A. Vardy, "List decoding of polar codes," IEEE Trans. Inf. Theory, vol. 61, no. 5, pp. 2213–2226, May 2015.
[22] S. A. Hashemi, A. Balatsoukas-Stimming, P. Giard, C. Thibeault, and W. J. Gross, "Partitioned successive-cancellation list decoding of polar codes," in Proc. IEEE Int. Conf. Acoust. Speech Signal Process. (ICASSP), Shanghai, China, Mar. 2016, pp. 957–960.
[23] S. A. Hashemi, M. Mondelli, S. H. Hassani, R. L. Urbanke, and W. J. Gross, "Partitioned list decoding of polar codes: Analysis and improvement of finite length performance," in Proc. IEEE Glob. Commun. Conf. (GLOBECOM), Singapore, Dec. 2017, pp. 1–7.

https://doi.org/10.17993/3ctecno.2022.v11n2e42.90-99


3C
tecnología
Glosas de innovacion aplicadas a la pyme